Thomas Ludwig Deppisch

A TALE OF SCALES

A TALE OF SCALES

Fermion Masses and Mixing in Minimal Supersymmetric SO(10)
and
Resummation of Gluino Contributions to the MSSM Higgs Potential

Zur Erlangung des akademischen Grades eines

Doktors der Naturwissenschaften

von der KIT-Fakultät für Physik des
Karlsruher Instituts für Technologie (KIT)
genehmigte

Dissertation

von

M.Sc. Thomas Ludwig Deppisch

Tag der mündlichen Prüfung:	26. April 2019
Referent:	Prof. Dr. Ulrich Nierste
Korreferent:	Prof. Dr. Margarete Mühlleitner

ABSTRACT

The first part of this work examines the Yukawa sector of a minimal supersymmetric SO(10) model. As a result of a global numerical analysis, the GUT predictions for fermion masses and mixing observables are challenged by recent data from neutrino experiments and lattice simulations. Moreover, the possible values for the SUSY threshold corrections to the Yukawa couplings turn out to be vastly constrained.

The second part concernes the quantum corrections to the MSSM Higgs potential from heavy gluinos. An explicit resummation of these effects to all orders in perturbation theory shows the relation to the renormalisation scheme of the top squarks with the result that for low-energy observables the on-shell scheme should be applied. The fine-tuning in the MSSM can furthermore be less severe compared to the leading order result if these contributions are taken into account.

ZUSAMMENFASSUNG

Der erste Teil dieser Arbeit untersucht den Yukawa Sektor eines minimalen supersymmetrischen SO(10) Modells. Eine globale Analyse ergibt, dass die GUT Vorhersagen für Fermionmassen und deren Minschungsobservablen von jüngsten Daten aus Neutrinoexperimenten und Gittersimulationen angefochten werden. Weiterhin zeigt sich, dass die möglichen Werte für SUSY Schwellenkorrekturen zu den Yukawa Kopplungen erheblich eingeschränkt sind.

Der zweite Teil befasst sich mit den Quantenkorrekturen von schweren Gluinos zum MSSM-Higgspotenzial. Die ausdrückliche Resummierung dieser Effekte zu allen Ordnungen der Störungstheorie zeigt den Zusammenhang zum Renormierungsschema der Topsquarks mit dem Ergbnis, dass für Niederenergieobservablen das *on-shell* Schema angewandt werden sollte. Ferner kann das *fine-tuning* im MSSM, verglichen mit dem Ergebnis in führender Ordnung, weniger drastisch sein, wenn diese Beiträge berücksichtigt werden.

CONTENTS

LIST OF FIGURES

LIST OF TABLES

ACRONYMS

QCD quantum chromodynamics

CKM Cabibbo-Kobayashi-Maskawa

PMNS Pontecorvo–Maki–Nakagawa–Sakata

EW electro-weak

EWSB electro-weak symmetry breaking

VEV vacuum expectation value

SM Standard Model of elementary particle physics

MSSM minimal supersymmetric extension of the Standard Model

NMSSM next-to-minimal supersymmetric extension of the Standard Model

EFT effective field theory

RGE renormalisation group equation

QFT quantum field theory

TC threshold correction

GUT grand unified theory

SUSY supersymmetry

LSP lightest supersymmetric particle

DREG dimensional regularisation

DRED dimensional reduction

1

SYNOPSIS

There is nothing so strange *and so unbelievable that it has not been said by one philosopher or another.*
— René Descartes

BREAKING THE FOURTH WALL. When I was a student and attended the lectures on quantum field theory (QFT) and particle physics I would more than once find myself puzzled with the consequences of quantum corrections: It seemed very strange to me that in perturbation theory "everything could influence everything". I wondered how one could make predictions from a theory whose values change at each and every order in the perturbative expansion. I needed some time to understand that many physical problems will become more comprehensible to oneself if they are formulated in a different way. Most of the time that question is: What is large and what is small? More precisely, in QFT, there are two powerful tools that help to seperate physics at small scales from physics at large scales: effective field theory and the renormalisation group.

Let us illustrate these theoretical concepts with a simple one-loop example before we actually apply them to physical problems. We will not so much focus on the calculations and the results but on the conclusions we can draw from them. Our conventions can be found in Appendix A.1. Some of them are explicitely mentioned in the text, some appear in the side margins as a reminder.

A TOY MODEL. PART I. Consider a complex scalar field ϕ (mass m) whose interaction with a Dirac fermion ψ (mass M) is described by the Lagrangian density

$\mathbb{P}_{R,L} = (\mathbb{1} \pm \gamma_5)/2\,.$

$$\mathcal{L}_{\text{int}} = -y\,\overline{\psi}\,\mathbb{P}_L\psi\,\phi - y^\star\,\overline{\psi}\,\mathbb{P}_R\psi\,\phi^\star\,. \tag{1.1}$$

We can calculcate the corrections to the scalar mass m coming from this fermion in perturbation theory, as depicted in diagram 3 of Figure 1.1. For zero momentum transfer the scalar self-energy in $d = 4 - 2\varepsilon$ dimensions is

The self-energy is evaluated at $p^2 = 0$ since we assume $M^2 \gg p^2$.

$$\begin{aligned} \mathrm{i}\,\Sigma(p^2 = 0) &= -\left|y\mu^\varepsilon\right|^2 \int \frac{\mathrm{d}^d k}{(2\pi)^d} \frac{\operatorname{tr}\left\{(M - \not{k})\mathbb{P}_L(M - \not{k})\mathbb{P}_R\right\}}{(k^2 - M^2)(k^2 - M^2)} \\ &= -\frac{2\mathrm{i}\left|y\right|^2 M^2}{(4\pi)^{d/2}} \left(\tfrac{1}{1-\varepsilon} + 1\right) \left(\frac{\mu}{M}\right)^{2\varepsilon} \Gamma(\varepsilon)\,, \end{aligned} \tag{1.2}$$

where the renormalisation scale μ has been introduced to keep the Yukawa coupling y dimensionless and the integral [1]

$$\int \frac{\mathrm{d}^d k}{(m^2 - k^2)^\lambda} = \frac{\mathrm{i}\,\pi^{d/2}}{(m^2)^{\lambda+\varepsilon-2}} \frac{\Gamma(\lambda + \varepsilon - 2)}{\Gamma(\lambda)}\,, \tag{1.3}$$

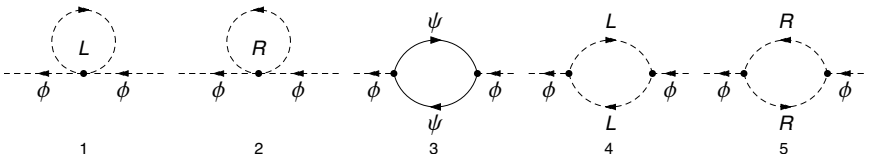

Figure 1.1: Diagrams contributing to the self-energy of ϕ.

has been used. The self-energy induces a shift in the pole of the Dyson resummed propagator of ϕ, i. e. the physical mass becomes

$$m^2_{\text{pole}} = m^2 - \Sigma(p^2) \,. \tag{1.4}$$

This simple example illustrates two important aspects of quantum corrections. Firstly, the integral in eq. (1.2) scales as $\sim \int \mathrm{d}k\, k^{d-3}$ for large values of the loop momentum. Hence, the integral does not converge in four spacetime dimensions. In dimensional regularisation (DREG) [2], this divergency becomes manifest as a pole in the Laurent series of the Γ function around $\varepsilon = 0$,

Numerically, the Euler-Mascheroni constant is $\gamma_{\text{E}} \approx 0.5772$.

$$\Gamma(\varepsilon) = \frac{1}{\varepsilon} - \gamma_{\text{E}} + \mathcal{O}(\varepsilon) \,. \tag{1.5}$$

Expanding now eq. (1.2) around $\varepsilon = 0$ gives

$$\begin{aligned} \mathrm{i}\,\Sigma(p^2 = 0) = \frac{-\mathrm{i}\,|y|^2 M^2}{16\pi^2} \Bigg(& \frac{4}{\varepsilon} - 4\,\gamma_{\text{E}} + 4\log 4\pi \\ & + 4\log\left(\frac{\mu^2}{M^2}\right) + 2 + \mathcal{O}(\varepsilon) \Bigg) \,. \end{aligned} \tag{1.6}$$

This expression is apparently not convergent in the limit $\varepsilon \to 0$. But we can deal with this divergency by replacing $m^2 \to m^2 + \delta m^2$ in the Lagrangian. The pole mass of the scalar ϕ then becomes

$$m^2_{\text{pole}} = m^2 - \Sigma(p^2) + \delta m^2 \,. \tag{1.7}$$

Choosing the counterterm δm^2 such that it cancels the $1/\varepsilon$ poles in eq. (1.6) makes m^2_{pole} finite in four dimensions. δm^2 must therefore at least contain all the $1/\varepsilon$ poles but one could add any term that is finite for $\varepsilon \to 0$. This leaves us with an arbitrariness in the choice of δm^2, namely the choice of the *renormalisation scheme*.

The *renormalisation scale* μ has been introduced in eq. (1.2) to keep the mass dimension of y fixed outside of four dimensions. Naively, μ^ε should give 1 for $\varepsilon \to 0$. But in combination with the $1/\varepsilon$ pole in the gamma function there remains a finite term $\propto \log(\mu^2/M^2)$ in eq. (1.6). Therefore $m^2_{\text{ren.}}$ now depends on the choice of both the renormalisation scheme and the renormalisation scale. At this point it is convenient to define the *modified minimal subtraction scheme* ($\overline{\text{MS}}$, [3]): We replace

The notation $\bar{\mu}$ is used in this work to avoid confusion with the MSSM parameter μ.

$$\mu^2 \to \bar{\mu}^2 \mathrm{e}^{\gamma_{\text{E}}}/4\pi \tag{1.8}$$

and then absorb only the $1/\varepsilon$ pole into δm^2. This is equivalent to absorbing not only the poles but also the $\log 4\pi$ and γ_E terms that always accompany them. We see that a different prescription of what to absorb into the counterterm is the same as a rescaling of the renormalisation scale.

We can express the dependence of m^2 on the renormalisation scale $\bar{\mu}$ in the following way

$$\frac{\mathrm{d}m^2_{\overline{\mathrm{MS}}}}{\mathrm{d}\log\bar{\mu}^2} = \frac{-4\left|y\right|^2 M^2}{16\pi^2}\,. \tag{1.9}$$

This so-called renormalisation group equation (RGE) tells us how the value of $m^2_{\overline{\mathrm{MS}}}$ changes if the value of $\bar{\mu}$ changes. This can be seen as one of the puzzling consquences of QFT mentioned at the beginning of this chapter: a physical quantity like a mass appears to depend on the renormalisation procedure. This fact may become clearer when we look at it from a different perspective: The renormalisation procedure is part of how a theory is defined. If we change it, the renormalisation group tells us how to change the other parameters of the theory in order *not* to change the physical predictions of the theory. Practically, one can think of the renormalisation group as a device to translate between renormalisation scales and thus will be used recurringly throughout this thesis.

Secondly, m^2_{ren} in eq. (1.7) also depends on y and M. It is a peculiarity of scalar fields that m^2_{ren} scales (naively) as M^2. If $M^2 \gg m^2$, the quantum corrections can easily become much larger than the value of m^2 itself. On the one hand, this is not a problem since one can absorb any finite contribution into δm^2. On the other hand, however, a relatively small change in the value of M may result in a relatively large change of m which needs to be compensated by tuning δm^2 accordingly. One can compare this to numerical operations on a computer: Adding and subtracting large numbers with small differences requires high floating point precision. Keeping in mind that this *fine-tuning* of the theory parameters must be done at every order in perturbation theory, it seems implausible that physics at the scale of m is so sensitive to physics at the scale of $M \gg m$. At this point our observation is general to scalar masses in QFT. Let us now have an overview of the Standard Model and particle physics to see the consequences of this observation.

If m is at the electroweak scale and M at the Planck scale, roughly 32 significant decimal digits, i. e. quadruple precision (128 bit), are required to get the right order of magnitude for m.

THE STANDARD MODEL. Since its development in the 1960s and 1970s the Standard Model of elementary particle physics (SM) has led to great success in describung the quantum nature of both the electro-weak (EW) interaction [4–6] and quantum chromodynamics (QCD) [7, 8]. The SM is a gauge theory with the gauge group $\mathrm{SU}(3)_C \times \mathrm{SU}(2)_L \times \mathrm{U}(1)_Y$. The corresponding gauge bosons are the gluons $G^{a,\mu}$

field	flavours	$SU(3)_C$	$SU(2)_L$	Y
e_R^i	e_R, μ_R, τ_R	**1**	**1**	-2
L^i	$\begin{pmatrix}\nu_{e,L}\\ e_L\end{pmatrix}, \begin{pmatrix}\nu_{\mu,L}\\ \mu_L\end{pmatrix}, \begin{pmatrix}\nu_{\tau,L}\\ \tau_L\end{pmatrix}$	**1**	**2**	-1
u_R^i	u_R, c_R, t_R	$\bar{\mathbf{3}}$	**1**	4/3
d_R^i	d_R, s_R, b_R	$\bar{\mathbf{3}}$	**1**	-2/3
Q^i	$\begin{pmatrix}u_L\\ d_L\end{pmatrix}, \begin{pmatrix}c_L\\ s_L\end{pmatrix}, \begin{pmatrix}t_L\\ b_L\end{pmatrix}$	**3**	**2**	1/3

Table 1.1: **Gauge representations of the fermions in the SM.** Subscripts L and R are used for left-handed and right-handed chiral fermions, respectively, such that $\psi_L = \mathbb{P}_L\psi$ and $\psi_R = \mathbb{P}_R\psi$ for a Dirac fermion ψ. Bold numbers stand for the representations of $SU(N)$. Y is the hypercharge and $i = 1, 2, 3$ is a flavour index.

($a = 1, ..., 8$) as well as the electroweak bosons $W^{1,\mu}$, $W^{2,\mu}$, $W^{3,\mu}$ and B^μ. They couple to the matter fermions ψ^i via the gauge kinetic term

$$\mathcal{L}^{\text{SM}}_{\text{kinetic}} = \overline{\psi}^i \, \mathrm{i}\not{D} \, \psi^i \, . \tag{1.10}$$

The covariant derivative D^μ here needs some clarification since it depends on the gauge representation of the matter fields. It is an important aspect of the electroweak interaction that it is chiral, i. e. treats left-handed fermions and right-handed fermions differently. Thus the SM accounts for the parity violation found in experiment [9]. Table 1.1 shows the gauge representations of the chiral fermions $\psi_L = \mathbb{P}_L\psi$ and $\psi_R = \mathbb{P}_R\psi$. In particular all right-handed fields are singlets under $SU(2)_L$ (i. e. weak interaction) and all leptons are singlets under $SU(3)_C$ (i. e. strong interaction). To fix the conventions we state the covariant derivative as it applies to the left-handed quark doublet,

$$D^\mu = \partial^\mu + \frac{\mathrm{i}g_Y}{2} B^\mu Y + \frac{\mathrm{i}g_2}{2} W_i^\mu \sigma^i + \frac{\mathrm{i}g_3}{2} G_a^\mu \lambda^a \, . \tag{1.11}$$

Y denotes the hypercharge of the field. The Pauli matrices $\sigma^i/2$ are the group generators acting on the weak doublets and the Gell-Mann matrices $\lambda^a/2$ act on the colour triplets. We note that colour indices for quarks (and also for squarks later on) will be suppressed in most expressions of this thesis.

All fermion fields in the SM come in three copies, or generations. We will often speak of *down-type quarks* meaning the quark *flavours* down, strange and bottom, as well as *up-type quarks* meaning the up, charm and top quark. The same applies to the charged leptons that come in the flavours electron, muon and tau. These three generations differ from each other in nothing but their masses. Mass terms in the Lagrangian, however, are forbidden by gauge symmetry since they would mix left-handed and right-handed fields. Fermion masses as

they are observed in nature therefore require spontaneous breaking of the electroweak interaction.

The electro-weak symmetry breaking (EWSB) is achieved with the Higgs mechanism [10, 11]. What we call the *Higgs field* is a complex scalar $SU(2)_L$ doublet field ϕ with hypercharge $Y = 1$ whose gauge kinetic term and self-interactions are

$$\mathcal{L}^{\text{SM}}_{\text{Higgs}} = \left(D_\mu \phi\right)^\dagger \left(D^\mu \phi\right) - m^2\, \phi^\dagger \phi - \frac{\lambda}{4}\left(\phi^\dagger \phi\right)^2 . \tag{1.12}$$

Numerically, $v = 174.104\,\text{GeV}$, replacing $v \to v/\sqrt{2}$ in our expressions will restore the other convention.

In the minimum of the classical scalar potential the Higgs field configuration can be written in $\text{SU}(2)_L$ space as

$$\langle \phi \rangle = \left\langle \begin{pmatrix} \phi^1 \\ \phi^0 \end{pmatrix} \right\rangle = \begin{pmatrix} 0 \\ v \end{pmatrix}, \quad \text{with } v^2 = -\frac{2m^2}{\lambda}, \qquad \text{for } m^2 < 0\,. \tag{1.13}$$

The vacuum expectation value (VEV) v breaks the $\text{SU}(2)_L \times \text{U}(1)_Y$ gauge symmetry to the electromagnetic gauge group $\text{U}(1)_{\text{EM}}$. The electric charge in our conventions is $Q = I_3 + Y/2$. The $W^\pm$ bosons and the Z boson which correspond to the generators of the broken symmetry receive a mass from the gauge kinetic term of the Higgs field, whereas the mass of the Higgs boson itself is determined by the curvature at the minimum of the classical scalar potential. In our conventions these masses read

I_3 is the third compent of the weak isospin. For a weak doublet that is $\sigma_3/2$.

$$m_W^2 = \frac{g_2^2}{2} v^2, \qquad m_Z^2 = \frac{g_Y^2 + g_2^2}{2}\, v^2, \qquad m_{\text{h}}^2 = \lambda v^2\,. \tag{1.14}$$

Although these particles were already predicted in the 1960s, it was not before 1983 until the W and Z bosons were discovered [12–15]. The long-standing search for all particles in the SM eventually came to its end with the finding of the Higgs boson in 2012 [16, 17].

Moreover, the Higgs mechanism also gives masses to quarks and leptons through the Yukawa interactions. The Yukawa sector of the SM consists of all gauge invariant interactions of the Higgs field with the chiral fermions,

$$\begin{aligned} \mathcal{L}^{\text{SM}}_{\text{Yukawa}} = &- Y_e^{ij}\, \overline{e_{Ri}}\, \phi^\dagger \cdot L_j - Y_d^{ij}\, \overline{d_{Ri}}\, \phi^\dagger \cdot Q_j - Y_u^{ij}\, \overline{u_{Ri}}\, Q_j^T \cdot \varepsilon \cdot \phi \\ &+ \text{H.c.} \end{aligned} \tag{1.15}$$

A dot denotes a matrix product, the metric tensor of $SU(2)$ is $\varepsilon = \left(\begin{smallmatrix} 0 & 1 \\ -1 & 0 \end{smallmatrix}\right)$.

Y_e, Y_d and Y_u are matrices in flavour space. We will use Y_x for Yukawa matrices and y_x for their singular values. Inserting the VEV of the Higgs field the mass matrices are

The singular values of a complex matrix A are the square roots of the eigenvalues of $A^\dagger A$.

$$M_x = v\, Y_x, \quad \text{for } x = u, d, e\,. \tag{1.16}$$

All mass matrices have a strong hierarchical structure with the first generation being the lightest one. The fermions of the second and third generation are heavier than the former ones by a factor of roughly 40 up to 100. This recurring pattern can be seen as a hint of an organising principle in the Yukawa sector.

BEYOND THE STANDARD MODEL. Coming back to our simple toy model from the beginning of this chapter, we can now compare it with the SM: The main similarity is the existence of a complex scalar field ϕ coupling to a fermion with a Yukawa interaction. The masses of all particles in the SM, however, are set by the VEV of the Higgs field (times some coupling). Therefore, there is no large mass hierarchy within the SM that destabilises the mass of the Higgs boson like in our simple example. The *hierarchy problem* arises if the Higgs doublet couples to physics at scales that are much higher than the electroweak scale. This could be the Planck scale at about 10^{19} GeV at which gravity becomes strong enough to compete with the forces of the SM. But it also could be any new particle heavier than the electroweak scale. This is a well-motivated scenario since we know that the SM—although quite accurate in its predictions—is at least an incomplete description of nature.

An obvious shortcoming of the SM is that it cannot—at the renormalisable level— explain the masses of neutrinos which are indicated by neutrino oscillations [18–21]. One possibility to generate neutrino masses without introducing new particles is the dimension five operator [22]

$\psi^C = -\mathrm{i}\gamma^2\gamma^0\bar{\psi}^T.$

$$\mathcal{L}_\kappa^{SM} = \frac{\kappa^{ij}}{4}\left(\overline{L^c}_i \cdot \varepsilon \cdot \phi\right)\left(L_j^T \cdot \varepsilon \cdot \phi\right) + \text{H.c.}\,. \tag{1.17}$$

The coupling κ has mass dimension minus one and hence is not renormalisable. This hints at a more fundamental theory that effectively generates this operator. A renormalisable model can e. g. introduce n species of right-handed neutrinos N_i. The most general way these gauge singlets can couple to the SM particles is

$$\mathcal{L}_N^{SM} = -\frac{1}{2}\, M^{ij}\, \overline{N}_i N_j^c - Y_\nu^{ij}\, \overline{N}_i\, L_j^T \cdot \varepsilon \cdot \phi + \text{H.c.} \tag{1.18}$$

Below the mass scale M of the right-handed neutrinos, they can be integrated out generating the effective *Weinberg operator* of eq. (1.17). All information from the fundamental theory is then incorporated in the Wilson coefficients κ^{ij} as the right-handed neutrinos and their dynamics are no longer part of the effective theory.

The effective masses for the left-handed neutrinos are of the order of v^2/M which lies in the eV range for $M = \mathcal{O}(10^{13})$ GeV in accordance with the current experimental bound on the SM neutrino masses [23]. This is one example of how physics from different scales can interfere with each other and a treatment in terms of an effective field theory becomes necessary. In this thesis the see-saw will be revisited in the context of SO(10) grand unification. One of the major findings of Chaper 2 is that the Yukawa sector of supersymmetric SO(10) becomes severely constrained with recent neutrino data. The setup of this model still needs another ingredient, namely supersymmetry (SUSY) which will be illustrated in the framework of our example from the beginning of this chapter.

A TOY MODEL. PART II. Let L and R be two complex scalar fields coupled to ϕ via the quartic couplings

$$\Delta\mathcal{L} = -|y|^2 \, L^\star L \, \phi^\star \phi - |y|^2 \, R^\star R \, \phi^\star \phi \,. \tag{1.19}$$

Let ϕ have a VEV of the form $\langle \phi \rangle = v$. Then $\Delta\mathcal{L}$ creates an additional mass term $M = yv$ for L and R (the same as for ψ in eq. (1.1)) as well as the trilinear coupling

$$-|y| \, v \, L^\star L(\phi + \phi^\star) - |y| \, v \, R^\star R(\phi + \phi^\star) \,. \tag{1.20}$$

Including these interactions, the diagrams 1,2,4 and 5 in Figure 1.1 also contribute to the self-energy of ϕ,

$$\begin{aligned} \mathrm{i}\,\Sigma(p^2 = 0) = {} & \frac{\mathrm{i}|y|^2 M^2}{(4\pi)^{d/2}} \left(\frac{\mu}{M}\right)^{2\varepsilon} \frac{\Gamma(\varepsilon)}{1-\varepsilon} \\ & + \frac{\mathrm{i}|y|^2 M^2}{(4\pi)^{d/2}} \left(\frac{\mu}{M}\right)^{2\varepsilon} \Gamma(\varepsilon) \\ & + \text{the same for diagrams 2 and 5} \,, \end{aligned}$$

where the first line corresponds to diagram 1, the second line to diagram 4 and the last line stands for the contributions of R. Surprisingly, these contributions exactly cancel that of the fermion ψ in eq. (1.2). Explicitly, this cancellation applies to the UV divergent terms as well as to the UV finite ones. The mass m hence does not need to be renormalised in our example and is stable against radiative corrections. But this cancellation only holds under the very specific assumptions we made: Introducing a complex scalar for each *chiral* component of ψ and coupling them to ϕ like in eq. (1.19). If there were another source of masses for L and R the cancellation would not be exact. Another subtlety is present: The fermion trace in eq. (1.2) must be evaluated in four dimensions, i. e. applying dimensional reduction (DRED) ($\overline{\text{DR}}$, [24, 25]) which will later be commented on.

The discussion will follow reference [26] which adopts the notation from [27].

Supersymmetry [28–33] puts this accidental cancellation on more formal grounds by postulating a symmetry between bosons and fermions. This has the benefit of stabilising the electroweak scale against radiative corrections from heavy particles at any order in perturbation theory. Instead of defining SUSY in a formal way we will use the minimal supersymmetric extension of the Standard Model (MSSM) as an example of a supersymmetric theory focusing on its phenomenological aspects.

THE MINIMAL SUPERSYMMETRIC STANDARD MODEL. A very useful tool to describe supersymmetric interactions is the *superpotential*. We can define it as a holomorphic function of the scalar fields with mass dimension three. The SUSY partners of the SM fermions are called squarks ($\tilde{Q}_i$, $\tilde{u}_R$, $\tilde{d}_R$) and sleptons ($\tilde{L}_i$, $\tilde{e}_R$) having the same

The superpotential of our toy model would be $\mathcal{W} = y\,\phi LR$.

gauge representations as the corresponding fermions in Table 1.1. The superpotential of the MSSM [27, 34–38] then can be written as

$$\begin{aligned}\mathcal{W}^{\text{MSSM}} = \mu\, H_1 \cdot \varepsilon \cdot H_2 + Y_e^{ij}\, e_{Ri}\, H_1 \cdot \varepsilon \cdot L_j \\ + Y_d^{ij}\, d_{Ri}\, H_1 \cdot \varepsilon \cdot Q_j + Y_u^{ij}\, u_{Ri}\, \cdot Q_j \cdot \varepsilon \cdot H_2\,,\end{aligned} \tag{1.21}$$

where $i, j = 1, 2, 3$ are flavour indices. The first observation is that two Higgs doublets H_1 (hypercharge $Y = -1$), H_2 ($Y = 1$) are needed because complex conjugation is not allowed in a holomorphic function. To generate masses for all fermions also two VEVs are needed, in $\text{SU}(2)_L$ space

$$\langle H_1 \rangle = \left\langle \begin{pmatrix} h_1^0 \\ h_1^- \end{pmatrix} \right\rangle = \begin{pmatrix} v_1 \\ 0 \end{pmatrix}, \qquad \langle H_2 \rangle = \left\langle \begin{pmatrix} h_2^+ \\ h_2^0 \end{pmatrix} \right\rangle = \begin{pmatrix} 0 \\ v_2 \end{pmatrix}. \tag{1.22}$$

Reproducing the gauge boson masses of the SM fixes $v^2 = v_1^2 + v_2^2$. The ratio of the VEVs is defined as $\tan\beta = v_2/v_1$. The Yukawa interactions for the scalars ϕ_i and their chiral partners ψ_i can be derived from the superpotential by

$$\mathcal{L}_{Yukawa} = -\frac{1}{2}\frac{\partial^2 \mathcal{W}}{\partial\phi_i\, \partial\phi_j}\psi_i\psi_j + H.c. \tag{1.23}$$

It is also useful to define so-called F-terms and D-terms, respectively,

$$F_i = \frac{\partial W}{\partial \phi_i}\,, \qquad D^a = g\, \phi_i^\star T_{ij}^a \phi_j\,, \tag{1.24}$$

where T^a is any matrix generator of the SM gauge groups and g denotes the corresponding gauge coupling. The scalar potential is

$$V = \frac{1}{2} D^a D^a + F_i^\star F_i\,. \tag{1.25}$$

The interactions of scalars and chiral fermions with the gauge bosons are given by their respective gauge kinetic term. In addition, the gauge bosons have superpartners, the gauginos λ^a (called bino $\tilde{b}$, wino $\tilde{w}^i$, gluino $\tilde{g}$). They are Majorana fermions in the adjoint representation of the gauge group. Their gauge interactions are described by

$$\mathcal{L}_{gaugino} = \mathrm{i} g f_{abc} \lambda^a \sigma^\mu \overline{\lambda^b}\, V_\mu^c + \mathrm{i}\sqrt{2}\, T_{ij}^a \left(\lambda^a \psi_j \phi_i^\star - \bar{\lambda}^a \overline{\psi_i} \phi_j \right)\,, \tag{1.26}$$

$\sigma^\mu = (1, \vec{\sigma})^\mu$, all further two-component spinor notation can be found in Appendix A.1

with the structure constants f_{abc} of the respective gauge group with gauge boson $V^{a,\mu}$.

In fact one further symmetry is required to forbid additional terms in the superpotential of eq. (1.21): R-parity. All SM fields and the Higgs doublets carry the multiplicative quantum number $R = 1$, whereas their respective superpartners have $R = -1$. This has the nice consequence that the lightest supersymmetric particle (LSP) is stable

and serves as a candidate for dark matter. The lack of such a candidate can be seen as another important shortcoming of the SM.

Finally, we have seen that supersymmetry demands particles and their superpartners to be degenerate in mass. Yet, this is not what we observe in nature and this fact hints at supersymmetry being not an exact but a broken symmetry. Although there exist ideas on how to break supersymmetry dynamically [39, 40], we will use general *soft-breaking* terms [41] in the Lagrangian, that is masses for the scalars and gauginos, namely

$$\mathcal{L} = -m_{ij}\,\phi_i\phi_j^\star - \frac{1}{2}M_1\,\bar{\tilde{b}}\tilde{b} - \frac{1}{2}M_2\,\bar{\tilde{w}}^i\tilde{w}^i - \frac{1}{2}M_3\,\bar{\tilde{g}}^a\tilde{g}^a\ , \tag{1.27}$$

as well as trilinear scalar couplings. They will be specified when we make use of them. The important condition for all soft terms is that they do not violate gauge symmetry. While phenomenologically additional scalar masses solve the problem of why we have not yet detected any SUSY particles they also introduce a theroretical problem: The cancellation of radiative corrections we have encountered in our toy model is spoiled. To make this statement more precise, let us suppose there is supersymmetry restored at some energy scale M_{SUSY}. That is, the SUSY scalar masses are set at this scale. Then radiative corrections of the order of M^2_{SUSY} can contribute to the mass parameters in the Higgs potential which destabilises the electroweak scale. Depending on how large M_{SUSY} actually is this behaviour reintroduces our problem from the beginning, this time called the *little hierarchy problem*.

OUTLINE. As we have seen in this introductory chapter, there are various reasons to speculate about new physics in the framework of supersymmetry. But the fact that we have not yet found any SUSY particles gives rise to problems of its own. This thesis tries to tackle some of them in two complementary ways: Chapter 2 will be concerned with SUSY SO(10) grand unification following a top-down approach. We will find that new data on quark masses and neutrino observables constrain the threshold effects of SUSY particles in the Yukawa sector. In Chapter 3 we will follow a bottom-up approach. We will consider the limit in which the gluino becomes much heavier than the top squarks as well as its implications on the Higgs sector and the little hierarchy problem. As we will see, this scenario poses the question of which renormalisation scheme should be adopted for radiative corrections stemming from heavy SUSY particles. In the end, we will summarise in Chapter 4 what we have learned from this *Tale of Scales*.

2

FERMION MASSES AND MIXING IN MINIMAL SUPERSYMMETRIC SO(10)

And what are two thousand years?... What, indeed, if you look from a mountain top down *the long wastes of the ages? The very stone one kicks with one's boot will outlast Shakespeare.*
—Virginia Woolf

SUPERSYMMETRIC GRAND UNIFICATION. In the course of its development, the SM not only provided a description of the electro-weak interaction, but delivered proof that the concept of non-abelian gauge theories [42] can function to describe nature at the quantum level. It was not before long that this finding inspired physicists to embed the SM into theories with simple gauge groups, so-called grand unified theories (GUTs). The first of such models that has been published is based on the gauge group SU(5) [43]. Interestingly, H. Georgi actually noticed earlier on that SO(10) is a valid candidate as well. This line of research was pursued later in references [44, 45]. GUTs became favoured by many theorists because of their elegance and simplicity: Once the SM is embedded into the GUT, all quantum numbers of the SM particles are fixed by gauge symmetry. In particular, GUTs explain why the electric charges of the proton and the positron are exactly equal. An SO(10) symmetric theory is also automatically free of gauge anomalies [46, 47], while their absence is merely accidental in the SM.

The spinorial representation **16** of SO(10) additionally can accommodate for all fifteen SM fermions of one generation plus a right-handed neutrino. Thus not only unification of the forces but also of the matter fields is achieved. As a result, in SO(10) symmetric theories, the Yukawa sectors of quarks and leptons are closely connected to each other. Parity is restored since SO(10) has a subgroup $SU(2)_R$ that couples to the right-handed SM fermions. Interestingly, in the MSSM all three gauge couplings meet at $M_{\text{GUT}} = 1.35 \times 10^{16}$ GeV as Figure 2.1 depicts. Although the unification is not quite perfect, it makes SUSY GUTs very attractive since gauge coupling unification can be achieved without additional particles below the GUT scale besides the SM particles and their superpartners. SUSY also has the advantage that it protects the EW scale against radiative corrections proportional to M_{GUT}^2 that stem from heavy gauge bosons and the Higgs fields necessary to break the gauge symmetry at M_{GUT}. Over the last decades a lot of studies on SUSY SO(10) models have been performed [48–61], some particularly focusing on one specific model, sometimes called the "(N)MSGUT" [62–81]. Nevertheless, we will not concern ourselves with the details of such complete models but rather with the features they all have in common: the Yukawa sector and its predictions for fermion masses and mixing in the SM.

The fact that relations among the Yukawa couplings predicted by GUTs are only valid at the GUT scale requires a thorough numerical

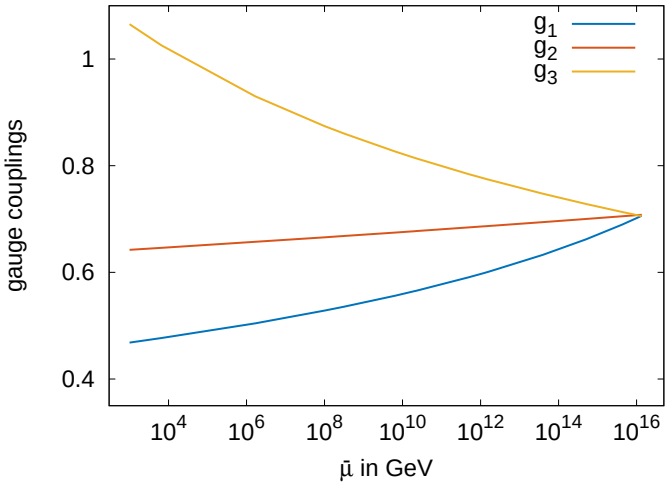

Figure 2.1: **RGE evolution of gauge couplings in the MSSM.** As input values the 1 TeV data from Table 2.3 is used. The GUT scale is determined by $M_{\text{GUT}} = 1.35 \times 10^{16}$ GeV and $g_1^2 = 3/5\, g_Y^2$. For greater detail see Section 2.1.4.

treatment of the RGE effects in order to fit the high-scale model to low-energy data, such as quark masses. Of the various studies that have been performed [55, 58–60, 82–88] we would like to point out references [89, 90] as being the most recent and elaborate ones. Dück and Rodejohann [90] perform a global fit to the fermion masses and their mixing in both the supersymmetric and the non-supersymmetric case while studying different combinations for the GUT Yukawa sector. Bertolini, Schwetz and Malinsky [89] additionally analyse the GUT potential regarding its influence on the see-saw scale. We will use both their results to set up what we will call the *minimal model*.

During the last couple of years, furthermore, a lot of progress has been made in improving the experimental data on quark and lepton observables. This counts especially for the light quark masses whose determination relies on lattice calculations [91]. Also the overall uncertainties in the global fits to the CKM [92] and PMNS [93] matrices have been reduced. As we will see, the new data severely challenges the predictions made by grand unification.

MINIMAL SUPERSYMMETRIC SO(10) Due to the tensor structure of SO(10), the only possible Yukawa couplings for fermions in the **16** representation are to Higgs fields in the **10**, **120** and $\overline{\mathbf{126}}$ representation, see, e. g., [94]. In supersymmetry, the corresponding superpotential reads, with flavour indices i and j

For simplicity, the name of the field indicates its representation.

$$\mathcal{W}_{\text{SO(10)}}^{\text{Yukawa}} = Y_{10}^{ij}\, \mathbf{16}_i \cdot \mathbf{16}_j \cdot \mathbf{10}_H + Y_{120}^{ij}\, \mathbf{16}_i \cdot \mathbf{16}_j \cdot \mathbf{120}_H + Y_{126}^{ij}\, \mathbf{16}_i \cdot \mathbf{16}_j \cdot \overline{\mathbf{126}}_H \,. \tag{2.1}$$

A flavour rotation $U \in \mathrm{U}(3)$ on the fields in the **16** representation

$$\mathbf{16}_i \to U_{ij}\,\mathbf{16}_j\,, \tag{2.2}$$

allows to choose one Yukawa matrix diagonal, e. g.

$$Y_{10} \to U^T Y_{10} U = \mathrm{diag}\left(y_1, y_2, y_3\right)\ . \tag{2.3}$$

A realistic model hence needs at least two Yukawa matrices to allow for flavour non-diagonal couplings. Due to the tensor structure of SO(10) one can further choose Y_{126} to be symmetric and Y_{120} to be antisymmetric without loss of generality. As the studies in [90] have shown, the combination of the Higgs representations **10** and $\overline{\mathbf{126}}$ is more suited to describe the fermion data than other combinations of two Higgs representations. We therefore will use this combination for our *minimal model*, introducing 19 free parameters in the Yukawa sector.

Because of its antisymmetry, Y_{120} can help to fit the mixing observables but not the fermion masses. Adding the 120 *representation would further introduce another* 12 *parameters.*

The $\overline{\mathbf{126}}$ representation does not only accommodate for two copies of the MSSM Higgs doublets but also features weak singlets and triplets. Their VEVs can trigger both Type I see-saw (stemming from weak singlets) and Type II see-saw (stemming from weak triplets). For a review, see e. g. [96]. In the analysis of [89], the authors find that fits to a complete SUSY GUT potential prefer Type I see-saw over Type II see-saw. We therefore will focus on Type I see-saw in order to keep the number of parameters in our model minimal.

The problems introduced by having several copies of the weak doublets and colour triplets in the Higgs representations can be solved in complete SO(10) *models via a mechanism called* missing vev mechanism, *see, e. g., [95].*

Besides their elegance GUTs make one spectacular prediction: They conserve neither lepton nor baryon number. Thus, the proton is unstable in those theories. In SUSY GUTs, its lifetime also depends on the absolute mass scale of the squarks. Analyses of minimal SUSY SO(10) models [97–99] have shown that the predictions for the lifetime of the proton are typically above the lower bounds given by the Super-Kamiokande experiment [100], being of the order of 10^{34} years.

2.1 FITTING SUSY SO(10) TO FERMION OBSERVABLES

The methodology of our global analysis will follow a top-down approach, i. e. the input parameters are set at the GUT scale and are compared to the data given at the SUSY scale after applying RGE corrections. Each step of the fitting procedure is shown in Figure 2.2 and explained in detail in the subsection labelled by the red numbers. The procedure can be roughly summarised as follows: The masses of the light quarks are evolved to the EW scale. Between M_Z and M_{SUSY}, the two-loop RGEs of the SM are used [101–103]. The GUT scale is determined by gauge coupling unification. At M_{GUT} the input parameters for the MSSM Yukawa couplings are set. Their values are then evolved in the MSSM with additional singlet fields to account for the right-handed neutrinos [104, 105] which are consecutively integrated out at their mass scale. The fit is finally performed at the matching scale

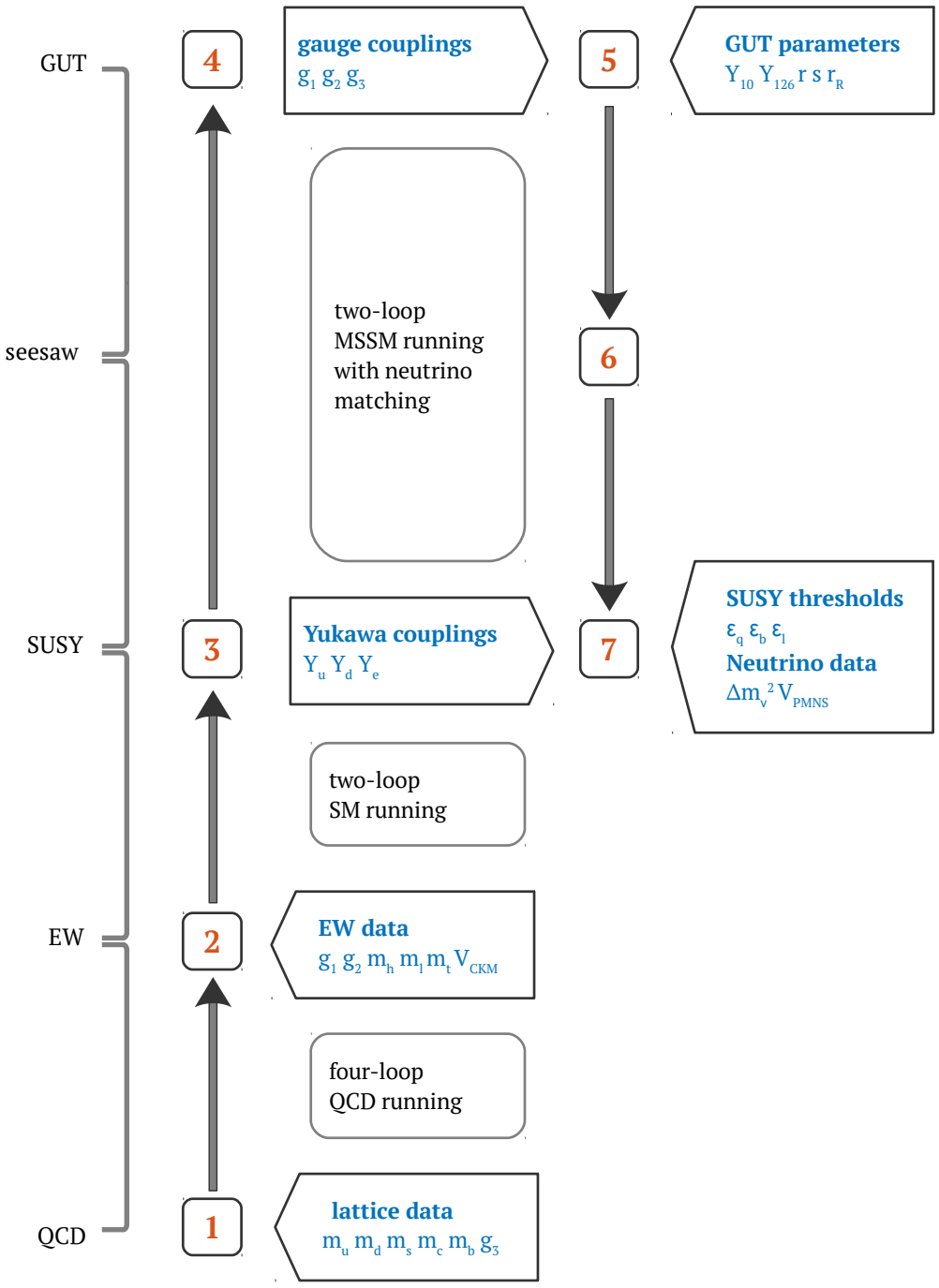

Figure 2.2: **Flow chart of the fitting procedure.** Input data is labelled in blue. The red numbers mark the subsections of Section 2.1

$M_{\text{SUSY}} = 1$ TeV, where also $\tan\beta$ enhanced threshold corrections (TCs) are taken into account.

A NOTE ON RUNNING AND DECOUPLING. If right-handed neutrinos are added to the MSSM, the superpotential additionally includes the following renormalisable couplings [106, 107]

$$\mathcal{W}_N = \frac{1}{2} M^{ij} N_i N_j + Y_\nu^{ij} N_i L_j \cdot \varepsilon^T \cdot H_2 \,. \tag{2.4}$$

Integrating out the right-handed neutrinos gives a contribution to the Weinberg operator, whose supersymmetric form is

The conventions are chosen to coincide with the non-supersymmetric version in eq. (1.17).

$$\mathcal{W}_\kappa = -\frac{\kappa^{ij}}{4}\Big(L_i \cdot \varepsilon \cdot H_2\Big)\Big(L_j \cdot \varepsilon \cdot H_2\Big) \,. \tag{2.5}$$

The Mathematica package `REAP` [108] features both the RGE running of these couplings as well as the automatic decoupling of the right-handed neutrinos at their threshold in the SM and the MSSM. For solving the RGEs of the Yukawa couplings and the gauge couplings at the two-loop level, we have rewritten `REAP` in `C++` to speed up the calculations. The RGEs themselves are coupled non-linear differential equations of the Yukawa couplings Y_x and gauge couplings g_i that take the general form

$$\frac{\mathrm{d}Y_x}{\mathrm{d}\log\bar{\mu}} = \beta_{Y_x} \,, \qquad \frac{\mathrm{d}g_i}{\mathrm{d}\log\bar{\mu}} = \beta_{g_i} \,, \tag{2.6}$$

where the beta functions β_{Y_x} and β_{g_i} are polynomials in Y_x and g_i. Our template-based implementation uses the libraries `odeint` [109] and `eigen3` [110]. On a desktop machine (i5, 3.3 GHz), the `C++` version is a hundred times faster than the Mathematica version making the time consuming computations of this analysis feasible. A generalised version of the code is planned to be publicly available [111].

A NOTE ON FERMION OBSERVABLES. At this point it should be clarified what the expression *fermion observables* means. In the SM, U(3) flavour rotations can be applied to the quark fields in the Lagrangian of eq. (1.15) by

$$u_{R,i} \to U_{ij}^{R,\dagger}\, u_{R,j} \,, \qquad Q_i \to U_{ij}^{L,\dagger}\, Q_j \,, \qquad d_{R,i} \to D_{ij}^{R,\dagger}\, d_{R,j} \,, \tag{2.7}$$

if at the same time the Yukawa matrices, Y_u and Y_d, are rotated as

$$Y_u \to U_R^\dagger\, Y_u\, U_L \,, \qquad Y_d \to D_R^\dagger\, Y_d\, U_L \,. \tag{2.8}$$

Hence the Yukawa matrices are not physical observables since they depend on the flavour basis that is chosen. Eq. (2.8) allows to choose one Yukawa matrix diagonal applying singular value decomposition. For Y_u that is

$$Y_u \to U_R^\dagger\, Y_u\, U_L = \mathrm{diag}(y_u, y_c, y_t) \,, \tag{2.9}$$

Matrices of the form $Y^\dagger Y$ and $YY^\dagger$ are hermitian and therefore can be diagnalised with unitary rotations.

by choosing U_L and U_R such that

$$U_L^\dagger\, Y_u^\dagger Y_u\, U_L = \mathrm{diag}\left(|y_u|^2, |y_c|^2, |y_t|^2\right) = U_R^\dagger\, Y_u Y_u^\dagger\, U_R\,. \tag{2.10}$$

The same procedure can not be applied to Y_d, however, since only one rotation, namely D_R, remains to be chosen. Yet we can introduce another unitary matrix D_L demanding that

$$Y_d \to D_R^\dagger\, Y_d\, U_L = D_R^\dagger\, Y_d\, D_L D_L^\dagger\, U_L \tag{2.11}$$

$$= \mathrm{diag}(y_d, y_s, y_b)\, D_L^\dagger U_L\,. \tag{2.12}$$

The unitary Cabibbo-Kobayashi-Maskawa (CKM)-matrix [112, 113] $V_{\mathrm{CKM}} = D_L^\dagger U_L$ describes the misalignement between Y_d and Y_u in the flavour basis where either of them is diagonal. V_{CKM} appears in the coupling of the $W^\pm$ bosons to quarks and can be parametrised by three mixing angles θ_{12}^q, θ_{13}^q, θ_{23}^q and one CP phase δ_{CP}^q. Other phases can be absorbed into the phases of the quark fields. Together with the six singular values of Y_u and Y_d, the four CKM parameters are the physisal observables of the quark Yukawa sector.

A similar procedure can be applied in the lepton sector. The rotations

$$e_{R,i} \to E_{ij}^{R,\dagger}\, e_{R,j}\,, \qquad L_i \to E_{ij}^{L,\dagger}\, L_j, \tag{2.13}$$

are sufficient to diagonalise

$$Y_e \to E_R^\dagger\, Y_e\, E_L = \mathrm{diag}(y_e, y_\mu, y_\tau)\,. \tag{2.14}$$

In the SM, the neutrinos are massless and there is no lepton flavour violation. However, in the presence of the Weinberg operator a neutrino mass is generated after EWSB by $m_\nu = -v^2\,\kappa/2$. Applying the flavour rotation to m_ν gives

$$m_\nu \to m_\nu' = E_L^T\, m_\nu\, E_L\,. \tag{2.15}$$

By construction, m_ν' is a complex symmetric matrix which can be diagonalised by

$$V_{\mathrm{PMNS}}^T\, m_\nu'\, V_{\mathrm{PMNS}} = \mathrm{diag}(m_1, m_2, m_3)\,. \tag{2.16}$$

In addition to the mixing angles θ_{12}^l, θ_{13}^l, θ_{23}^l and the CP phase δ_{CP}^l, the Pontecorvo–Maki–Nakagawa–Sakata (PMNS) matrix V_{PMNS} has additional phases that might be physical. But neither of them nor the absolute mass of the neutrinos has been measured yet. Neutrino oscillation experiments are only sensitive to their mass squared differences $\Delta m_{ij}^2 = m_i^2 - m_j^2$. Altogether there are three singular values of Y_e, two mass squared differences and the elements of V_{PMNS} as observables in the lepton sector.

For extracting the mixing angles and the phases from the Yukawa matrices and the neutrino mass matrix we have also implemented the routines of `REAP` in `C++` using the `eigen3` library for the singular value decomposition. The algorithms are described in the `REAP` manual [108].

obs.	input value	input scheme	ref.	value at $\bar{\mu} = M_Z$
m_u	2.36(24) MeV	$\bar{\mu} = 2\,\text{GeV}$	[91, 114]	1.36(15) MeV
m_d	5.03(26) MeV	$\bar{\mu} = 2\,\text{GeV}$	[91, 114]	2.90(11) MeV
m_s	93.9(1.1) MeV	$\bar{\mu} = 2\,\text{GeV}$	[91, 114, 115]	54.05(63) MeV
m_c	996(25) MeV	$\bar{\mu} = 3\,\text{GeV}$	[91, 114, 115]	635(16) MeV
m_b	4.190(21) GeV	$\overline{m}_b(\overline{m}_b)$	[91, 115, 116]	2.866(14) GeV
α_s	0.1182(12)	$\alpha_s^{(5)}(M_Z)$	[91, 115–119]	0.1170(12)
m_t	174.2(1.4) GeV	pole	[120]	172.3(1.5) GeV

Table 2.1: **Used input data and values at $\bar{\mu} = M_Z$ for the quark masses and α_s.** All values in the right column are given in the $\overline{\text{MS}}$ scheme at $M_Z = 91.1876\,\text{GeV}$ with six active flavours. Conversions of the renormalisation scheme have been applied where necessary.

2.1.1 *Running the light quark masses to the EW scale*

Since the masses of the light quarks are set in the energy range where QCD cannot be treated perturbatively their determination depends on non-perturbative techniques. In the recent years, the precision that can be achieved with lattice gauge theory has significantly improved.

The $N_f = 2+1+1$ combination from reference [91] summarises these results and gives averages for masses of the five light quark flavours and the strong coupling α_s. The QCD running of the quark masses and α_s as well as the transition between the various flavour schemes is performed with the Mathematica package `RunDec` [121] at four-loops accuracy. Table 2.1 gives the input values from [91] and [120] together with the results we obtain at $M_Z = 91.1876\,\text{GeV}$ [120] in the six flavour $\overline{\text{MS}}$ scheme. In all cases the errors from variation of the decoupling scales are negligible compared to the experimental uncertainty.

2.1.2 *Extrapolating the SM parameters to higher scales*

Above M_Z it is more appropriate to consider the RGE running of the Yukawa matrices rather than that of the fermion masses. As we have discussed at the beginning of this section, the singular values of the Yukawa matrices are given at the EW scale by the fermion masses m_i via $y_i = m_i/v$. Choosing Y_u und Y_e diagonal, Y_d is given by $\text{diag}(y_d, y_s, y_b)\, V_{\text{CKM}}$. The global fit of the CKM matrix V_{CKM} by the CKMfitter group [92, 122–161] was updated at the ICHEP conference 2016. Translating their results from the Wolfenstein parametrisation [162] into that of the PDG [120] yields the values of the CKM parameters $\theta_{12}^q, \theta_{13}^q, \theta_{23}^q, \delta_{\text{CP}}^q$. Furthermore, the electro-weak gauge couplings $g_1 = \sqrt{3/5} g_Y$ and g_2 as well as the lepton Yukawa couplings are taken

from [163]. All data at M_Z can be found in Table 2.2 together with the extrapolated values at 1 TeV, 3 TeV and 10 TeV, respectively.

This procedure can simply be put as applying Bayes' theorem with a normal distribution as prior.

For the propagation of errors, normally distributed random numbers are generated at M_Z. Each sample point is run up to the respective energy scale. Then a normal distribution is fitted to the set of sample points. That way, the relative errors of the observables increases during running due to the uncertainty of the other observables, mostly the top Yukawa coupling.

In addition to the observables in Table 2.2, the SM Higgs quartic coupling is needed for the two-loop running of the Yukawa couplings. It can be extracted from the Higgs mass measurement [120] via $\lambda = m_{\text{Higgs}}^2/v^2$.

2.1.3 *Matching the SM to the MSSM*

As we have mentioned before, the matching between the SM and the MSSM is performed at the scale of 1 TeV. In the supersymmetric phase of the theory the $\overline{\text{DR}}$ scheme is adopted. The finite shift between the $\overline{\text{MS}}$ and $\overline{\text{DR}}$ scheme for the Yukawa couplings and gauge couplings g_i are [164]

$C(G) = N$ and $C(r) = (N^2-1)/2N$ for $SU(N)$.

$$g_i^{\overline{\text{MS}}} = g_i^{\overline{\text{DR}}}\left(1 - \frac{g_i^2}{96\,\pi^2}\,C(G)\right), \tag{2.17}$$

$$Y_u^{\overline{\text{MS}}} = Y_u^{\overline{\text{DR}}}\left(1 + \frac{1}{32\,\pi^2}\left(-\frac{g_1^2}{60} - \frac{3\,g_2^2}{4} + \frac{8\,g_3^2}{3}\right)\right), \tag{2.18}$$

$$Y_d^{\overline{\text{MS}}} = Y_d^{\overline{\text{DR}}}\left(1 + \frac{1}{32\,\pi^2}\left(-\frac{13\,g_1^2}{60} - \frac{3\,g_2^2}{4} + \frac{8\,g_3^2}{3}\right)\right), \tag{2.19}$$

$$Y_e^{\overline{\text{MS}}} = Y_e^{\overline{\text{DR}}}\left(1 + \frac{1}{32\,\pi^2}\left(\frac{9\,g_1^2}{20} - \frac{3\,g_2^2}{4}\right)\right). \tag{2.20}$$

Table 2.3 shows all results from Table 2.2 converted to the $\overline{\text{DR}}$ scheme.

Moreover, the MSSM Yukawa couplings also depend on $\tan\beta$. Besides, there are additional one-loop TCs from SUSY particles, in particular those which scale with $\tan\beta$: They can lead to changes of $\mathcal{O}(10\%)$ in the Yukawa couplings and hence have a large impact on Yukawa unification in GUTs [59, 84, 165–170]. We introduce three parameters $\epsilon_q, \epsilon_b, \epsilon_l$ that encode these corrections to the Yukawa matrices. The

	M_Z	1 TeV	3 TeV	10 TeV
g_1	$0.461425^{+0.000044}_{-0000043}$	0.467773 ± 0.000045	0.470766 ± 0.000046	0.474109 ± 0.000047
g_2	$0.65184^{+0.00018}_{-0.00017}$	0.63935 ± 0.00016	0.63383 ± 0.00016	0.62792 ± 0.00016
g_3	1.2127 ± 0.0061	1.0549 ± 0.0040	1.0009 ± 0.0034	0.9503 ± 0.0029
$y_u/10^{-6}$	7.80 ± 0.86	6.73 ± 0.74	6.37 ± 0.70	6.03 ± 0.66
$y_c/10^{-3}$	3.646 ± 0.091	3.147 ± 0.79	2.976 ± 0.074	2.816 ± 0.071
y_t	0.9897 ± 0.0086	0.8723 ± 0.0088	0.8317 ± 0.0088	0.7934 ± 0.0089
$y_d/10^{-5}$	1.663 ± 0.064	1.438 ± 0.056	1.361 ± 0.053	1.289 ± 0.050
$y_s/10^{-4}$	3.104 ± 0.036	2.685 ± 0.032	2.541 ± 0.030	2.407 ± 0.029
$y_b/10^{-2}$	1.646 ± 0.0082	1.3940 ± 0.0079	1.3091 ± 0.0071	1.2303 ± 0.0070
$y_e/10^{-6}$	$2.794745^{+0.000015}_{-0.000016}$	2.8491 ± 0.0022	2.8659 ± 0.0031	2.8800 ± 0.0040
$y_\mu/10^{-4}$	$5.899863^{+0.000019}_{-0.000018}$	6.0146 ± 0.0046	6.0501 ± 0.0065	6.080 ± 0.0086
$y_\tau/10^{-2}$	$1.002950^{+0.000090}_{-0.000091}$	1.02246 ± 0.00078	1.0285 ± 0.0011	1.0336 ± 0.0014
θ^q_{12}	$0.22704^{+0.00030}_{-0.00029}$	0.22704 ± 0.00029	0.22704 ± 0.00029	0.22705 ± 0.00029
$\theta^q_{13}/10^{-3}$	$3.71^{+0.13}_{-0.14}$	3.79 ± 0.14	3.82 ± 0.14	3.85 ± 0.14
$\theta^q_{23}/10^{-2}$	$4.181^{+0.047}_{-0.067}$	4.270 ± 0.058	4.303 ± 0.058	4.337 ± 0.059
$\delta^q_{\rm CP}$	$1.143^{+0.011}_{-0.011}$	1.143 ± 0.011	1.143 ± 0.011	1.143 ± 0.011

Table 2.2: **SM parameters in the $\overline{\rm MS}$ scheme at M_Z, 1 TeV, 3 TeV and 10 TeV.**

	M_Z	1 TeV	3 TeV	10 TeV
g_1	$0.461425^{+0.000044}_{-0000043}$	0.467773 ± 0.000045	0.470766 ± 0.000046	0.474109 ± 0.000047
g_2	0.65243 ± 0.00018	0.63990 ± 0.00017	0.63437 ± 0.00016	0.62844 ± 0.00016
g_3	1.2185 ± 0.0062	1.0587 ± 0.0040	1.00415 ± 0.0034	0.9530 ± 0.0029
$y_u/10^{-6}$	7.71 ± 0.85	6.68 ± 0.74	6.32 ± 0.70	5.99 ± 0.66
$y_c/10^{-3}$	3.60 ± 0.090	3.120 ± 0.078	2.954 ± 0.074	2.797 ± 0.071
y_t	0.9785 ± 0.0086	0.8651 ± 0.0087	0.8255 ± 0.0087	0.7881 ± 0.0088
$y_d/10^{-5}$	1.64441 ± 0.064	1.426 ± 0.056	1.351 ± 0.053	1.281 ± 0.050
$y_s/10^{-4}$	3.06979 ± 0.036	2.663 ± 0.032	2.523 ± 0.030	2.392 ± 0.029
$y_b/10^{-2}$	1.6274 ± 0.0082	1.3825 ± 0.0073	1.2995 ± 0.0071	1.2224 ± 0.0070
$y_e/10^{-6}$	2.796719 ± 0.000016	2.8510 ± 0.0022	2.8677 ± 0.0031	2.8818 ± 0.0041
$y_\mu/10^{-4}$	5.904029 ± 0.000019	6.0186 ± 0.0046	6.0540 ± 0.0065	6.0836 ± 0.0086
$y_\tau/10^{-2}$	1.003658 ± 0.000091	1.0231 ± 0.0078	1.0292 ± 0.0011	1.0342 ± 0.0015
θ^q_{12}	$0.22704^{+0.00030}_{-0.00029}$	0.22704 ± 0.00029	0.22704 ± 0.00029	0.22705 ± 0.00029
$\theta^q_{13}/10^{-3}$	$3.71^{+0.13}_{-0.14}$	3.79 ± 0.14	3.82 ± 0.14	3.85 ± 0.14
$\theta^q_{23}/10^{-2}$	$4.181^{+0.047}_{-0.067}$	4.270 ± 0.058	4.303 ± 0.058	4.337 ± 0.059
$\delta^q_{\rm CP}$	$1.143^{+0.011}_{-0.011}$	1.143 ± 0.011	1.143 ± 0.011	1.143 ± 0.011

Table 2.3: **SM parameters in the $\overline{\rm DR}$ scheme at M_Z, 1 TeV, 3 TeV and 10 TeV.**

matching between the SM and the MSSM is described in the $\overline{\text{DR}}$ scheme by

$$Y_u^{\text{SM}} = \sin\beta \; Y_u^{\text{MSSM}} \,, \tag{2.21}$$

$$Y_e^{\text{SM}} = \cos\beta \, (1 + \epsilon_l \tan\beta) \; Y_e^{\text{MSSM}} \,, \tag{2.22}$$

$$Y_d^{\text{SM}} = \cos\beta \, \text{diag}\left(1 + \epsilon_q \tan\beta, 1 + \epsilon_q \tan\beta, 1 + \epsilon_b \tan\beta\right) \; Y_d^{\text{MSSM}} \,. \tag{2.23}$$

The parametrisation is valid provided that the squark mass matrices are nearly degenerate with small off-diagonal elements and the trilinear scalar couplings are hierarchical with dominant third generation elements [163, 171–173]. Note that the TCs do not decouple for large values of M_{SUSY} but rather depend on ratios of the SUSY parameters. This allows us to study the influence of SUSY corrections without being specific about the actual SUSY spectrum. In the fit we allow for the following ranges

$$-0.05 \leq \epsilon_q \leq 0.05 \,, \tag{2.24}$$

$$-0.10 \leq \epsilon_b \leq 0.10 \,, \tag{2.25}$$

$$-0.03 \leq \epsilon_l \leq 0.03 \,. \tag{2.26}$$

Note that ϵ_l stems from electro-weak one-loop corrections whereas ϵ_q and ϵ_b also receive contributions from QCD. That is why the absolut values of the latter ones are allowed to be larger. ϵ_b additionally can be enhanced by soft trilinear couplings of the bottom squarks. For the up-type quarks there we ignore such corrections since corresponding contributions scale with $\cot\beta$ and are hence suppressed.

2.1.4 *Determining the GUT scale*

For the MSSM running of the gauge and Yukawa couplings two-loop RGEs are used. We first determine the GUT scale by minimising the squared differences of the gauge couplings. Neglecting the SUSY TCs we find $M_{\text{GUT}} = 1.35 \times 10^{16}$ and

$$g_1 = 0.706 \,, \qquad g_2 = 0.708 \,, \qquad g_3 = 0.705 \,, \tag{2.27}$$

at M_{GUT}. Since the influence of the Yukawa couplings on the gauge couplings is a very small two-loop effect we keep the GUT scale and the gauge couplings at M_{GUT} fixed in all fits to GUT parameters.

2.1.5 *Matching SO(10) to the MSSM*

In the minimal SO(10) setup discussed in the beginning of this chapter, the MSSM Yukawa matrices are set by the GUT Yukawa matrices, see for instance [58, 59, 90, 174, 175]

The factor of 3 in front of Y_{126} is a Clebsch-Gordan coefficient of SO(10).

$$Y_u = r\,(Y_{10} + s\,Y_{126})\,, \tag{2.28}$$
$$Y_d = Y_{10} + Y_{126}\,, \tag{2.29}$$
$$Y_\nu = r\,(Y_{10} - 3\,s\,Y_{126})\,, \tag{2.30}$$
$$Y_e = Y_{10} - 3\,Y_{126}\,, \tag{2.31}$$
$$M = r_R\,Y_{126}\,. \tag{2.32}$$

The mixing of the Higgs doublets from the GUT representations into the MSSM Higgs doublets H_1 and H_2 is described by the complex parameter s. The parameters r and r_R denote ratios of VEVs of the GUT Higgs fields that can be chosen real. r_R also sets the see-saw scale by giving a Majorana mass M to the right-handed neutrinos. A flavour rotation of the GUT fields (i. e. of $\mathbf{16}_i$) allows to choose Y_{10} real and diagonal. From the tensor structure of SO(10) follows that Y_{126} is a complex symmetric matrix. In this setup, there are altogether 19 real parameters that determine the MSSM Yukawa matrices at the GUT scale: r (one parameter), r_R (one parameter), s (two parameters), Y_{10} (three parameters), Y_{126} (twelve parameters).

2.1.6 *Decoupling of the right-handed neutrinos*

When solving the RGEs for the MSSM with additional singlets from M_{GUT} to M_{SUSY} one comes across the thresholds where the heavy right-handed neutrinos N_i need to be integrated out. The procedure is described in great detail in [176] and can be sketched as follows: The thresholds are determined from the eigenvalues of M. At each threshold M_n the Wilson coefficient of the Weinberg operator κ receives a contribution from the Yukawa coupling Y_ν

$$\overset{(n)}{\kappa}_{ij} = \overset{(n+1)}{\kappa}_{ij} + 2\left(\overset{(n+1)}{Y}_\nu{}^{T}\right)_{in} M_n^{-1} \left(\overset{(n+1)}{Y}_\nu\right)_{nj}\,, \tag{2.33}$$

The equation holds in a flavour basis where M is diagonal and at the renormalisation scale $\bar{\mu} = M_n$.

with no sum over n and flavour indices i, j, where $\overset{(n)}{\kappa}$ stands for the matrix κ with the last n rows deleted. After EWSB κ generates the masses for the left-handed neutrinos. As a result of the see-saw mechanism these masses are suppressed by M_n.

2.1.7 *Fitting the GUT parameters to the experimental data*

It is convenient to perform the global fit at M_{SUSY} treating the SM fermion observables as experimental data to compare the GUT prediction with.

The 19 GUT parameters from Section 2.1.5 give the input for the MSSM Yukawa matrices and M, which are evolved to $M_{\text{SUSY}} = 1$ TeV. Note thatM_{SUSY} is a matching scale and not necessarily the mass scale of SUSY particles.The SM model Yukawa couplings are determined according to eqs. (2.21)-(2.23). The TCs ϵ_q, ϵ_b, ϵ_l give three additional

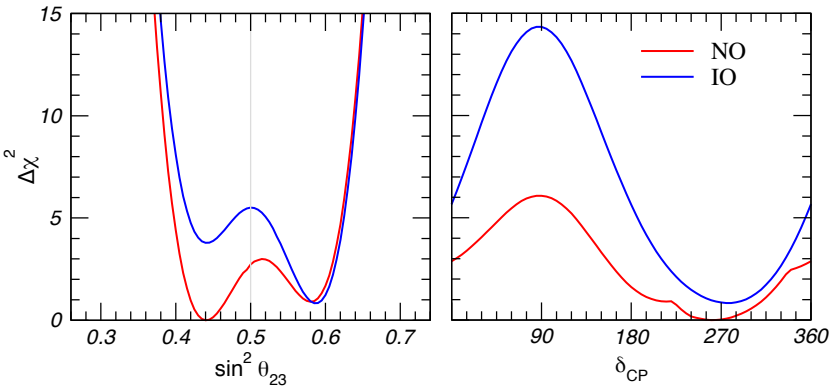

Figure 2.3: $\Delta\chi^2$ distribution of the atmospheric mixing angle θ_{23} and the CP phase δ_{CP} in degrees. The plots are taken from `NuFit3.0` [93].

input parameters for the fit. The fermion observables are extracted as described at the beginning of this section.

For the comparison of the GUT prediction with the experimental data a χ^2 function is defined by

$$\chi^2 = \sum_{i=1}^{15} \left(\frac{\mathcal{O}_i^{\text{theo}} - \mathcal{O}_i^{\text{exp}}}{\sigma_i} \right)^2 + \sum_{i=1}^{4} \chi^2_{\text{PMNS},i} \,. \tag{2.34}$$

The experimental uncertainties, σ_i, of the 15 observables $\mathcal{O}_i$ are assumed to be Gaussian. Firstly, these are the quark and charged lepton Yukawa couplings y_i (nine observables) and the CKM parameters (four observables), whose extrapolated values at 1 TeV can be found in Table 2.3. Secondly, one has the neutrino mass squared differences (two observables). The data from the global analysis of `NuFit3.0` [93, 177–192] also depend on the mass ordering, in case of normal neutrino mass ordering

$$\Delta m^2_{21} = (7.50 \pm 0.18) \times 10^{-5}\,\text{eV}^2 \,, \tag{2.35}$$

$$\Delta m^2_{31} = (2.524 \pm 0.0395) \times 10^{-3}\,\text{eV}^2 \,. \tag{2.36}$$

For the PMNS parameters (four observables) the one-dimensional χ^2 distributions from `NuFit3.0` are included (depending on the respective mass ordering). The reason is that the uncertainties of the PMNS parameters are not Gaussian but rather exhibit more complicated likelihood profiles. Figure 2.3 shows the $\Delta\chi^2$ distribution of the atmospheric mixing angle θ^l_{23} with two competing minima together with the $\Delta\chi^2$ distribution of the CP phase δ^l_{CP} which—although it has not been measured yet—prefers values between 180° and 360°.

The χ^2 function is minimised by varying the 19 input parameters (22 with TCs) to fit the 19 experimental observables. The minimisation is performed with the `Sbplx/Subplex` [193] and `ISRES` algorithms [194, 195] from the `C++` implementation of the `NLopt2.4.2` library [196].

2.2 RESULTS OF THE GLOBAL MINIMISATION

A NOTE ON YUKAWA UNIFICATION. Before discussing the results of the global analysis, let us illustrate the challenge for the Yukawa sector that arises from SO(10) grand unification. We will do so by making some rough estimates in order to understand the numerical results later on. From eqs. (2.28)-(2.31) follows that the third generation Yukawa couplings at the GUT scale are, neglecting mixing to other generations,

$$y_t = r\,(Y_{10}^{33} + s\,Y_{126}^{33})\,, \tag{2.37}$$
$$y_b = Y_{10}^{33} + Y_{126}^{33}\,, \tag{2.38}$$
$$y_\tau = Y_{10}^{33} - 3\,Y_{126}^{33}\,. \tag{2.39}$$

Assuming r and s to be of order one, we have $y_t \approx y_b$ at M_{GUT}, implicating that $\tan\beta \approx m_t/m_b \approx 60$. Realistically, the ratio can be smaller than 60, as y_t decreases and y_b increases between M_Z and M_{GUT} due to RGE effects. Nevertheless, *bottom-top unification* will prefer values of $\tan\beta$ of the order of ten and larger. For smaller values of $\tan\beta$ the mass hierarchy between the top and bottom quark must stem from r and/or s.

Note that the two parameters r and s are universal for all three generations, the respective hierarchy between up-type quarks and down-type quarks, howewer, is not ($m_c/m_s \approx 10$ and $m_u/m_d \approx 0.5$). In that case, there must be cancellations between the matrix elements of Y_{10} and Y_{126} in order to reproduce the hierarchy between up-type and down-type quark masses correctly in all generations.

Furthermore, the third generation Yukawa couplings also affect the mixing between the second and third generation of fermions. It has been noticed that a large atmospheric mixing angle θ_{23}^l demands $y_\tau = y_b$ at M_{GUT} [197], neglecting SUSY TCs. This fact gives rise to another constraint on the Yukawa sector which will be commented later on in Section 2.2.3.

The same discussion can be continued for the second and first generation. Nevertheless, due to hierarchical structure of the Yukawa matrices, a tension in the observables related to the third (second) generation cannot necessarily be resolved by tuning the parameters related to the second (first) generation.

2.2.1 *Discussion of the global minima*

In the global minimisation $\tan\beta$ is not treated as a free parameter but its value is rather kept fixed to $\tan\beta = 10\,, 38\,, 50$, respectively, to ensure numerical stability. These particular values are merely chosen for historical reasons, see e. g. [90]. The minimisation of the χ^2 function is performed both with and without including SUSY TCs in the fit. Thus,

		without TC			with TC		
	$\tan\beta$	10	38	50	10	38	50
	χ^2	127.0	94.69	75.43	40.37	1.74	3.71
pull	y_u	0.19	0.29	0.12	0.01	0.25	-0.17
	y_c	2.73	2.71	2.44	1.66	0.19	0.11
	y_t	-2.06	-2.01	-1.85	-1.26	-0.35	0.06
	y_d	-7.42	-8.08	-6.30	-4.53	0.82	1.26
	y_s	0.90	2.12	1.17	-0.12	-0.17	-0.42
	y_b	-0.36	-0.55	0.39	-0.22	-0.04	-0.15
	θ^q_{12}	0.62	0.45	0.38	0.11	-0.05	-0.08
	θ^q_{13}	-0.71	-1.03	-0.42	2.81	0.35	-0.11
	θ^q_{23}	-0.38	-0.58	0.40	-1.61	0.52	-0.49
	δ^q_{CP}	1.51	0.64	0.77	0.38	-0.12	-0.16
	y_e	0.01	0.01	0.04	0.17	-0.08	-0.04
	y_μ	-0.30	-0.73	-0.33	0.28	-0.15	0.04
	y_τ	0.42	0.14	0.19	0.30	-0.17	0.00
	Δm^2_{21}	0.81	0.17	0.49	-0.30	-0.05	0.03
	Δm^2_{32}	-0.25	-0.11	-0.31	0.19	0.03	-0.02
	θ^l_{12}	-1.30	-0.45	-0.87	-1.07	-0.02	-0.01
	θ^l_{13}	-4.13	-0.40	-0.93	0.72	0.00	-0.04
	θ^l_{23}	-5.74	-2.67	-4.29	-0.48	0.18	-0.26
	δ^l_{CP}	-1.83	-1.73	-1.78	1.61	0.56	1.24
best-fit values	$m_{\nu,1}$ in meV	2.4	2.6	2.4	1.8	2.4	2.0
	$m_{\nu,2}$ in meV	9.1	9.1	9.0	8.8	9.0	8.9
	$m_{\nu,3}$ in meV	50.2	50.3	50.2	50.3	50.3	50.3
	$\epsilon_q/10^{-2}$	–	–	–	5.00	2.80	4.72
	$\epsilon_b/10^{-2}$	–	–	–	-7.35	-4.06	-0.60
	$\epsilon_l/10^{-2}$	–	–	–	-3.00	-0.60	0.13

Table 2.4: **Best-fit points of the global minimisation.** The table shows the minimal χ^2, the corresponding pulls of the observables in the $\overline{\mathrm{DR}}$ scheme for different values of $\tan\beta$ as well as the best-fit values for the light neutrino masses and SUSY threshold corrections (TC) if included in the fit.

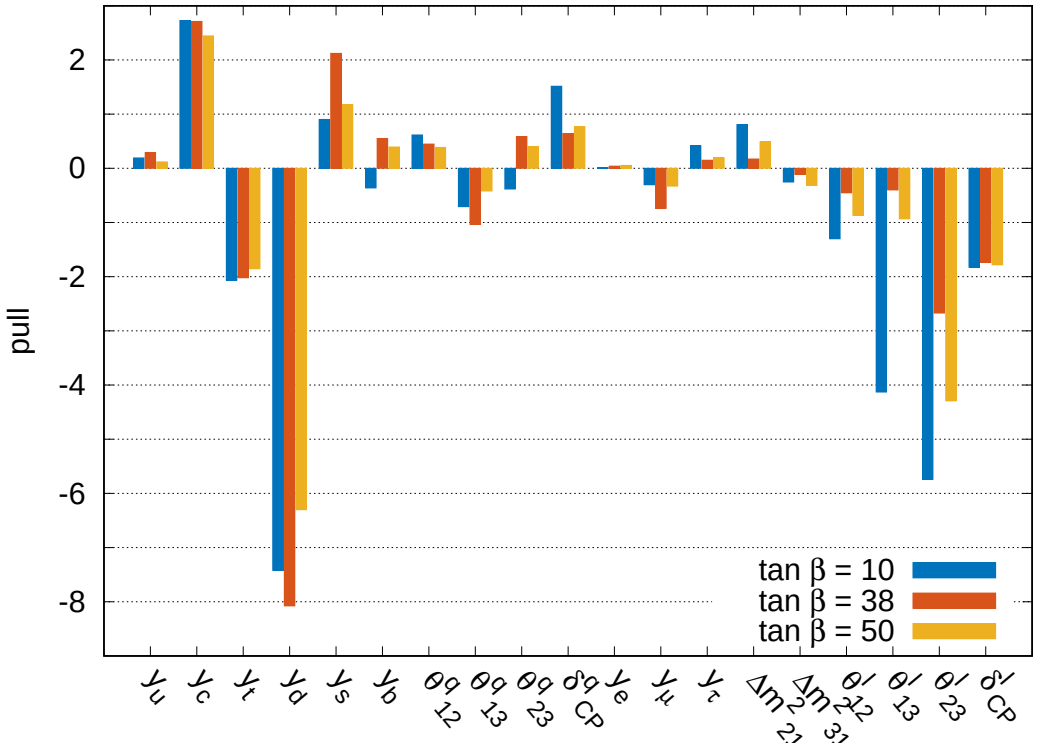

(a) Pulls for the global minima without SUSY threshold corrections.

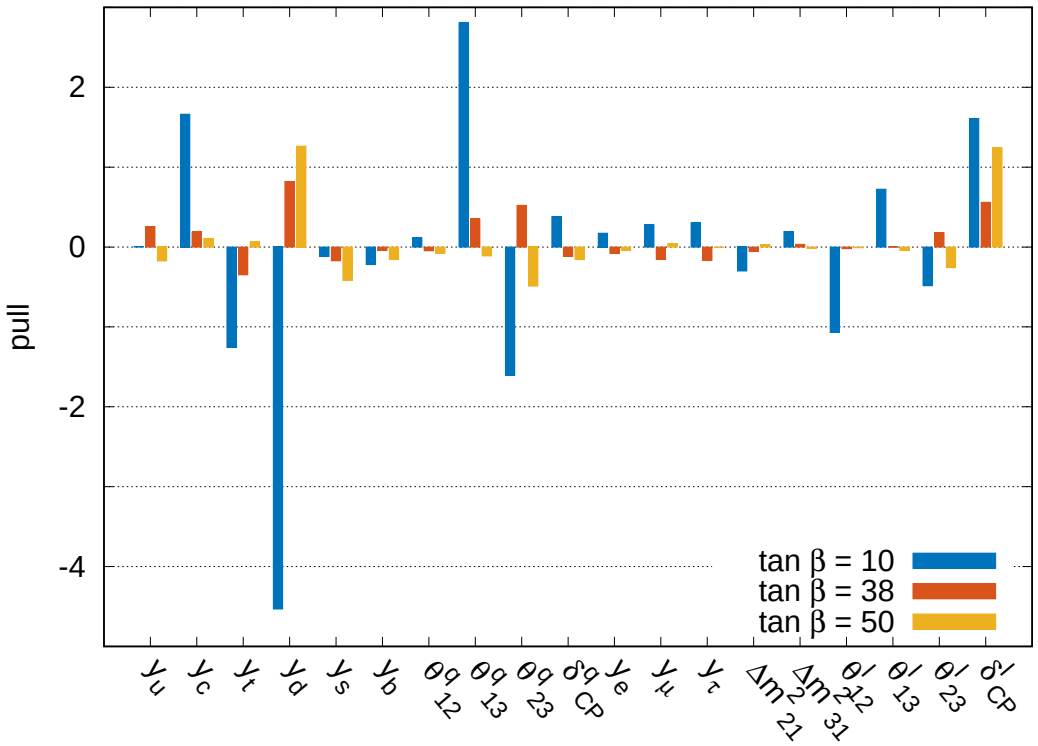

(b) Pulls for the global minima including SUSY threshold corrections.

Figure 2.4: **Pulls of all global minima.** The minimisation is performed separately for $\tan\beta = 10, 38, 50$ both including and neglecting SUSY threshold corrections.

there are, in total, six global minima (best-fit points) which will be discussed in the following.

The pulls of the Gaussian observables in eq. (2.34) are defined by

$$\text{pull}_i = \frac{\mathcal{O}_i^{\text{theo}} - \mathcal{O}_i^{\text{exp}}}{\sigma_i} \,. \tag{2.40}$$

For the PMNS parameters the χ^2_{PMNS}-distributions and the best-fit values $\mathcal{O}_i^{\text{best-fit}}$ of `NuFit3.0` are employed to define the pull as

$$\text{pull}_i = \text{sign}\left(\mathcal{O}_i^{\text{theo}} - \mathcal{O}_i^{\text{best-fit}}\right) \sqrt{\chi^2_{\text{PMNS,i}}} \,. \tag{2.41}$$

The pulls of all observables for the six global minima are given in Table 2.4 and visualised as bar charts in Figure 2.4. The input parameters at the GUT scale are listed in Appendix A.2 for all six global minima.

THE CASE WITHOUT SUSY THRESHOLD CORRECTIONS. If SUSY TCs are not included in the fit one finds a poor description of the fermion data, indicated by minimal χ^2 values of $75 \ldots 127$. This holds for all values of $\tan\beta$, although the tensions become smaller for larger $\tan\beta$. The largest pulls ($> 6\sigma$) are found in the down-quark Yukawa coupling y_d. Note that, opposite to the second and third generation, in the first generation, the down-type quark is heavier than the up-type quark posing a challenge on Yukawa unification. The tension in y_d has already been seen in previous analyses [89, 90] albeit then it has been less severe. It can directly be traced back to the improved precision of lattice calculations [91]. Similar observations can be made concerning the atmospheric mixing angle θ_{23}^l where the experimental uncertainty has been reduced compared to data used in former analyses.

For a statistical interpretation of the χ^2 function, one has to consider the degress of freedom in the fit. Given the fact that there are as many parameters as there are observables, the number of degrees of freedom is actually zero. Naively, one would therefore expect a perfect fit, i. e. $\chi^2 = 0$. As we have argued at the beginning of this section, the input parameters do not influence all observables alike due to the non-linearity of the problem (numerical integration and singular value decomposition) and the hierarchical structure of the Yukawa matrices. Still, the χ^2 function and the pulls of the various observables provide useful information for a qualitative discussion of the results.

THE CASE WITH SUSY THRESHOLD CORRECTIONS. Allowing for the $\tan\beta$ enhanced threshold corrections, the minimal χ^2 values significantly decrease for all values of $\tan\beta$. One should keep in mind that the TCs get multiplied by $\tan\beta$. For $\tan\beta = 10$, the combintation of $\epsilon_{q,b,l} \tan\beta$ is absolutely smaller than for $\tan\beta = 38$ and 50. These correction are in turn not as able to resolve the tensions encountered without TCs.

For $\tan\beta = 10$, one again finds large tensions in the down-quark Yukawa coupling y_d ($> 4\sigma$) and the quark mixing angle θ_{13}^q ($> 2\sigma$). In addition to the pulls, Table 2.4 also shows the respective best-fit values of the threshold corrections ϵ_q, ϵ_b and ϵ_l. For $\tan\beta = 10$, some of them lie on the borders of the allowed ranges, namely $\epsilon_q = 0.05$ and $\epsilon_l = -0.03$. This fact indicates that the goodness of fit would improve if the allowed ranges for ϵ_q and ϵ_l were larger and TCs had a larger impact. Overall, for $\tan\beta = 10$ the minimal model can hardly reproduce the fermion data.

The best fit in all our studies is obtained for $\tan\beta = 38$, with $\chi^2 = 1.74$. For this best-fit point we only find slight pulls in the down-quark yukawa coupling y_d and in the CP phase of the PMNS matrix, δ_{CP}^l. It has already been noticed in reference [88], that SO(10) grand unification has a predictive power for δ_{CP}^l. This fact will be important if, in the future, the CP phase is known precisely.

For $\tan\beta = 50$, the best-fit point has $\chi^2 = 3.71$. Again there are slight pulls in y_d and δ_{CP}^l making the overall picture quite similar to that for $\tan\beta = 38$.

For all values of $\tan\beta$ we find a preference for positive ϵ_q and negative ϵ_b. This means that the predicted value from the GUT is enhanced for y_b, whereas it is reduced in the case of y_d and y_s. ϵ_l, does not have a distinct preference for its sign. This observation is confirmed by the likelihood profiles for ϵ_b, ϵ_q and ϵ_l in Section 2.2.2.

ADDITIONAL CONSTRAINS AND PREDICTIONS. Although the fit can only account for the mass squared differences of the neutrinos, the model actually predicts the absolute neutrino mass scale. The neutrino masses for the respective best-fit points are listed in Table 2.4. In all cases the masses are hierarchical with normal mass ordering, which is caused by the hierarchical structure of the Yukawa matrices. The neutrinos have a typical mass of 2, 9, 50 meV, rather independent of $\tan\beta$ and TCs. Their sum is in all cases below bounds from cosmology [198]

$$\sum_{i=1}^{3} m_{\nu,i} < 0.23\,\mathrm{eV}\,. \tag{2.42}$$

The effective β-decay masses are also below the current bound from the Troitsk experiment [23]

$$m_{\nu,\beta}^2 = \sum_{i=1}^{3} |V_{ei}^l|^2 m_{\nu,i}^2 < 2.05\,\mathrm{eV}\,, \tag{2.43}$$

and below the expected sensitivity of the KATRIN [199] experiment.

2.2.2 *Likelihood profiles for threshold corrections*

The global analysis of Section 2.2.1 has shown the importance of $\tan\beta$ enhanced threshold corrections. Since they may have important

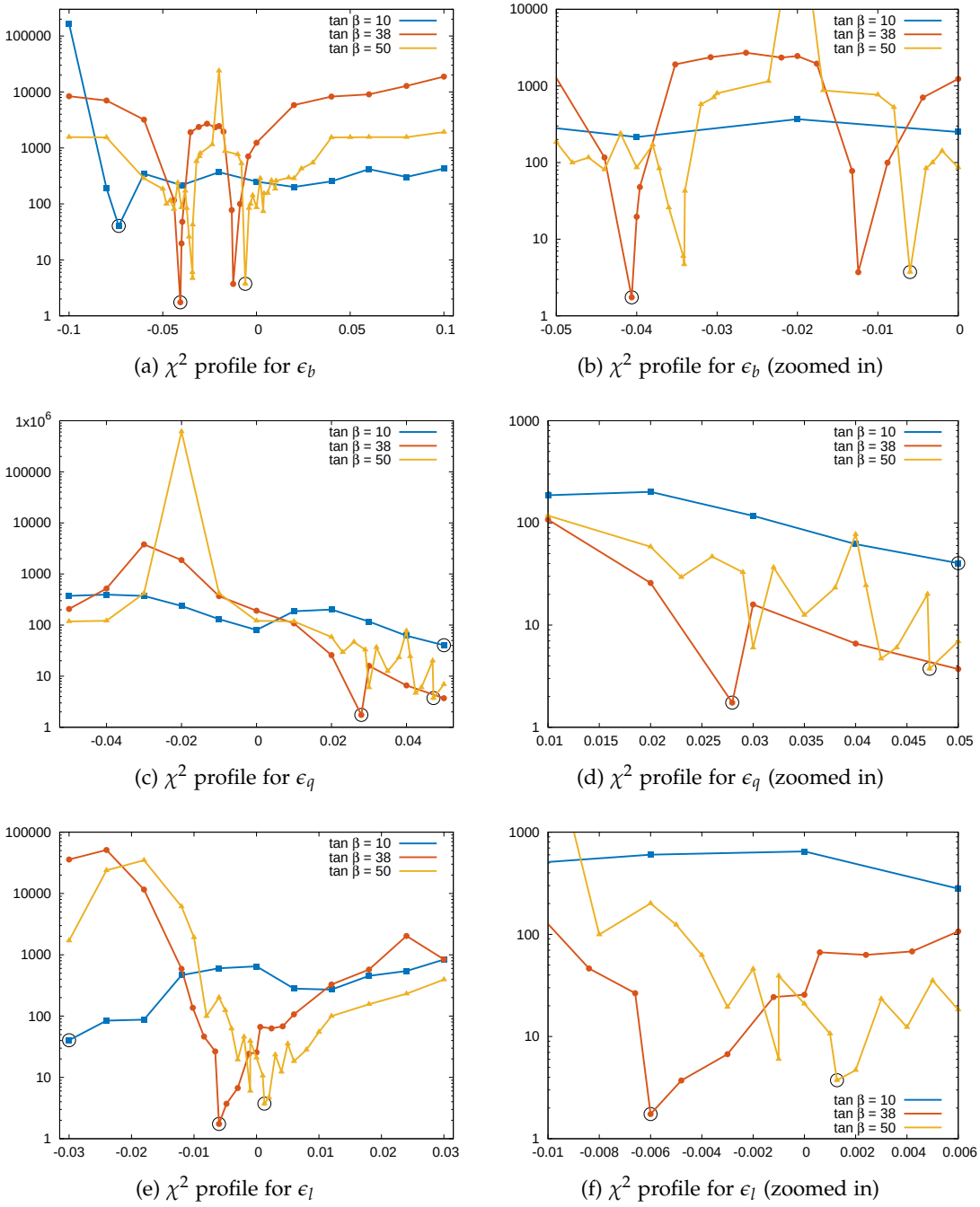

(a) χ^2 profile for ϵ_b

(b) χ^2 profile for ϵ_b (zoomed in)

(c) χ^2 profile for ϵ_q

(d) χ^2 profile for ϵ_q (zoomed in)

(e) χ^2 profile for ϵ_l

(f) χ^2 profile for ϵ_l (zoomed in)

Figure 2.5: **Likelihood profiles for fixed values of the threshold corrections ϵ_b, ϵ_q and ϵ_l.** The minima of the global minimisation are marked with circles.

consequences for flavour model building in SUSY, it is an interesting question how sensitive the fits actually are to these corrections. For this study, the minimisation of the χ^2 is performed with one of the threshold corrections ϵ_b, ϵ_q and ϵ_l fixed. This procedure is then repeated for different values of the particular TC and for $\tan\beta = 10$, 38 and 50, respectively. As a result, the likelihood profiles for the TCs are shown in Figure 2.5. On the left, the profiles over the complete ranges of ϵ_b, ϵ_q and ϵ_l are shown. On the right, the same plots are zoomed into the regions of interest. The density of points on the x-axis is increased around the minima for better numerical convergence. Also the global minima of Section 2.2.1 have been added to the plots and marked by circles.

For $\tan\beta = 10$, the χ^2 profiles exhibit in general less features than for larger values of $\tan\beta$. The χ^2 function has a minimum for $\epsilon_b = -0.0735$. For both ϵ_q and ϵ_l, the best-fit points lie on the edges of the allowed ranges, as has been noticed before. The profiles also show a preference of larger values for ϵ_q and smaller values for ϵ_l.

For $\tan\beta = 38$ and $\tan\beta = 50$ the χ^2 profiles for ϵ_q and ϵ_l are qualitatively similar. There is a preference for positive values of ϵ_q. In contrast to $\tan\beta = 10$, all minima are within the allowed ranges. The χ^2 profiles for ϵ_l, both show a minimum around zero. Therefore, rather small corrections are preferred in the lepton sector.

The most distinct features in the plots are two competing minima in the profile of ϵ_b for both $\tan\beta = 38$ and $\tan\beta = 50$. The local minima are nearly degenerate with the global ones, having χ^2 values of 3.71 ($\tan\beta = 38$) and 4.69 ($\tan\beta = 50$). Both being steep and narrow, the four minima actually shrink the possible values for ϵ_b to very fine-tuned regions. The pulls of this minima compared to those of the global minima are shown in Figure 2.6. Interestingly, for $\tan\beta = 38$ the minimum with smaller ϵ_b is the preferred one, whereas for $\tan\beta = 50$ the one with larger ϵ_b is preferred. The effective corrections are also rather large, especially for those minima with the smaller values of ϵ_b we have $\epsilon_b \tan\beta < -1$. It has been pointed out, that the $\tan\beta$ enhancement of the threshold corrections occurs at one-loop, but does not repeat itself at higher loop orders. To be precise, there are no corrections scaling as $\epsilon_b^n \tan^n\beta$ at $n > 1$ loops, see e. g. [200].

2.2.3 *Bottom-Tau unification and the atmospheric mixing angle*

It has been analysed in detail in [66, 73, 197] that there is an intricate connection between the atmospheric mixing angle θ_{23}^l and unification of the bottom and tau Yukawa couplings, y_b and y_τ, in SO(10) grand unification. In these studies, however, SUSY TCs have not been taken into account. As we will see, considering these corrections gives us a qualitative understanding of the numerical fit results.

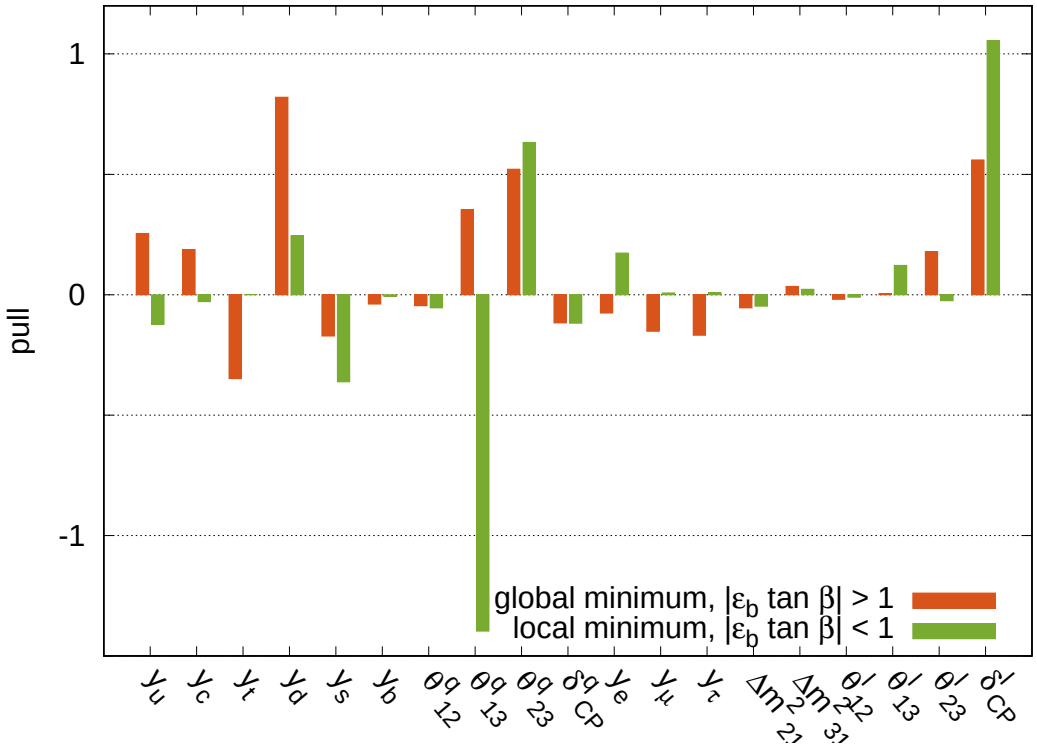

(a) Comparison of the two minima for $\tan\beta = 38$.

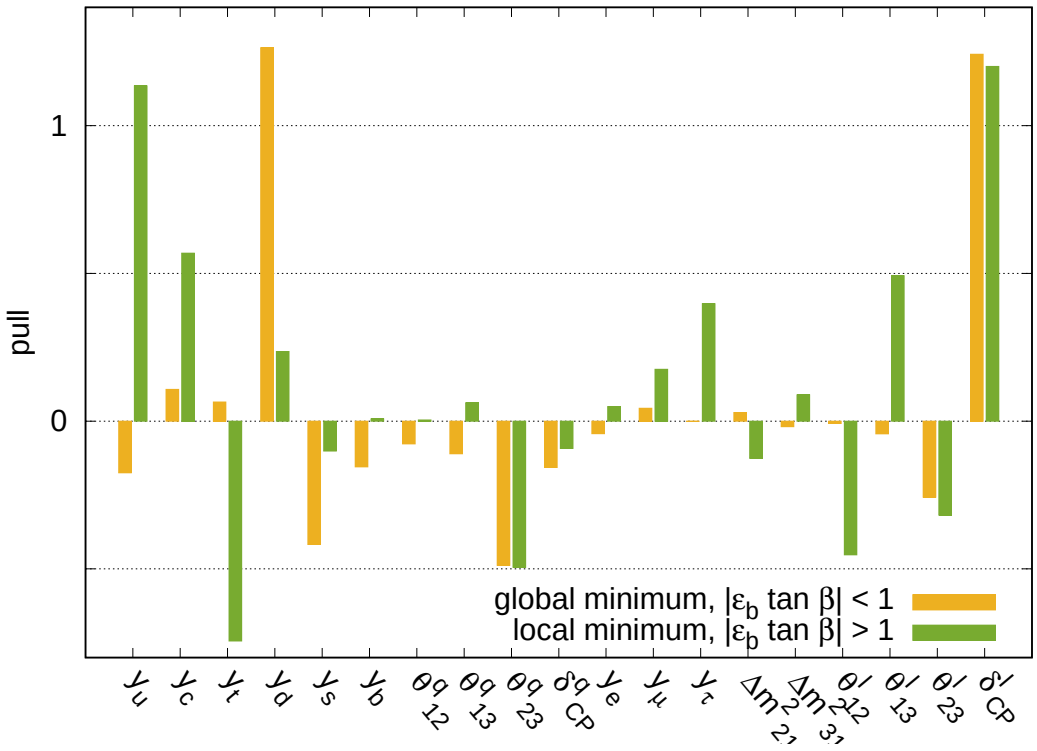

(b) Comparison of the two minima for $\tan\beta = 50$.

Figure 2.6: **Comparison of global and local minima.** The local minima appear in the likelihood profile of ϵ_b in Figure 2.5.

Neglecting the second generation Yukawa couplings, there is a relation between the mixing angles in the quark and lepton sector at the GUT scale [66]

$$\tan 2\theta_{23}^{l} = \frac{\sin 2\theta_{23}^{q}}{2\sin^2\theta_{23}^{q} + y_\tau/y_b - 1} \,. \tag{2.44}$$

This relation can be expanded for small θ_{23}^{q}

$$\frac{y_\tau}{y_b} = 1 + \frac{2\theta_{23}^{q}}{\tan 2\theta_{23}^{l}} \,. \tag{2.45}$$

The right-hand side of the equation is to a good approximation one, as θ_{23}^{q} is of order one permille and $\tan 2\theta_{23}^{l}$ is of order one. To reproduce the lepton and quark mixing angles between the second and third generation fermions, y_b and y_τ must be equal at the GUT scale to a rather high precision. That explains, why we find large tensions in the atmospheric mixing angle θ_{23}^{l}. Applying the SUSY TCs to this relation gives at M_{SUSY}, neglecting RGE corrections

$$\frac{y_\tau(1+\epsilon_l\tan\beta)}{y_b(1+\epsilon_b\tan\beta)} = 1 + \frac{2\theta_{23}^{q}(1+(\epsilon_q-\epsilon_b)\tan\beta)}{\tan 2\theta_{23}^{l}} \,. \tag{2.46}$$

On the right-hand side, the picture does not change qualitatively. On the left-hand side, however, SUSY corrections can loosen the strict constraint from bottom tau unification. For $\epsilon_b\tan\beta < -1$ the left-hand side can become negative. The two competing minima in the likelihood profiles of ϵ_b actually correspond to $\epsilon_b\tan\beta < -1$ and $-1 < \epsilon_b\tan\beta < 0$, respectively. This sign does not necessarily need to be physical since singular values can always be chosen real and positive. The simplified two generation model used here can also not account for physical phases. But it is interesting to note that the occurence of this sign seems to allow for two distinct solutions.

For illustration, the absolute value of the left-hand side of eq. 2.46 is plotted in Figure 2.7. In the case where no TCs are included, $|y_\tau/y_b|$ is much larger than one at the GUT scale explaining the bad convergence of the fit. For the global minima including TCs, we find a big deviation from one for $\tan\beta = 10$. The deviation is smallest for $\tan\beta = 38$ and a bit larger for $\tan\beta = 50$. Thus the goodness of fit is qualitatively reproduced for all global minima. This also holds for the local minima in the χ^2 profile of ϵ_b in Figure 2.5. Note that, for $\tan\beta = 50$, the global and local minimum are nearly degenerate.

2.3 CONCLUSIONS

We have studied fermion observables in a minimal SUSY SO(10) model. The results of Section 2.2.1 clearly suggest that the predictions of minimal SUSY SO(10) for the fermion sector of the SM can only be

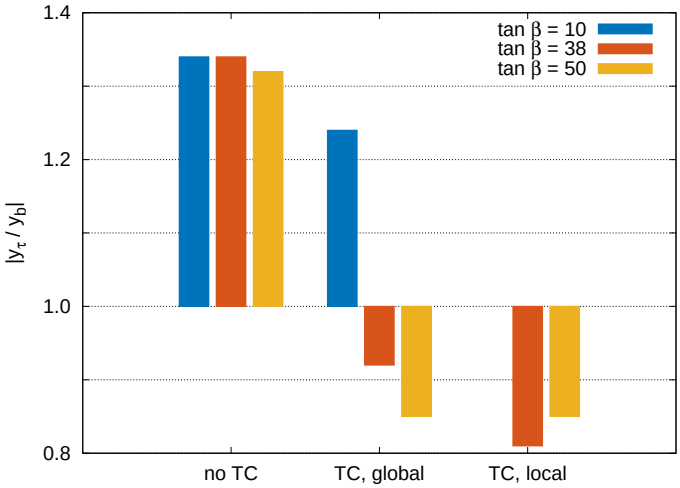

Figure 2.7: **Best-fit values of $|y_\tau/y_b|$ at M_{GUT}.** The directions of the bars shows the deviation from one.

viable in the presence of large $\tan\beta$ and sizable TCs from heavy SUSY particles. In comparison to previous studies with similar approaches, updated values for the fermion observables in the SM are used. The reduced uncertainty in lattice and neutrino data leads to tensions in the GUT predictions for the down quark yukawa coupling y_d and the atmospheric mixing angle θ_{23}^l. Both quantities are expected to become more precisely known in the future. Lattice and neutrino data hence will be able to provide insight on models of grand unification.

Improvements on the experimental side, however, call for improvements on the theoretical side. The global analysis of this chapter, therefore, focuses on a elaborate treatment of all energy scales in the problem in terms of effective field theory (EFT). The procedure includes integrating out right-handed neutrinos at their respective mass scale and consistent use of two-loop RGE evolution. For this purpose efficient code has been written in `C++` that will be made publicly available. Not only is this to our knowledge the first fit to SUSY GUTs that features threshold corrections, but this work also provides likelihood profiles for their values. As a result of Section 2.2.2, the likelihood profile for the correction to the bottom Yukawa coupling, ϵ_b, shows two narrow, deep and nearly degenerate minima. These specific values for the TCs may be of interest for model building since they depend on the flavour structure of the SUSY spectrum.

When the τ and the bottom quark were discoverd in the 1970s, the idea of grand unification has already been around. It must have been an astonishing insight for the pioneers of particle physics that there is not only a third family of fermions but more than that it would fit into the bigger picture of grand unification. More than twenty years after the discovery of the top quark, all fermions of the SM have been discovered and their couplings have been measured ever

more precisely. This data and modern computing power now allow us to take the predictions of GUTs seriously and question them at a quantitative level. QFT thus can provide us with insight on physics that might happen at much higher energy scales by carefully connecting them to the physics we find in experiment.

3

RESUMMATION OF GLUINO CONTRIBUTIONS TO THE MSSM HIGGS POTENTIAL

If there is going to be change, real change, it will have to work its way from the bottom up, *from the people themselves. That's how change happens.*
—Howard Zinn

THE FINE-TUNING IN THE MSSM. The existence of the Higgs boson as a particle is one of the central predictions of the SM. Before its discovery in 2012, the value of its mass was therefore subject to widespread speculation among physicists. In contrast to the SM, the mass of the Higgs boson can be calculated in the MSSM once the SUSY mass spectrum is known.

At the tree-level, the mass of the lightest CP even Higgs boson m_h must be below M_Z via $m_h^2 \leq M_Z^2 \cos 2\beta$. This mass range had already been excluded in the 1990s by the LEP experiments that set a lower bound on the Higgs mass. A combined analysis of all experimental results from LEP excludes Higgs masses below 114.4 GeV at the 95% confidence level [201]. Loop corrections, however, can shift the Higgs mass above M_Z. Since the discovery of the Higgs boson [16, 17], the measurements of its mass have constantly been improved. The current PDG average for the mass of the SM model Higgs boson is [202]

$$m_h = 125.18 \pm 0.61\,\text{GeV} \,. \tag{3.1}$$

In the MSSM this particular value requires soft SUSY breaking parameters in the TeV range, see e. g. [203]. SUSY particles with masses above several TeV are also suggested by recent bounds from direct searches. The recent study in [204] finds e. g. mass bounds for the top squark of $m_{\tilde{t}} > 1.23\,\text{TeV}$ and the gluino of $m_{\tilde{g}} > 2.12\,\text{TeV}$, both at the 95% confidence level. These bounds yet depend on theoretical assumptions regarding the mass of the LSP (typically the neutralino, i. e. the mass eigenstate of the mixed higgsino, bino and wino states after EWSB) and the branching fractions of those particles into their respective final states.

But let us return from these recent developments to the more general aspects of supersymmetry. Recalling the arguments of Chapter 1, heavy particles with mass M yield large corrections to the self-energy of scalars that scale as M^2. In the context of softly broken supersymmetry, these corrections give rise to the little hierarchy problem that is induced by the fact that SUSY particles appear to be heavier than the electro-weak scale. Thus, the electro-weak scale receives corrections of the order of M_{SUSY} and the counterterms have to be tuned accordingly at every order in perturbation theory. This issue raised concern even

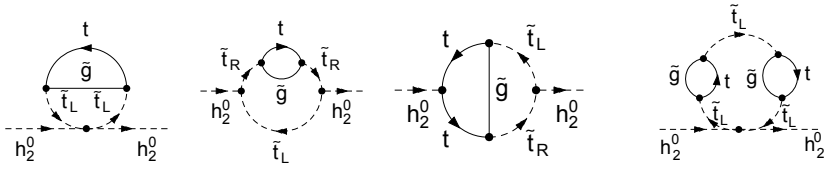

(a) (b)

Figure 3.1: **Feynman diagrams with gluinos.** The two-loop diagrams (Figure 3.1a) lead to large contributions to $m^2_{\tilde{t}_{ij}}$ in case the gluino is heavy. The three-loop diagram (Figure 3.1b) is an example of how these contributions appear recurringly at higher orders in perturbation theory.

before the days of LEP and the little hierarchy problem was quantified by introducing the fine-tuning measure [205, 206]

$$\Delta(p) = \left| \frac{p}{M_Z(p)} \frac{\partial M_Z(p)}{\partial p} \right| . \tag{3.2}$$

$\Delta(p)$ is a measure of the logarithmic dependence of the electro-weak scale, i. e. M_Z, on a soft SUSY parameter p.

If the Z boson is renormalised on-shell and used as input, as usually done in SUSY Higgs mass calculations, the fine-tuning is found in the counterterm of M_Z.

Here, M_Z is a function of p in the sense that if one calculates the corrections to the Higgs potential as a function of p and then determines M_Z from the minimum of the Higgs potential, M_Z depends on p. As an example, consider a top squark mass of the order of 1 TeV. Thus, in the determination of M_Z^2, contributions of the order of $(1\,\text{TeV})^2$ appear. The fine-tuning $\Delta(m_{\text{stop}})$ then is roughly 100. That means that when adding up contributions of the order of $(1\,\text{TeV})^2$ they need a tuning of 1% (1 in 100) to give a result of the order of $(100\,\text{GeV})^2$.

What concerned physicists about the LEP results? The fine-tuning in a SUSY theory is smallest, when all SUSY parameters are of the same order as the EW scale. The higher the lower bounds on the masses of SUSY particles become, the larger the fine-tuning becomes. This development continued from the LEP experiments until today [207–211].

OUTLINE. In this chapter, we will study the fine-tuning in the MSSM from a novel perspective. We will consider the SUSY spectrum itself to be hierarchical with the gluino being heavier than the top squarks. The gluino couples to the Higgs fields at the two-loop level via the strong coupling to the top quarks and top squarks, see Figure 3.1a. For the study of the fine-tuning, we calculate the corrections to the parameters in the MSSM potential in an EFT approach. Since we want to focus on the impact of the hierarchy between top squarks and the gluino, we only include corrections induced by the top Yukawa coupling y_t and

In GUT models with bottom-top unification values of $\tan\beta > 1$ are typically preferred, see e. g. Chapter 2.

the corresponding trilinear scalar coupling A_t. These contributions are typically also the largest ones for $\tan\beta > 1$. The parameters in the Higgs potential are all renormalised in the $\overline{\text{DR}}$ scheme in order not to hide the fine-tuning by absorbing finite pieces into the counterterms. We also assume a GUT scenario, or at least the existence of a theory at higher scales than the SUSY scale, where the soft parameters are set and evolved to the SUSY scale by RGE running. For that reason, all soft parameters are given at the SUSY scale in the $\overline{\text{DR}}$ scheme.

This chapter is structured as follows: The details of the MSSM Higgs potential are discussed in Section 3.1. Section 3.2 contains all technical details about the calculation. It is divided into subsections as follows: At first the two-loop calculation is described in Section 3.2.1 and the fixed order results in the $\overline{\text{DR}}$ scheme are discussed in Section 3.2.2. For large gluino masses, the two-loop corrections to the potential can be quite sizeable. These corrections require an all-order resummation that is explicitely performed in Section 3.2.3. However, this resummation can be avoided by renormalising the top squarks in an on-shell scheme. We demonstrate in Section 3.2.4 that these procedures are equivalent. The gluino contributions cause a large scheme difference between the $\overline{\text{DR}}$ mass and the OS mass. Section 3.2.5 investigates the matching scale at which the SUSY particles should be integrated out in our scenario. In Section 3.2.6 the mass of the lightest CP even Higgs boson in the MSSM is discussed in the light of the contributions to the Higgs potential we have calculated. Before the fine-tuning in the MSSM is studied in a numerical scan in Section 3.3, we summarise, all results from the previous sections. As an illustration of how these results can be generalised to SUSY phenomenology beyond the Higgs sector, the implications on Kaon mixing are studied in Section 3.4, before we conclude this chapter with Section 3.5.

3.1 THE HIGGS SECTOR OF THE MSSM

This section follows the pedagogical introductions of [212] and [213].

The scalar potential of the MSSM contains terms from three distinct sources: D-terms, F-terms and SUSY breaking terms. Its subpart describing the neutral components h_1^0 and h_2^0 of the Higgs doublets that is responsible for EWSB and the masses of the Higgs bosons can be written as, including one-loop corrections

$$\begin{aligned} V_H = {} & m_{11}^2 \left|h_1^0\right|^2 + m_{22}^2 \left|h_2^0\right|^2 - \left(m_{12}^2 \, h_1^0 \, h_2^0 + \text{H.c.}\right) \\ & + \frac{g_Y^2 + g_2^2}{8} \Big((1+\Delta_{11}) \left|h_1^0\right|^4 + (1+\Delta_{22}) \left|h_2^0\right|^4 \\ & \qquad - 2\,(1+\Delta_{12}) \left|h_1^0\right|^2 \left|h_2^0\right|^2 \Big) \,. \end{aligned} \tag{3.3}$$

The Δ_{ij} encode the quantum corrections to the quartic couplings, the m_{ij}^2 stand for the loop corrected mass parameters. At the minimum of the potential, h_1^0 and h_2^0 acquire VEVs defined by

$$\left\langle h_1^0 \right\rangle = v_1 = v \cos\beta \,, \qquad \left\langle h_2^0 \right\rangle = v_2 = v \sin\beta \,, \tag{3.4}$$

where $v = 174.10$ GeV. The necessary condition that the gradient of V_H vanishes at its minimum yields for $v_1 \neq 0 \neq v_2$

$$0 = m_{11}^2 - m_{12}^2 \tan\beta + \rho\, M_Z^2 \,, \tag{3.5}$$
$$0 = m_{22}^2 - m_{12}^2 \cot\beta - \varphi\, M_Z^2 \,, \tag{3.6}$$

where we have used that $M_Z^2 = v^2(g_Y^2 + g_2^2)/2$ and

$$2\,\rho = \cos(2\beta) + \cos^2\beta \left(\Delta_{11} - \Delta_{12}\tan^2\beta\right) \,, \tag{3.7}$$
$$2\,\varphi = \cos(2\beta) - \sin^2\beta \left(\Delta_{22} - \Delta_{12}\cot^2\beta\right) \,. \tag{3.8}$$

The necessary condition now allows us to write M_Z and m_{12}^2 as a function of m_{11}^2, m_{22}^2, $\tan\beta$ and the Δ_{ij}

$$m_{12}^2 = \frac{\varphi\, m_{11}^2 + \rho\, m_{22}^2}{\varphi\tan\beta + \rho\cot\beta} \,, \qquad M_Z^2 = \frac{m_{22}^2\tan\beta - m_{11}^2\cot\beta}{\varphi\tan\beta + \rho\cot\beta} \,. \tag{3.9}$$

Moreover, the potential must be bounded from below. For classical field configurations with $h_1^0 \neq h_2^0$ this is ensured by the quartic terms. Along the so-called *D-flat directions* where $|h_1^0| = |h_2^0|$ one must further require, at the tree-level

$$m_{11}^2 + m_{22}^2 - 2\,m_{12}^2 > 0 \,. \tag{3.10}$$

After EWSB the complex Higgs fields h_1^0 and h_2^0 mix into their mass eigenstates. Writing these fields as $h_i^0(x) = \left(\phi_i(x) + \mathrm{i}\,\sigma_i(x)\right)/\sqrt{2}$ the mass squared matrix of the CP odd scalars is

$$\mathcal{M}_{ij}^2 = \left\langle \frac{\partial^2 V_H}{\partial\sigma_i\,\partial\sigma_j} \right\rangle \tag{3.11}$$

with

$$\mathcal{M}_{11}^2 = m_{11}^2 + \rho M_Z^2 = m_{12}^2\tan\beta \,, \tag{3.12}$$
$$\mathcal{M}_{22}^2 = m_{22}^2 - \varphi M_Z^2 = m_{12}^2\cot\beta \,, \tag{3.13}$$
$$\mathcal{M}_{12}^2 = m_{12}^2 \,. \tag{3.14}$$

This also shows the existence of one neutral (would-be) Goldstone boson which then becomes the longitudinal polarisation of the Z boson.

From $\det\mathcal{M}^2 = 0$ follows that at least one eigenvalue is zero. The other eigenvalue is given by the trace of $\mathcal{M}^2$

$$\mathrm{tr}\,\mathcal{M}^2 = \frac{2\,m_{12}^2}{\sin 2\beta} \equiv m_A^2 \,. \tag{3.15}$$

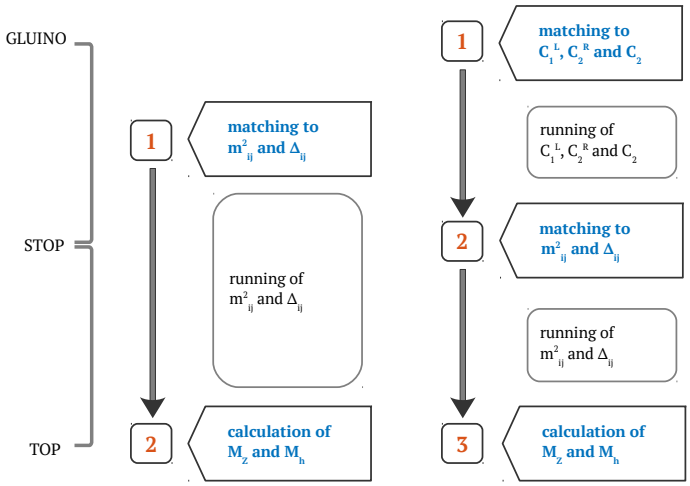

Figure 3.2: **Overview of the relevant scales in Section 3.2.** In Section 3.2.2 the contributions to the parameters in the MSSM Higgs potential are calculated in an EFT approach at the matching scale $\bar{\mu}$ as depicted on the left. On the right the matching at separate scales M_3 and M_{SUSY} is shown with the RGE running performed between those scales. Section 3.2.5 compares the two approaches in order to find a suitable value for $\bar{\mu}$.

Analogously for the CP even scalars the mass squared matrix is

$$\mathcal{M}^2_{ij} = \left\langle \frac{\partial^2 V_H}{\partial\phi_i\,\partial\phi_j} \right\rangle \tag{3.16}$$

with

$$\mathcal{M}^2_{11} = m^2_{12}\tan\beta + M^2_Z\cos^2\beta\,(1+\Delta_{11})\,, \tag{3.17}$$
$$\mathcal{M}^2_{22} = m^2_{12}\cot\beta + M^2_Z\sin^2\beta\,(1+\Delta_{22})\,, \tag{3.18}$$
$$\mathcal{M}^2_{12} = -m^2_{12} - M^2_Z\sin\beta\cos\beta\,(1+\Delta_{12})\,. \tag{3.19}$$

The masses of the CP even Higgs boson can be obtained by diagonalising $\mathcal{M}^2$. In analogy to the SM, one of the eigenvalues must be negative to trigger EWSB.

From the last equation it also follows that the lightest CP even Higgs boson must be lighter than the Z boson at the tree-level, i. e. $m^2_h \leq M^2_Z\cos 2\beta$. The corrections to the quartic couplings then can shift its mass above M_Z.

3.2 QUANTUM CORRECTIONS TO THE HIGGS POTENTIAL

The gluino couples the MSSM Higgs fields via squarks loops at the two-loop level. We are interested in the limit where these corrections become as sizeable as the one-loop corrections. This section will deal with the more technical details of this limit. To point out its implications, namely the renormalisation scheme applied to the top squarks,

we will restrict ourselves to the contributions from the top and stop sector of the MSSM, i. e. those governed by the superpotential

$$\mathcal{W} = \mu \left(h_1^0 h_2^0 - h_1^- h_2^+ \right) + y_t \left(\tilde{t}_R \tilde{t}_L h_2^0 - \tilde{t}_R \tilde{b}_L h_2^+ \right) , \tag{3.20}$$

In this chapter, y_t is the Yukawa coupling as it appears in the superpotential. Its relation to the SM Yukawa coupling is $y_t = \frac{y_t^{\mathrm{SM}}}{\sin\beta} = \frac{m_t}{v \sin\beta}$ a the tree-level.

where the obvious colour indices have been suppressed. The corresponding Lagrangian is derived according to [26] and given in Appendix A.3. There, also the SUSY QCD interactions are listed.

The calculation is performed in an EFT approach, i. e. the SUSY particles are integrated out at the matching scale $\bar{\mu}$, and in the unbroken electro-weak phase of the MSSM. In particular, the top quark is massless in this limit and the gauge eigenstates of the top squarks, t_L and t_R do not mix.

For a review of the two-Higgs-doublet model see e. g. [214].

Below the matching scale $\bar{\mu}$ the RGE running of the parameters in the Higgs potential is the same as in a two-Higgs-doublet model of Type II. At the mass scale of the top quark m_t the solutions of the RGEs for the mass parameters are to leading order in y_t [215]

$$m_{11}^2(m_t) = m_{11}^2(\bar{\mu}) , \qquad m_{11}^2(m_t) = m_{11}^2(\bar{\mu}) , \tag{3.21}$$

$$m_{22}^2(m_t) = \left(1 - \frac{6 \left| y_t \right|^2}{16 \pi^2} \log\left(\frac{\bar{\mu}}{m_t} \right) \right) m_{22}^2 \left(\bar{\mu} \right) . \tag{3.22}$$

The RGE effects to the Δ_{ij} are neglected which is commented on later.

Regarding the fine-tuning we would like to point out the difference between the electro-weak scale and the masses of the Higgs bosons: The loop corrections to the m_{ij}^2 affect the electro-weak scale and therefore are relevant for the discussion of the hierarchy problem. The Δ_{ij} can only have a logarithmic dependence on the SUSY masses by power counting and set the masses of the Higgs bosons after EWSB. For that reason, we consider two-loop contributions to the mass parameters but only one-loop corrections to the quartic couplings. Thus we only obtain a rough estimate of the masses of the Higgs bosons. Nonetheless, that estimate is sufficient for the discussion of the fine-tuning.

We renormalise the parameters of the potential in eq. (3.3) in the $\overline{\mathrm{DR}}$ scheme. We then compute M_Z from the input parameters m_{11}^2 and m_{22}^2 with eq. (3.9) of the previous section, that also fixes m_{12}^2 via the choice of $\tan\beta$.

Albeit our considerations lack some accuracy by not including the complete SUSY spectrum, they have the advantage of less complicated analytic results that allow for a comparison of different methodologies. Sections 3.2.2-3.2.4 weigh the differences between the renormalisation scheme of the stops. Section 3.2.5 deals with the choice of the matching scale $\bar{\mu}$ by comparing the previous results to the matching at two separate scales M_3 and $\bar{\mu}$, see Figure 3.2. The uncertainty regarding the masses of the Higgs bosons is estimated in Section 3.2.6.

The structure of this comparably long and technical section is a pedagogical one that aims at developing our methodology step by

(a) (b) (c) (d)

Figure 3.3: **Counterterm conventions.** Counterterms for scalar propagators, fermion propagators and vertices. The respective Feynman rules are given in consecutive order in eqs. (3.25), (3.26), (3.28) and eq. (3.36)

step. We will sometimes remind the reader of previous results or postpone certain questions to later discussions. To begin with, all results of this section are summarised at the beginning of Sections 3.3 where the fine-tuning in the MSSM is considered.

SOFT TERMS AND HIGGSINOS. We define soft terms for SUSY breaking by

$$\begin{aligned} -\mathcal{L}_{\text{soft}} = {} & A_t \left(\tilde{t}_R \tilde{t}_L h_2^0 - \tilde{t}_R \tilde{b}_L h_2^+\right) + A_t^\star \left(\tilde{t}_L^\star \tilde{t}_R^\star h_2^{0,\star} - \tilde{b}_L^\star \tilde{t}_R^\star h_2^{+,\star}\right) \\ & + m_L^2 \left(\tilde{t}_L^\star \tilde{t}_L + \tilde{b}_L^\star \tilde{b}_L\right) + m_R^2 \, t_R t_R^\star \\ & + m_{h_1}^2 \left(h_1^{0,\star} h_1^0 + h_1^{-,\star} h_1^-\right) + m_{h_2}^2 \left(h_2^{0,\star} h_2^0 + h_2^{+,\star} h_2^+\right) \\ & + \frac{1}{2} M_3 \, \overline{\psi_{\tilde{g}}} \psi_{\tilde{g}} \,, \end{aligned} \tag{3.23}$$

The Higgs fields also have a supersymmetric mass term, such that their tree-level mass terms are $m_{11}^{2,tree} = |\mu|^2 + m_{h_1}^2$ and $m_{22}^{2,tree} = |\mu|^2 + m_{h_1}^2$, respectively.

where $\psi_{\tilde{g}}$ is the Majorana spinor of the gluino, see Appendix A.3.

In the basis of gauge eigenstates the higgsinos $\tilde{h}_1^0$ and $\tilde{h}_2^0$ as well as their $SU(2)_L$ partners $\tilde{h}_1^-$ and $\tilde{h}_2^+$ have a common mass term μ and we therefore use $|\mu|$ as the higgsino mass which is correct if they do not mix with the bino and the neutral wino. The four-component spinors of the neutral higgsinos are Majorana spinors and those of the charged higgsinos are Dirac spinors. Their definition and interactions are also given in Appendix A.3.

THE FEYNARTS MODEL FILE. For the generation of Feynman diagrams and the corresponding amplitudes, the interactions described by the Lagrangian in eqs. (A.34)-(A.38) are implemented in a `FeynArts` [216] model file. Fermion number violating interactions are implemented in `FeynArts` according to [217].

RENORMALISATION. For the two-loop calculation the Higgs fields need to be renormalised at the two-loop level and all internal particles and vertices at the one-loop level. For later reference, we explicitly state our conventions for renormalisation. For scalars, field and mass

renormalisations are introduced by the following replacements in the Lagrangian

$$\phi \to \sqrt{Z}\,\phi\,, \qquad m^2 \to m^2 + \delta m^{(1),2} + \delta m^{(2),2}\,, \tag{3.24}$$

with $Z = 1 + \delta Z^{(1)} + \delta Z^{(2)}$, where the number in brackets marks the counter term order in the perturbative expansion. The renormalisation is done diagrammatically in renormalised perturbation theory, i. e. by introducing additional Feynman rules for counterterms that are also implemented in the `FeynArts` model file. The propagator counterterm (Figure 3.3a) for scalars at the one-loop level is

$$\mathrm{i}\,p^2\,\delta Z^{(1)} - \mathrm{i}\left(\delta m^{(1),2} + m^2\,\delta Z^{(1)}\right)\,, \tag{3.25}$$

and at the two-loop level (Figure 3.3b)

$$\mathrm{i}\,p^2\,\delta Z^{(2)} - \mathrm{i}\left(\delta m^{(2),2} + m^2\,\delta Z^{(2)} + \delta m^{(2),2}\,\delta Z^{(1)}\right)\,. \tag{3.26}$$

For chiral fermions analogous replacements are made,

$$\psi_{L,R} \to \sqrt{Z_{L,R}}\,\psi_{L,R}\,, \qquad m \to m + \delta m\,, \tag{3.27}$$

with $Z_{L,R} = 1 + \delta Z^{(1)}_{L,R}$ in the perturbative expansion. The subscripts L and R denote the left-handed and right-handed components of four-component fermions. The propagator counterterm (Figure 3.3c) for fermions is

$$\mathrm{i}\,\not{p}(\delta Z_L\,\mathbb{P}_L + \delta Z_R\,\mathbb{P}_R) - \mathrm{i}\left(\delta m + m(\delta Z_L + \delta Z_R)/2\right)(\mathbb{P}_L + \mathbb{P}_R)\,. \tag{3.28}$$

For Majorana fermions $Z_L = Z_R$.

A diagram is called one-particle-irreducible *if it cannot be cut into two disconnected pieces by dropping one internal line.*

Self-energies Σ are defined such that the sum of all connected and one-particle-irreducible diagrams with two external legs equals $\mathrm{i}\,\Sigma(p^2)$, where p is the external momentum. $\hat{\Sigma}$ denotes the renormalised self-energy. The Dyson resummed propagator then becomes, see Figure 3.4

$$\sum_{n=0}^{\infty} \frac{\mathrm{i}}{p^2 - m^2}\left(\mathrm{i}\,\Sigma(p^2)\,\frac{\mathrm{i}}{p^2 - m^2}\right)^n = \mathrm{i}\left(p^2 - m^2 + \Sigma(p^2)\right)^{-1}\,. \tag{3.29}$$

It has its pole at $m^2 - \hat{\Sigma}(p^2)$. The renormalised self-energy for scalars in terms of field and mass renormalisation constants is, at the one-loop level

$$\hat{\Sigma}(p^2) = \Sigma(p^2) - \delta m^2 - m^2\,\delta Z + p^2\,\delta Z\,. \tag{3.30}$$

At the two-loop level also one-loop diagrams with counterterm insertions must be considered. When the mass corrections are calculated in an EFT approach adopting the $\overline{\mathrm{DR}}$ scheme, the self-energy is asymptotically expanded around $p^2 = 0$

$$\Sigma(p^2) = \Sigma^{(0)} + \Sigma^{(1)}\,p^2 + \ldots \tag{3.31}$$

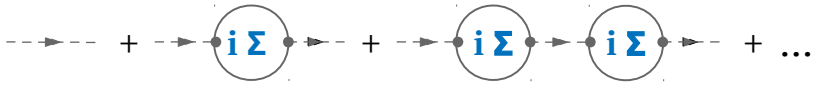

Figure 3.4: **Dyson resummation.** The insertion of n self-energies into a scalar propagator are formally summed to all orders.

After comparing coefficients of p^2, the $\overline{\text{DR}}$ renormalisation constants are defined by subtracting the ε poles only

div *denotes the UV divergent part rather than the divergence of a vector field.*

$$\delta Z = -\operatorname{div}\Sigma^{(0)}\,, \tag{3.32}$$

$$\delta m^2 = \operatorname{div}\Sigma^{(0)} + m^2 \operatorname{div}\Sigma^{(1)}\,. \tag{3.33}$$

In an OS scheme, $\hat{\Sigma}(p^2)$ is defined such that the Dyson resummed propagator in eq. (3.29) has a pole at $p^2 = m^2$, i. e. when the particle is *on-shell*, with residue one. It follows that

$$\delta m^2 = \Sigma(p^2 = m^2)\,, \qquad \delta Z = -\frac{\mathrm{d}}{\mathrm{d}p^2}\Sigma(p^2 = m^2)\,. \tag{3.34}$$

The couplings y_t, g_3 and A_t are renormalised by substituting in the Lagrangian

$$y_t \to Z_{y_t}\, y_t\,, \qquad g_3 \to Z_g\, g_3\,, \qquad A_t \to Z_{A_t}\, A_t\,, \tag{3.35}$$

where $Z_x = 1 + \delta Z_x$ for $x = y_t, g_3, A_t$. Expanding to the given order in perturbation theory gives the one-loop counterterms for vertices, see Figure 3.3d. E. g. for the top Yukawa coupling we have

$$\frac{-\mathrm{i}}{2}\, y_t \left(2\,\delta_{y_t} + \delta Z_{h_2^0} + \delta Z_{t_L} + \delta Z_{t_R}\right) \mathbb{P}_L + \text{H.c.} \tag{3.36}$$

3.2.1 *Two-loop calculations with Medusa*

THE PACKAGE. `Medusa` [218, 219] is a yet unpublished `Mathematica` package for the automated calculation of one-loop and two-loop diagrams. It has been developed by Christoph Wiegand and is particularly designed for calculating contributions of heavy particles in the loops. For that reason `Medusa` adopts asymptotic expansions in external momenta and large masses as described in [220]. This procedure allows to reduce general two-loop integrals to the tensorial vacuum integral

This overview is based on the upcoming manual of `Medusa` which was kindly provided by C. Wiegand.

$$\int \mathrm{d}^d k\, \mathrm{d}^d l\, \frac{l^{\nu_1} \dots l^{\nu_r}\, k^{\mu_1} \dots k^{\mu_s}}{(m_1^2 - k^2)^\alpha\, (m_2^2 - l^2)^\beta\, (m_3^2 - (l+k)^2)^\gamma}\,, \tag{3.37}$$

with arbitrary powers of the denominators and masses m_1, m_2, m_3. `Medusa` contains an implementation of a closed form solution of this

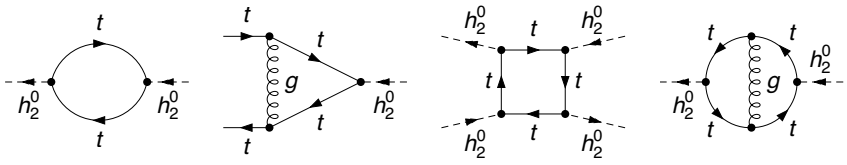

(a) (b) (c) (d)

Figure 3.5: **Massless diagrams.** Several classes of massless diagrams that appear in our calculations and cannot naively be calculated with `Medusa`.

integral that has been derived based on the solutions in [221–223]. Various one-loop integrals are implemented based on d dimensional results in [224, 225]. For the Laurent expansion of the integrals in $\varepsilon = (4-d)/2$ `HypExp` [226] is used and the Dirac algebra is solved with `TRACER` [227]. `Medusa` loads these packages into different namespaces to avoid conflicts due to homonymous internal variables.

After loading the package into the `Mathematica` kernel, the interface to `Medusa` is provided by the function `ComputeAmplitudes`. This function takes analytic expressions generated with `FeynArts` as input. Further necessary arguments are the depth of the expansions in momenta and masses as well as the mass hierarchy of all occurring particles. In our case that is

$$m_{22}^{\text{tree}} < |\mu| < m_{11}^{\text{tree}} < m_R < m_L < M_3 \,. \tag{3.38}$$

`ComputeAmplitudes` takes several optional arguments including the possibility to switch off the large mass expansion and the momentum expansion, too. In all two-loop amplitudes propagator diagrams the large mass expansion is therefore switched off. `ComputeAmplitudes` also allows to obtain higher powers in the expansion in ε, which are needed for one-loop diagrams with counterterm insertions.

The use of asymptotic expansion poses a problem for diagrams with only massless propagators. At this stage, `Medusa` does in addition not support DRED or the calculation of colour factors from QCD vertices. In the following we exemplify how these issues can be avoided.

MASSLESS DIAGRAMS. Figure 3.5 shows several diagrams that only contain loops with massless particles. In the corresponding integrals, logarithms of the form $\log(p^2/\bar{\mu}^2)$ appear, where p is an external momentum. Hence the expansion in small momenta is ill-defined since these logarithms cannot be expanded around $p^2 = 0$. One must therefore sort all diagrams of an amplitude into two categories depending on whether they contain massive internal particles or not. For the latter ones the momentum expansion in `Medusa` has to be switched off. Nevertheless not all the necessary loop integrals are implemented

in Medusa as it is designed to calculate contributions of heavy particles. We explain in the following how we treat the different classes of diagrams in Figure 3.5.

Figure 3.5a shows a diagram which is needed for the field renormalisation of h_2^0 at one-loop. Medusa can calculate tensorial propagator integrals of the form

$$\int \mathrm{d}^d k \, \frac{k^{\mu_1} \dots k^{\mu_r}}{((k+p)^2 - m_1^2)^\alpha (k^2 - m_2^2)^\beta} \,, \tag{3.39}$$

for arbitrary external momenta p, masses m_1, m_2 and powers α, β of the denominators. For that reason, massless one-loop propagator diagrams are not an issue once the momentum expansion is turned off. In this way also the OS self-energies in Section 3.2.4 are calculated.

The diagram in Figure 3.5b gives a QCD contribution to the renormalisation constant of y_t. Integrals with three massless propagators cannot be calculated in Medusa and a unique placeholder denoting

$$\int \mathrm{d}^d k \, \frac{\text{numerator}}{k^2 \, (k+p_1)^2 \, (k+p_2)^2} \,, \tag{3.40}$$

is returned instead of a result. In our cases, the numerators of this integral are 1, k^μ or $k^\mu k^\nu$. The respective integrals are calculated with Package-X [228, 229] and saved as a set of rules to substitute the placeholders after the calculation with Medusa.

Diagrams like those in Figure 3.5c are regularised with a finite top quark mass. The diagrams can then be evaluated with Medusa. For greater detail see Section 3.2.6.

Figure 3.5d shows a two-loop self-energy diagram with massless propagators only that cannot be reduced to the vacuum master integral in (3.37). Also in that case Medusa returns placeholders for these integrals. To cross-check our results and the renormalisation we were kindly provided with private results from [230] for all massless two-loop diagrams that appear in our calculation.

DIMENSIONAL REDUCTION. In SUSY calculations DRED is preferably used to regularise loop integrals since it is consistent with supersymmetry as opposed to DREG which explicitly breaks SUSY. The reason is that the symmetry between bosons and fermions only holds in four spacetime dimensions, while in DREG loop integrals are evaluated in d dimensions. In [231], it is shown how DRED can be constructed consistently such that fermions and vector bosons are treated in "quasi" four dimensions and loop integrals in d dimensions.

Formally, one defines d dimensional space (with metric tensor $\hat{g}^{\mu\nu}$) as in DREG, for details see e. g. [232]. $(4-d)$ dimensional space is defined analogously (with metric tensor $\tilde{g}^{\mu\nu}$). "Quasi-four-dimensional" space (with metric tensor $g^{\mu\nu}$) is defined as the direct sum of these

The direct sum of two infinite dimensional vector spaces is also infinite dimensional.

(a) (b)

Figure 3.6: **Gluon contributions to the top self-energy.** Sample diagrams at the one-loop level (left) and two-loop level (right).

vector spaces, such that $g^{\mu\nu} = \hat{g}^{\mu\nu} + \tilde{g}^{\mu\nu}$. The respective metric tensors fulfil

$$g^{\mu\nu} g_{\mu\nu} = 4 \,, \qquad \hat{g}^{\mu\nu} \hat{g}_{\mu\nu} = d \,, \qquad \tilde{g}^{\mu\nu} \tilde{g}_{\mu\nu} = 4 - d = 2\,\varepsilon \,, \tag{3.41}$$

and also serve as projectors onto d and $4 - d$ dimensional space

$$g^{\mu\nu} \hat{g}_{\nu\rho} = \hat{g}^{\mu}_{\rho} \,, \qquad g^{\mu\nu} \tilde{g}_{\nu\rho} = \tilde{g}^{\mu}_{\rho} \,, \qquad \hat{g}^{\mu\nu} \tilde{g}_{\nu\rho} = 0 \,. \tag{3.42}$$

Over each vector space a Dirac algebra is defined such that

$$\{\gamma^{\mu}, \gamma^{\nu}\} = 2\, g^{\mu\nu} \,, \qquad \{\hat{\gamma}^{\mu}, \hat{\gamma}^{\nu}\} = 2\, \hat{g}^{\mu\nu} \,, \qquad \{\tilde{\gamma}^{\mu}, \tilde{\gamma}^{\nu}\} = 2\, \tilde{g}^{\mu\nu} \,, \tag{3.43}$$

and $\gamma^{\mu} = \hat{\gamma}^{\mu} + \tilde{\gamma}^{\mu}$. We additionally define $\{\gamma_5, \gamma^{\mu}\} = 0$ which demands

$$\operatorname{tr}\{\gamma^{\mu_1} \cdots \gamma^{\mu_n} \gamma_5\} = 0 \,. \tag{3.44}$$

Momenta are treated in d dimensions, i. e. $p^{\mu} = \hat{p}^{\mu}$, since they are subject to the d dimensional Lorentz group. Contractions with Dirac matrices actually project onto d dimensional space, i. e. $\not{p} = p_{\mu}\gamma^{\mu} = \hat{p}_{\mu}\hat{\gamma}^{\mu} = \hat{\not{p}}$.

In contrast to DREG, vector bosons are four dimensional quantities. They can be decomposed as $A^{\mu} = \hat{A}^{\mu} + \tilde{A}^{\mu}$. In Feynman gauge, the propagator of vector bosons is then proportional to $g^{\mu\nu} = \hat{g}^{\mu\nu} + \tilde{g}^{\mu\nu}$. `Medusa` interprets all Lorentz structures and therefore also metric tensors as d dimensional which is not consistent with DRED.

As an example of how this issue affects our calculations let us discuss the Dirac part of the gluon contribution to the top self-energy, see Figure 3.6a. The d dimensional part of the gluon propagator is

$$\gamma_{\mu} \not{p} \gamma_{\nu}\, \hat{g}^{\mu\nu} = \hat{\gamma}^{\mu} \not{p} \hat{\gamma}_{\mu} = (2 - d)\, \not{p} \,, \tag{3.45}$$

where p is the momentum flowing through the top propagator. The $(4 - d)$ dimensional part of the gluon propagator is

$$\gamma^{\mu} \not{p} \gamma^{\nu}\, \tilde{g}^{\mu\nu} = \tilde{\gamma}^{\mu} \not{p} \tilde{\gamma}_{\mu} = -(4 - d)\, \not{p} \,. \tag{3.46}$$

This additional contribution is formally of order ε but yields a finite contribution in the presence of ε poles from loop integrals. The sum of both contributions (eqs. (3.45) and (3.46)) gives the same result as treating all quantities in four dimensions

$$\gamma^\mu \not{p} \gamma^\nu \, g^{\mu\nu} = \gamma^\mu \not{p} \gamma_\mu = -2 \not{p} \, . \tag{3.47}$$

At leading order in QCD, it is therefore sufficient to treat all Dirac objects and metric tensors as four dimensional and all loop integrals and momenta as d dimensional. In practice, the Dirac algebra must be solved separately and all four dimensional quantities must be encapsulated before passing the amplitudes to `Medusa`. The results from `Medusa` then contain only d dimensional quantities since they purely stem from loop integrals. When contracting the results afterwards eqs. (3.41) and (3.42) must be applied.

Beyond leading order in QCD, additional gluon propagators as in Figure 3.6b will generate combinations of metric tensors like $g^{\mu\nu} g^{\rho\sigma} = (\hat{g}^{\mu\nu} + \tilde{g}^{\mu\nu})(\hat{g}^{\rho\sigma} + \tilde{g}^{\rho\sigma})$. This problem is typically solved by treating $\tilde{A}^\mu$ as a separate field, called *epsilon scalar*, with own Feynman rules and renormalisation constants, which can e. g. be found in [233].

COLOUR ALGEBRA. In the current version, `Medusa` cannot deal with the QCD expressions that are generated in `FeynArts`. The colour algebra hence is also solved before the evaluation with `Medusa`. The relevant formulae are given in Appendix A.1.

CHECKS FOR CONSISTENCY. As `Medusa` is still in the stage of development and testing, we perform various cross-checks on final and intermediate results. All calculations and testing routines are fully automated, including the export from `Mathematica` to `C++` for numerical evaluation. Thus, it has been possible to rerun and test the computational setup after each update of `Medusa` providing useful feedback for the developer.

Beta functions for the couplings and masses can be extracted from the renormalisation constants, for details see e. g. [102]. They are listed in Appendix A.3 and compared to the one-loop and two-loop results in [104] finding perfect agreement. All renormalisation constants are calculated from all vertices to test the `FeynArts` model file and to ensure that the SUSY, QCD and $\mathrm{SU}(2)_L$ relations between different vertices hold also beyond leading order. The finite pieces of one-loop integrals are additionally cross-checked with `FormCalc` [234] and `Package-X`. The corrections to the quartic Higgs couplings are further compared to the compact analytic expressions in [235]. Finally, it is analytically checked that the self-energies for charged and neutral Higgs fields yield the same results as expected in the unbroken phase of the MSSM.

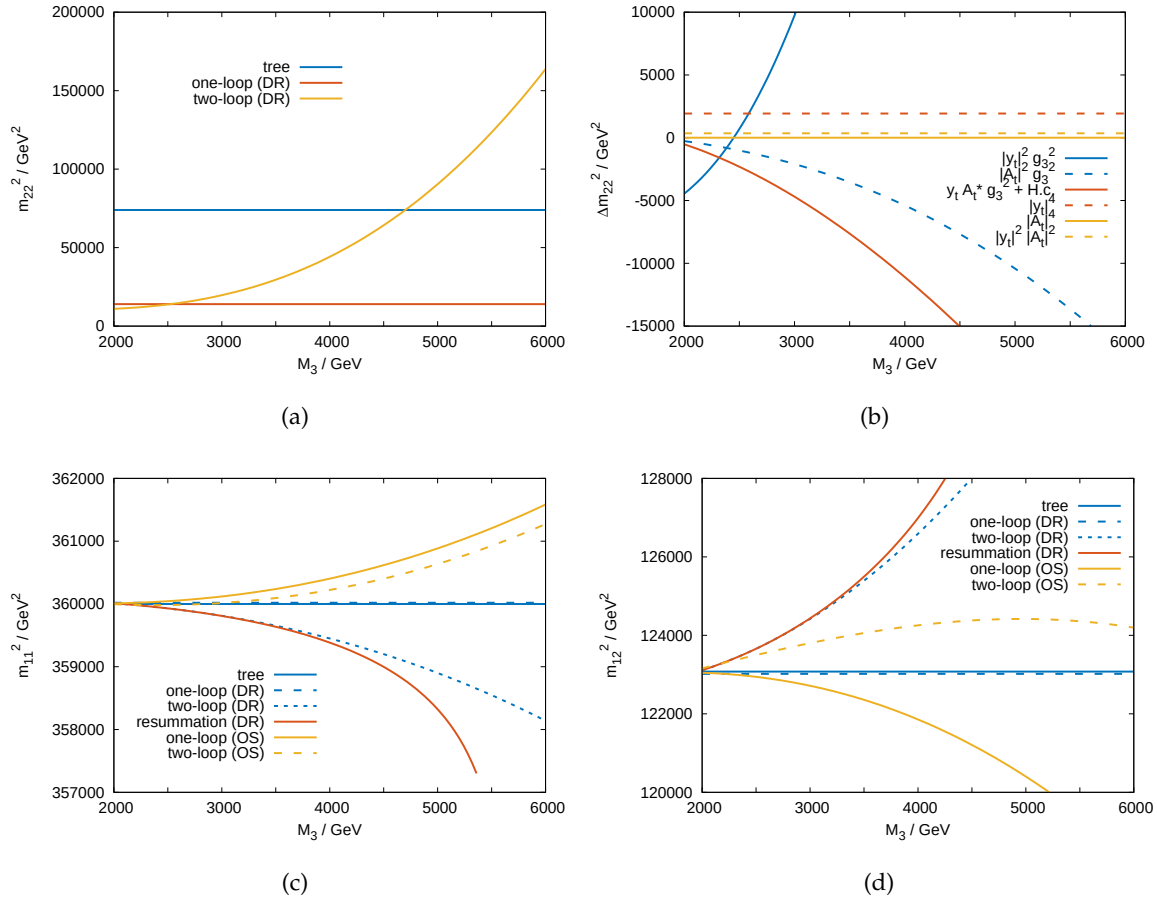

Figure 3.7: **Numerical results of the two-loop calculation.** The numerical input values are defined in eqs. (3.48)-(3.51). Figure 3.7a shows that the two-loop corrections to m_{22} are of comparable size as a the one-loop corrections for gluino masses of several TeV. The various two-loop contributions to m_{22} are compared to each other in Figure 3.7b. The two-loop corrections to m_{11} and m_{12} in Figures 3.7c and 3.7d, respectively, are of the order of percent for our choice of parameters. This is also the case if the top squarks are renormalised on-shell or if the $\overline{\text{DR}}$ contributions from gluino loops are resummed to all orders.

3.2.2 *Fixed order results for m_{ij}^2*

This section deals with the numerical results for the corrections to the mass parameters m_{ij}^2. For the corrections to the quartic couplings Δ_{ij} see the discussion of the Higgs masses in Section 3.2.6.

Figure 3.7a shows the one-loop and two-loop corrections to the mass parameter m_{22}^2 as a function of M_3 where the following input parameters have been used

The values for the couplings y_t and g_3 are the $\overline{\text{DR}}$ values at 1 TeV taken from Table 2.3.

$$y_t \sin\beta = 0.8651\,, \qquad g_3 = 1.004\,, \tag{3.48}$$
$$m_{11}^{\text{tree}} = 600\,\text{GeV}\,, \qquad m_{22}^{\text{tree}} = 272\,\text{GeV}\,, \tag{3.49}$$
$$m_R = 1300\,\text{GeV}\,, \qquad m_L = 1600\,\text{GeV} \tag{3.50}$$
$$|\mu| = 300\,\text{GeV}\,, \qquad \tan\beta = 5\,. \tag{3.51}$$

The choice of the renormalisation scale $\bar{\mu} = \sqrt{m_L\, m_R}$ is investigated in Section 3.2.5. These parameters evade bounds from experimental searches for stops, see e. g. [204] and for neutralinos if the bino and wino states are heavy enough to leave the higgsino states nearly degenerate at $\mu = 300\,\text{GeV}$, see e. g. [236].

For $M_3 < 3000\,\text{GeV}$, the two-loop correction are rather small compared to the one-loop corrections. For larger values of M_3, the two-loop corrections nonetheless become larger than the one-loop corrections. Figure 3.7b shows the different two-loop contributions. All non-QCD corrections at two-loop are small, i. e. at the level of view percent, compared to the one-loop results.

For $M_3 > 3000\,\text{GeV}$, the $g_3^2|y_t|^2$ contributions are largest in magnitude and of the order of the one-loop corrections. The $g_3^2|A_t|^2$ terms as well as the mixed $g_3^2 y_t A_t^\star + \text{H.c.}$ contributions are at the level of 10% of the one-loop corrections. The analytic result for the dominant contributions proportional to $g_3^2|y_t|^2 M_3^2$ also shows the scaling of the two-loop corrections with M_3^2

The dilogarithm is defined in eq. (A.12). For $M_3 \gg m_{L,R}$ we approximately have $\text{Li}_2(1) = \pi^2/6$.

$$\Delta m_{22}^2 = \frac{4\,N\,C_F\,g_3^2\,|y_t|^2\,M_3^2}{256\,\pi^4}\left(\left(2\log\left(\frac{M_3}{\bar{\mu}}\right)-1\right)\left(1+2\log\left(\frac{\bar{\mu}\,M_3}{m_L\,m_R}\right)\right)\right.$$
$$\left. + \text{Li}_2\left(1-m_L^2/M_3^2\right) + \text{Li}_2\left(1-m_R^2/M_3^2\right)\right)\,. \tag{3.52}$$

These contributions originate from gluino loops like in Figure 3.1a. For large values of M_3 they do not only become larger than the one-loop corrections but reappear at higher loop orders in perturbation theory, see Figure 3.1b.

Before we resum these large gluino contributions to all orders, let us note that the two-loop corrections to m_{11} and m_{12} are relatively small, i. e. at the percent level, see Figures 3.7c and 3.7d. These figures also anticipate the results of Section 3.2.3 where the gluino loops have

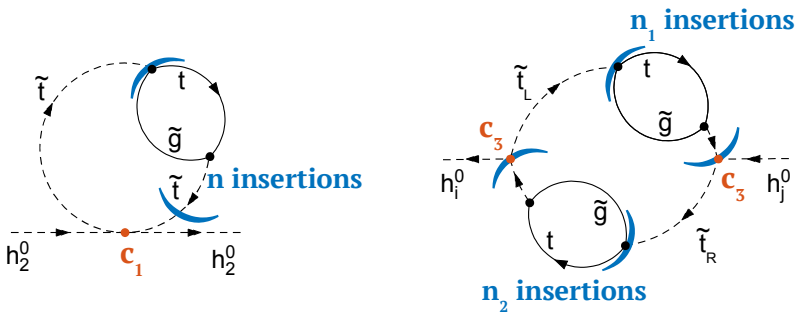

(a) Topology I (b) Topology II

Figure 3.8: **Topologies for the all-order resummed diagrams.** Blue brackets mark the repeated insertions of gluino-top-loops into the stop propagator. Topology I exists for both $\tilde{t}_L$ and $\tilde{t}_R$. Topology II includes both species of top squarks. The coupling constants c_1, c_2 and c_3 (in red) are given in Table 3.1 for the respective self-energies.

been resummed and those of Section 3.2.4 where the top squarks are renormalised on-shell. Also in this cases the contributions to m_{11}^2 and m_{12}^2 are much smaller than those to m_{22}^2.

3.2.3 *All-order resummation of the gluino contributions*

The gluino contributions that are recurring at all orders appear in two topologies, see Figure 3.8. In both topologies gluino-top-loops are inserted into the stop propagators. In Topology I, the top squarks couple to h_2 via the F-term proportional to $|y_t|^2$ and only one species of the top squarks is present, i. e. either $\tilde{t}_L$ and $\tilde{t}_R$. In Topology II, there are two arches of propagators, one with a left-handed and one with a right-handed stop. They couple to the external Higgs fields through trilinear scalar couplings: for h_2 that is A_t and for h_1 that is $\mu\, y_t^\star$. All couplings are encoded in the coefficients c_1, c_2 and c_3 where the latter one resembles all colour and Dirac factors from the gluino-top-subloop. The c_i are listed in Table 3.1 for the different contributions to the Higgs self-energies.

In all expressions, the integral measure is defined by

$$\int \mathrm{d}^d\tilde{k} = \mathrm{e}^{\gamma_E \varepsilon} \left(\frac{\bar{\mu}^2}{4\pi}\right)^{\varepsilon} \int \mathrm{d}^d k\,, \tag{3.53}$$

and we write m for the respective stop mass (m_L or m_R) and M for the gluino mass (M_3) to keep expressions short.

self-energy	correction to	$\hat{c}_1$	$\hat{c}_2$	$\hat{c}_3$
$h_1^0 \to h_1^0$	m_{11}^2	$\frac{-N\lvert y_t\rvert^2}{16\pi^2}$	$\frac{-4\,C_F\,g_3^2}{16\pi^2}$	$\frac{-N\lvert A_t\rvert^2}{16\pi^2}$
$h_1^0 \to h_2^{0,\star}$	m_{12}^2	0	$\frac{-4\,C_F\,g_3^2}{16\pi^2}$	$\frac{N\,y_t^\star\,\mu\,A_t}{16\pi^2}$
$h_2^0 \to h_2^0$	m_{22}^2	0	$\frac{-4\,C_F\,g_3^2}{16\pi^2}$	$\frac{-N\lvert y_t\rvert^2\lvert\mu\rvert^2}{16\pi^2}$

Table 3.1: **Coupling constants for different self-energies.** The coefficients c_1 and c_2 appear in Topology I while the coefficients c_2 and c_3 appear in Topology II, see Figure 3.8. For shortness, we define $\hat{c}_i = \pi^{d/2}\,c_i/(4\pi)^\varepsilon$. The colour factors are $N = 3$ and $C_F = 4/3$.

TOPOLOGY I. The first topology (Figure 3.8a) with n gluino-top-loops inserted corresponds to the loop integral

$$\Sigma_I^{(n)} = \int d^d\tilde{k}\,\frac{i\,c_1}{k^2-m^2}\left(\frac{i\,c_2}{k^2-m^2}\,J(k^2)\right)^n, \tag{3.54}$$

where $J(k^2)$ denotes the subloop with gluino and top quark

$$J(k^2) = \int d^d\tilde{q}\,\frac{q^2 - k\cdot q}{q^2\,((q-k)^2-M^2)}\,. \tag{3.55}$$

The function $J(k^2)$ is logarithmically divergent in the UV by power counting. But each insertion of $J(k^2)$ comes with a corresponding counterterm diagram that renormalises this subloop. The integral over k in eq. (3.54) is logarithmically divergent for $n = 1$ and UV finite for $n > 1$ because of the increasing number of propagators. Therefore an exact two-loop calculation is needed for $n = 1$ since nested divergences can appear resulting in double logarithmic terms, see eq. (3.52). For $n > 1$, our strategy is to extract those contributions from $J(k^2)^n$ that are large in the limit $m \ll M$. Afterwards the integration over k can be performed, yielding a UV finite result that can be summed to all orders. Thus the perturbative expansion is reorganised in powers of M and subleading logarithms $\log m/M$.

Moreover, $J(k^2)$ depends on two mass scales, k and M. Logarithms of the form $\log(m^2/M^2)$ therefore come from the kinematic region where $k \simeq m$. Expanding $J(k^2)$ around $k^2 = m^2$ gives

$$J(k^2) = \frac{i\,\pi^{d/2}}{(4\pi)^\varepsilon}\left(J_0 + (k^2-m^2)\,J_1 + (k^2-m^2)^2\,J_2 + \dots\right). \tag{3.56}$$

The coefficient functions J_i are determined by the small momentum expansion of two-point functions according to [237]

$$J_j = \frac{(4\pi)^\varepsilon}{i\,\pi^{d/2}}\,\frac{\Gamma(d/2)}{4^j\,\Gamma(j+1)\,\Gamma(j+d/2)}\left(\frac{\partial^2}{\partial k_\mu\cdot\partial k^\mu}\right)^j J(k^2)\Big|_{k^2=m^2}. \tag{3.57}$$

The d dimensional result for $J(k^2)$ can be obtained from its Feynman parameter representation

The hypergeometric function is defined in eq. (A.15).

$$\begin{aligned} J(k^2) =& \frac{\mathrm{i}\,\pi^{d/2}\,\mathrm{e}^{\gamma_\mathrm{E}\varepsilon}\,\bar{\mu}^{2\varepsilon}\,\Gamma(\varepsilon)}{2\,(1-\varepsilon)\,(4\pi)^\varepsilon\,\left(M^2\right)^{\varepsilon-1}} \\ & \times\left(1+\left(1-\tfrac{k^2}{M^2}\right)^{1-\varepsilon}\,{}_2\mathrm{F}_1\left(\varepsilon,1-\varepsilon;2-\varepsilon;-\tfrac{k^2}{M^2-k^2}\right)\right)\,. \end{aligned} \tag{3.58}$$

The coefficient functions J_i are calculated by taking the derivatives according to (3.57) and expanding the hypergeometric ${}_2\mathrm{F}_1$ function in ε with `HypExp`. The first four coefficient functions are

$$\begin{aligned} J_0 =& \frac{2M^2-m^2}{2\,\varepsilon}+\frac{1}{2}\left(3\,M^2-2\,m^2\right)+\left(M^2-\frac{m^2}{2}\right)\log\left(\frac{\bar{\mu}^2}{M^2}\right) \\ & -\frac{\left(M^2-m^2\right)^2}{2\,m^2}\log\left(\frac{M^2}{M^2-m^2}\right)+\mathcal{O}(\varepsilon)\,, \end{aligned} \tag{3.59}$$

$$J_1 = -\frac{1}{2\,\varepsilon}+\frac{1}{2}\left(\log\left(1-\frac{m^2}{M^2}\right)+\log\left(\frac{M^2}{\bar{\mu}^2}\right)\right)+\mathcal{O}(\varepsilon)\,, \tag{3.60}$$

$$J_2 = \frac{m^2-2M^2}{12\left(m^2-M^2\right)^2}+\mathcal{O}(\varepsilon)\,, \tag{3.61}$$

$$J_3 = -\frac{M^4}{24\left(m^2-M^2\right)^4}+\mathcal{O}(\varepsilon)\,. \tag{3.62}$$

The leading terms in J_0 are proportional to M^2 while the leading terms in J_1 depend logarithmically on M^2. J_2 is power suppressed by M^2 and each following coefficient function is supppressed by an additional power of M^2. For large M we therefore have

$$J_0 > m^2\,J_1 > m^4\,J_2 > \ldots \tag{3.63}$$

Figure 3.9 shows the expansion of $J(k^2)$ compared to the full result.

This expansion of $J(k^2)$ is inserted into $\Sigma_\mathrm{I}^{(n)}$ in eq. (3.54)

$$\begin{aligned} \Sigma_\mathrm{I}^{(n)} =& \int \mathrm{d}^d\tilde{\mathrm{k}}\,\frac{\mathrm{i}c_1}{k^2-m^2}\left(\frac{-\hat{c}_2}{k^2-m^2}\right)^n \\ & \times\left(\hat{J}_0+(k^2-m^2)\,\hat{J}_1+(k^2-m^2)^2\,\hat{J}_2+\ldots\right)^n\,, \end{aligned} \tag{3.64}$$

where $\hat{c}_i = \pi^{d/2}\,c_i/(4\pi)^\varepsilon$ and $\hat{J}_i$ denote the renormalised coefficient functions. For the moment, we will only consider the $\overline{\mathrm{DR}}$ scheme, where in $\hat{J}_i$ only the ε poles are subtracted from the coefficient functions J_i. The OS scheme will be discussed in Section 3.2.4.

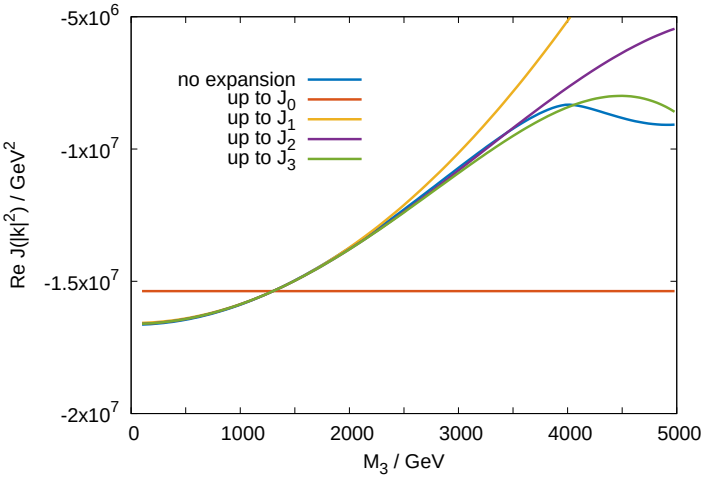

Figure 3.9: **Expansion of $J(k^2)$.** The plot shows the real part of $J(k^2)$ compared to expansion around $k^2 = m^2$. The coefficients of the expansion are given in eqs. (3.59)-(3.62). Numerical values from eq. (3.48) are used with $m = 1300\,\text{GeV}$, $M = 4000\,\text{GeV}$.

To perform the integration over k the integrand in eq. (3.64) is reorganised in powers of denominators resulting in one-loop vacuum integrals

$$\Sigma_{\text{I}}^{(n)} = \int \mathrm{d}^d\tilde{\mathrm{k}}\, \frac{\mathrm{i}c_1}{k^2-m^2}\left(\frac{-\hat{c}_2}{k^2-m^2}\right)^n \hat{J}_0^n \times\left(1+n(k^2-m^2)\frac{\hat{J}_1}{\hat{J}_0}+(k^2-m^2)^2\left(n\frac{\hat{J}_2}{\hat{J}_0}+n(n-1)\frac{\hat{J}_1^2}{\hat{J}_0^2}\right)+\dots\right). \tag{3.65}$$

The first term in the second line gives the leading contribution in powers of $\hat{J}_0/m^2 \propto M^2/m^2$. The loop integral for this term gives

$$\Sigma_{\text{I,1}}^{(n)} = \hat{c}_1\, m^2\, \mathrm{e}^{\gamma_{\text{E}}\varepsilon}\left(\frac{\bar{\mu}}{m}\right)^{2\varepsilon}\left(\frac{\hat{c}_2\hat{J}_0}{m^2}\right)^n \frac{\Gamma(n+\varepsilon-1)}{\Gamma(n+1)}\,, \tag{3.66}$$

which is UV finite for $n > 1$, as mentioned before. For $n > 1$, these contributions from all orders are summed

$$\Sigma_{\text{I,1}} = \sum_{n=2}^{\infty}\Sigma_{\text{I,1}}^{(n)} = \hat{c}_1\, m^2 \sum_{n=2}^{\infty}\xi^n\,\frac{\Gamma(n-1)}{\Gamma(n+1)} \tag{3.67}$$

$$= \hat{c}_1\, m^2\,\left(\xi+(1-\xi)\log(1-\xi)\right)\,, \tag{3.68}$$

with $\xi = \hat{c}_2\,\hat{J}_0/m^2$.

The second term in the second line of eq. (3.65) resembles the next-to-leading contribution in the powercounting of M. It has an additional combinatorical factor of n since the power in eq. (3.64) contains n terms

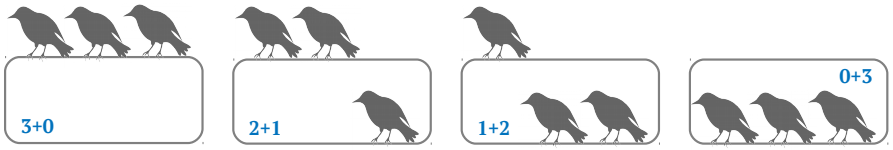

Figure 3.10: **Combinatorics of three indistinguishable birds on two wires.** The case for $n = 3$ is depicted above. For placing n birds on two wires one has $n + 1$ possibilities since there can be $0, 1, 2, \ldots n$ birds on the upper wire, corresponding to also $n, n-1, \ldots, 0$ birds on the lower wire.

of the form $J_1 J_0^{n-1}$. The integration over k gives for the second term in eq. (3.65)

$$\Sigma_{\mathrm{I},2}^{(n)} = (\mathrm{i}c_1)\,(-\hat{c}_2)^n \frac{n\,\hat{J}_1}{\hat{J}_0}\,\hat{J}_0^n \int \mathrm{d}^d\tilde{k}\,\frac{1}{(k^2-m^2)^n} \tag{3.69}$$

$$= -\hat{c}_1\,m^2\,\frac{\mathrm{e}^{\gamma_\mathrm{E}\varepsilon}\,\bar{\mu}^{2\varepsilon}}{m^{2\varepsilon}} \left(\frac{\hat{J}_1 m^2}{\hat{J}_0}\right) \left(\frac{\hat{c}_2\hat{J}_0}{m^2}\right)^n \frac{n\;\Gamma(n+\varepsilon-2)}{\Gamma(n)}\,. \tag{3.70}$$

The result is UV finite for $n > 2$. We note that the nested divergencies for $n = 2$ can only be resolved in a complete three-loop calculation. Hence we sum all terms starting with $n = 3$

$$\Sigma_{\mathrm{I},2} = \sum_{n=3}^{\infty} \Sigma_{\mathrm{I},2}^{(n)} = -\hat{c}_1\,m^2\,\chi_1\,\xi\,\big(\xi + (1-2\xi)\log(1-\xi)\big)\;, \tag{3.71}$$

with the additional abbreviation $\chi_i = (m^2)^i\,\hat{J}_i/\hat{J}_0$.

Analogously, the third term of eq. (3.65) is integrated over k and gives a UV finite result for $n > 3$. Resumming these contributions to all orders gives

$$\Sigma_{\mathrm{I},3} = \hat{c}_1\,m^2\,\xi^2 \Bigg(\Big(2\chi_2 - \frac{\chi_1^2(\xi-2)}{1-\xi}\Big)\xi + \Big((2-3\xi)\chi_2 + \chi_1^2(2-6\xi)\Big)\log(1-\xi)\Bigg)\,. \tag{3.72}$$

TOPOLOGY II. In the second topology (Figure 3.8b), there are n_1 gluino-top-loop insertions on the upper stop propagator with mass m_R and n_2 on the lower stop propagator with mass m_L. The corresponding loop integral therefore is

$$\int \mathrm{d}^d\tilde{k}\,\frac{\mathrm{i}\,c_3}{(k^2-m_R^2)((k+p)^2-m_L^2)} \left(\frac{\mathrm{i}\,c_2\,J(k^2)}{(k^2-m_R^2)}\right)^{n_1} \left(\frac{\mathrm{i}\,c_2\,J((k+p)^2)}{(k+p)^2-m_L^2}\right)^{n_2}\,.$$

Expanding to leading order in the external momentum p and neglecting the mass splitting between m_R and m_L simplifies this topology to

$$\Sigma_{\mathrm{II}}^{(n)} = (n+1)\int \mathrm{d}^d\tilde{k}\,\frac{\mathrm{i}\,c_3}{(k^2-m^2)^2} \left(\frac{\mathrm{i}\,c_4\,J(k^2)}{k^2-m^2}\right)^n\,, \tag{3.73}$$

with $n = n_1 + n_2$ and $m = (m_L + m_R)/2$. The combinatorical factor $n+1$ counts the possibilities to distribute n gluino-top-loops on both propagators, see Figure 3.10.

In comparison to Topology I there is one additional propagator and the factor $n+1$ that has to be considered in the summation. We therefore adopt the same strategy as in the previous case and expand $\Sigma_{\text{II}}^{(n)}$ in terms of the coefficient functions J_i analogously to eq. (3.65)

$$\Sigma_{\text{II}}^{(n)} = (n+1) \int \mathrm{d}^d\tilde{k}\, \frac{\mathrm{i}c_3}{(k^2-m^2)^2} \left(\frac{-\hat{c}_2}{k^2-m^2}\right)^n \hat{J}_0^n \times \left(1 + n(k^2-m^2)\frac{\hat{J}_1}{\hat{J}_0} + (k^2-m^2)^2\left(n\frac{\hat{J}_2}{\hat{J}_0} + n(n-1)\frac{\hat{J}_1^2}{\hat{J}_0^2}\right) + \dots\right) . \tag{3.74}$$

The integral over the first term gives

$$\Sigma_{\text{II},1}^{(n)} = -\hat{c}_3\, \mathrm{e}^{\gamma_{\text{E}}\varepsilon}\, (n+1) \left(\frac{\bar{\mu}}{m}\right)^{2\varepsilon} \left(\frac{\hat{c}_2\hat{J}_0}{m^2}\right)^n \frac{\Gamma(n+\varepsilon)}{\Gamma(n+2)} . \tag{3.75}$$

Although the integral is UV finite for $n \geq 1$ the sum must start at $n = 2$ to avoid double counting the two-loop contribution

$$\Sigma_{\text{II},1} = \sum_{n=2}^{\infty} \Sigma_{\text{II},1}^{(n)} = -\hat{c}_3 \sum_{n=2}^{\infty} \xi^n \frac{(n+1)\,\Gamma(n)}{\Gamma(n+2)} = -\hat{c}_3\, (\xi + \log(1-\xi)) , \tag{3.76}$$

where $\xi = \hat{c}_2\hat{J}_0/m^2$ as before.

Analogous to Topology I, integration and summation for the second term of eq. (3.74) yield

$$\Sigma_{\text{II},2} = -\hat{c}_3\, \frac{\chi_1\,\xi}{\xi-1} \Big(\xi(3\,\xi-2) + 2\,(\xi-1)\,\log(1-\xi)\Big) . \tag{3.77}$$

The result for the third term of eq. (3.74) finally is

$$\begin{aligned}\Sigma_{\text{II},3} = \hat{c}_3\,\xi \Bigg(&\frac{\xi}{(1-\xi)^2}\Big(\chi_1^2\,\xi\,(6 - 19\,\xi + 12\,\xi^2) \\ &- \chi_2\,(2 - 9\,\xi + 13\,\xi^2 - 6\,\xi^3)\Big) \\ &+ \Big(6\,\chi_1^2\,\xi + \chi_2(6\,\xi - 2)\Big)\log(1-\xi)\Bigg) .\end{aligned} \tag{3.78}$$

NUMERICAL RESULTS. Recalling the fact that the resummation sums terms starting at three-loop and including the fixed order re-

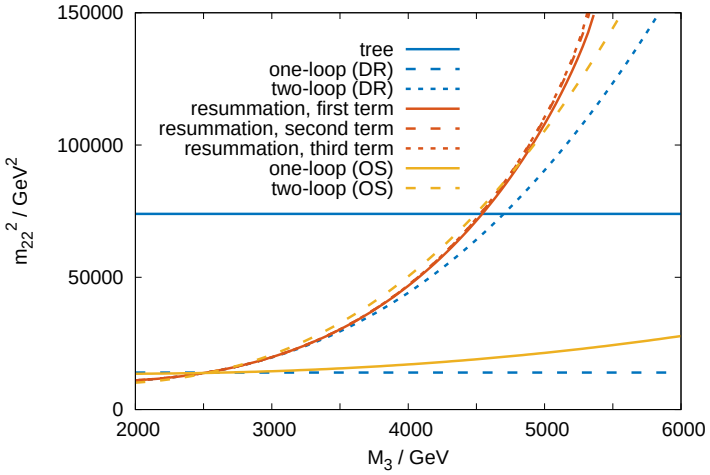

Figure 3.11: **Numerical comparison of the different schemes.** The plot shows the fixed order results up to two-loop and the all order resummed contributions to m_{22}^2, see Section 3.2.3. In the OS scheme *only* the stops are renormalised on-shell and for comparison with the $\overline{\text{DR}}$ scheme the stop masses are converted from the $\overline{\text{DR}}$ to the OS scheme, see Section 3.2.4.

sults of the previous section, we have for the corrections to the mass parameters

$$\begin{aligned} m_{ij}^2 = m_{ij}^{2,\text{tree}} &- \hat{\Sigma}_{ij}^{\text{one-loop}} - \hat{\Sigma}_{ij}^{\text{two-loop}} \\ &- \Sigma_{\text{I},1}^{(ij)}(m = m_R) - \Sigma_{\text{I},2}^{(ij)}(m = m_R) - \Sigma_{\text{I},3}^{(ij)}(m = m_R) \\ &- \Sigma_{\text{I},1}^{(ij)}(m = m_L) - \Sigma_{\text{I},2}^{(ij)}(m = m_L) - \Sigma_{\text{I},3}^{(ij)}(m = m_L) \\ &- \Sigma_{\text{II},1}^{(ij)} - \Sigma_{\text{II},2}^{(ij)} - \Sigma_{\text{II},3}^{(ij)} \,. \end{aligned} \tag{3.79}$$

Note that for the first topology, denoted by $\Sigma_{\text{I}}^{(ij)}$, the contributions of both species of top squarks need to be added, while in the second topology, $\Sigma_{\text{II}}^{(ij)}$, both species are already included. Figure 3.11 shows the numerical results as function of M using the parameters from eqs. (3.48)-(3.51). Compared to the two-loop result, the resummed results grow even faster with M. The first terms of the resummation give the largest additional contribution while the contribution of the second term is comparably small. The difference of the second and third term, however, is hardly recognisable in the plot. Hence the expansion converges well for the given set of parameters.

CONVERGENCE AND VALIDITY. For both topologies, the expansion and resummation depends on three assumptions which we like to evaluate in the light of the numerical results.

Firstly, the self-energy insertions are expanded around $k^2 = m^2$ to extract logarithms of the form $\log m/M$. Other kinematic regions of

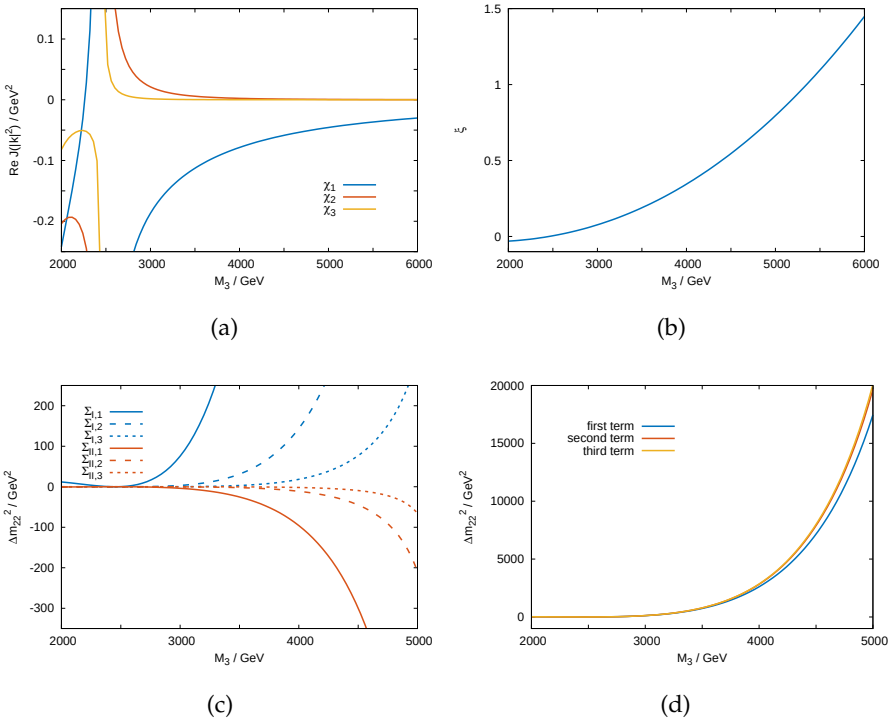

(a) (b)

(c) (d)

Figure 3.12: **Numerical evaluation of the expansion parameters.** The input values for y_t and g_3 are those of eq. (3.48) and $m = 1300\,\text{GeV}$. The upper plots show the expansion parameters $\chi_i = m^2 J_0 / J_i$ (Figure 3.12a) and $\xi = \hat{c}_2 \hat{J}_0 / m^2$ (Figure 3.12b) as a function of M. The lower plots show the relative (Figure 3.12a) and absolute (right) size of the terms in the expansion and resummation of Section 3.2.3.

the loop integrals do not contribute to these logarithmic terms and therefore are not parametrically enhanced.

Secondly, the powers of the coefficient functions J_i in eq. (3.64) have been rearranged assuming that $\hat{J}_0 > m^2 \hat{J}_1 > m^4 \hat{J}_2 > \dots$ In other words, we have assumed that the series of the expansion parameters $\chi_i = m^2 \hat{J}_i / \hat{J}_0$ converges fast enough. Numerically, this is verified in Figure 3.12a for the first three terms in the expansion. For the given set of parameters, χ_1 still is of the order of percent but the higher order terms are rather small for values of M larger than 3000 GeV.

Thirdly, the powers of $J_0 \propto M^2$ are summed to all orders, resulting in logarithms of the form

$$\sum_{n=1}^{\infty} \xi^n / n = -\log(1-\xi)\,. \tag{3.80}$$

This series converges for $\xi = \hat{c}_2 \hat{J}_0 / m^2 < 1$. But ξ scales proportional to M^2, see Figure 3.12b. Hence there is a maximal value of M_{max} for that the series converges. For the given set of parameters, that is $M_{\text{max}} \approx 5.4\,\text{TeV}$. By reconstructing the imaginary part of ξ from the

branch cut of $J(k^2)$ for $k^2 > M^2$ one can analytically continue these logarithms to the region outside the disc with $|\xi| < 1$. This allows the expansion to be valid beyond $M_{\text{max}} \approx 5.4\,\text{TeV}$.

Nevertheless, let us restate this issue from a different perspective: We have explicitly demonstrated that for large mass hierarchies between M_3 and m_L, m_R, the application of the $\overline{\text{DR}}$ scheme leads to large corrections that demand an all order resummation.

3.2.4 *The top squark mass*

Since the resummation sums the renormalised subloops $\hat{J}_0$, the question of how the resummation depends on the renormalisation scheme arises. Let us for instructional purposes go back to eq. (3.54) now performing the summation before the integration

This equation is practically nothing else but Dyson resummation.

$$\sum_{n=0}^{\infty} \frac{1}{k^2 - m^2} \left(\frac{\mathrm{i}\, c_2\, J(k^2)}{k^2 - m^2} \right)^n = \frac{1}{k^2 - m^2 - \hat{c}_2 \left(\hat{J}_0 + (k^2 - m^2)\hat{J}_1 + \dots \right)} ,$$

where again the hats on top of variables denote renormalised quantities. Writing the integrals of the previous section in this form would make them quite hard to evaluate. In this way it should become clearer, what the implications of the renormalisation scheme for the top squark mass m are. In an OS scheme, the conditions for pole and residue of the resummed propagator yield $\hat{J}_0 = 0 = \hat{J}_1$. Regarding the resummation of the previous section, this implies that there are no higher order terms of the form $\hat{J}_0^n$ that need to be resummed. As a major result of this chapter, we conclude that in case of a heavy gluino the OS scheme should be applied for top squarks in order to avoid resumming large corrections from all orders.

SCHEME CONVERSION. Having in mind a high-scale scenario where the stop masses are set, it is useful to translate between the $\overline{\text{DR}}$ and the OS scheme. Assuming the stop masses are evolved from a high scale, the $\overline{\text{DR}}$ scheme is the obvious choice for the renormalisation group evolution. The contributions to the Higgs potential and low-energy observables should be calculated using the OS definition of the stop mass. For this conversion the scheme difference of the stop masses Δm^2 is needed. Since the bare mass m_0 is the same in both schemes, Δm^2 is given by the difference of the counterterms

$$\begin{aligned} \Delta m^2 &= m^{2,\text{OS}} - m^{2,\overline{\text{DR}}} \\ &= m_0^2 + \delta m^{2,\text{OS}} - m_0^2 - \delta m^{2,\overline{\text{DR}}} \\ &= \delta m^{2,\text{OS}} - \delta m^{2,\overline{\text{DR}}} . \end{aligned} \tag{3.81}$$

The scheme difference is always UV finite because UV divergences are universal for all renormalisation schemes.

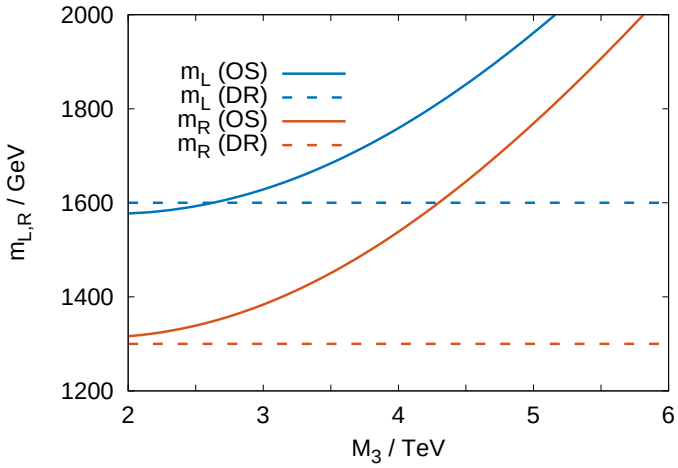

Figure 3.13: **Scheme dependence of the stop mass as function of the gluino mass M_3.** The gluino contributions can shift the OS stop masses by several hundreds of GeV compared to the $\overline{\text{DR}}$ mass parameters. The numerical input values are defined in eqs. (3.48)-(3.51).

For heavy gluinos the leading terms proportional to M_3^2 in Δm^2 are

$$\Delta m^2 = \frac{g_3^2}{6\,\pi^2}\Bigg(- m^2\,\log\Big(\frac{M_3^2}{m^2}\Big) - 3\,M_3^2 + 2\,M_3^2\,\log\Big(\frac{M_3^2}{\bar{\mu}^2}\Big) + M_3^2\Big(2 - \frac{M_3^2}{m^2}\Big)\,\log\Big(1 - \frac{m^2}{M_3^2}\Big)\Bigg)\,, \tag{3.82}$$

We have checked that this result coincides with the corresponding terms $\propto M_3^2$ of $(-\hat{c}_2\hat{J}_0)$ in eq. (3.59).

for $m = m_L,\, m_R$. We note that in all calculations the complete one-loop result for the stop mass counterterm is used rather than the leading terms only.

Figure 3.13 shows the on-shell masses of the top squarks as function of the $\overline{\text{DR}}$ masses and the gluino mass M_3. The given set of parameters (eqs. (3.48)-(3.51)) is especially interesting. As we recall from the beginning of this chapter bounds from direct searches typically exclude scenarios with stop masses below 1 TeV. Collider experiments, however, test the physical masses. Figure 3.13 shows that $\overline{\text{DR}}$ masses can be several hundreds of GeV lower than the on-shell masses if the gluino is heavy enough. It is an important result that in case of hierarchical SUSY spectra the renormalisation scheme difference must be kept in mind when confronting theory to collider experiments.

In Section 3.2.2, the two-loop contributions to the Higgs mass parameters have been calculated in the $\overline{\text{DR}}$ scheme. The yellow curves in Figure 3.11 show the same calculation with the top squarks renor-

malised on-shell. To compare both results the OS result is expanded in terms of the $m_{L,R}^{2,\overline{\text{DR}}}$. To leading order in g_3^2 we have

$$\begin{aligned} f(m^{2,\text{OS}}) &= f(m^{2,\overline{\text{DR}}} + \Delta m^2) \\ &= f(m^{2,\overline{\text{DR}}}) + \Delta m^2 \, \frac{\mathrm{d}f(m^{2,\overline{\text{DR}}})}{\mathrm{d}m^{2,\overline{\text{DR}}}} + \mathcal{O}(g_3^4) \, . \end{aligned} \tag{3.83}$$

For the two-loop results the scheme difference is formally of three loop order and is consequently not included. For the one-loop result f is formally of the same order as a two-loop result and therefore included. That is why the one-loop OS result in Figure 3.11 has a dependence on M_3. Figure 3.11 also shows the resummed contributions in the $\overline{\text{DR}}$ scheme. For moderately large gluino masses, the OS result numerically reproduces the resummed result but also turns out to be numerically stable around $M_3 > 5400\,\text{GeV}$, where the expansion parameter ξ becomes larger than one, as can be seen in Figure 3.12b.

In most computations it will be more convenient to numerically calculate the OS stop mass from the SUSY spectrum and use this value, e. g. to compute flavour observables. As an application of these techniques kaon mixing is considered in Section 3.4.

It has already been mentioned that heavy gluinos can have large two-loop effects on the mass parameters m_{ij}^2 proportional to M_3^2, see e. g. [238] and that these corrections can partially be absorbed in the OS scheme, see e. g. [239]. The corrections to dimensionless couplings as well as to the Higgs mass, however, in this case are logarithmic in M_3, see e. g. [240, 241]. Our resummation performed in Section 3.2.3 explicitly shows that when working in the $\overline{\text{DR}}$ scheme the corrections from higher orders in perturbation theory actually make the situation worse and that these corrections are absent in the OS scheme. Interestingly, in [242] it is mentioned that corrections from a heavy gluino are *critical* in terms of the little hierarchy problem because they lift the stop masses. The authors of [242] also note, that in a numerical study the fine-tuning can become smaller if $M_3 > m_{L,R}$. Nonetheless, in Section 3.3 we will show that this scenario can in contrast be helpful concerning the little hierarchy problem.

3.2.5 *The choice of the renormalisation scale*

In the previous sections, the contributions to the mass parameters in the Higgs potential m_{ij}^2 from eq. 3.3 have been calculated. From the EFT perspective, all SUSY particles were integrated out at once at the matching scale $\bar{\mu} = \sqrt{m_L m_R}$. As there are two separate mass scales, namely that of the top squarks and that of the gluino, that choice of the renormalisation scale is not obvious. This ambiguity also concerns the mass scale at which the couplings g_3 and y_t are evaluated.

As a consequence we will study the influence on the matching scale $\bar{\mu}$. We will do so by first integrating out the gluino at its mass

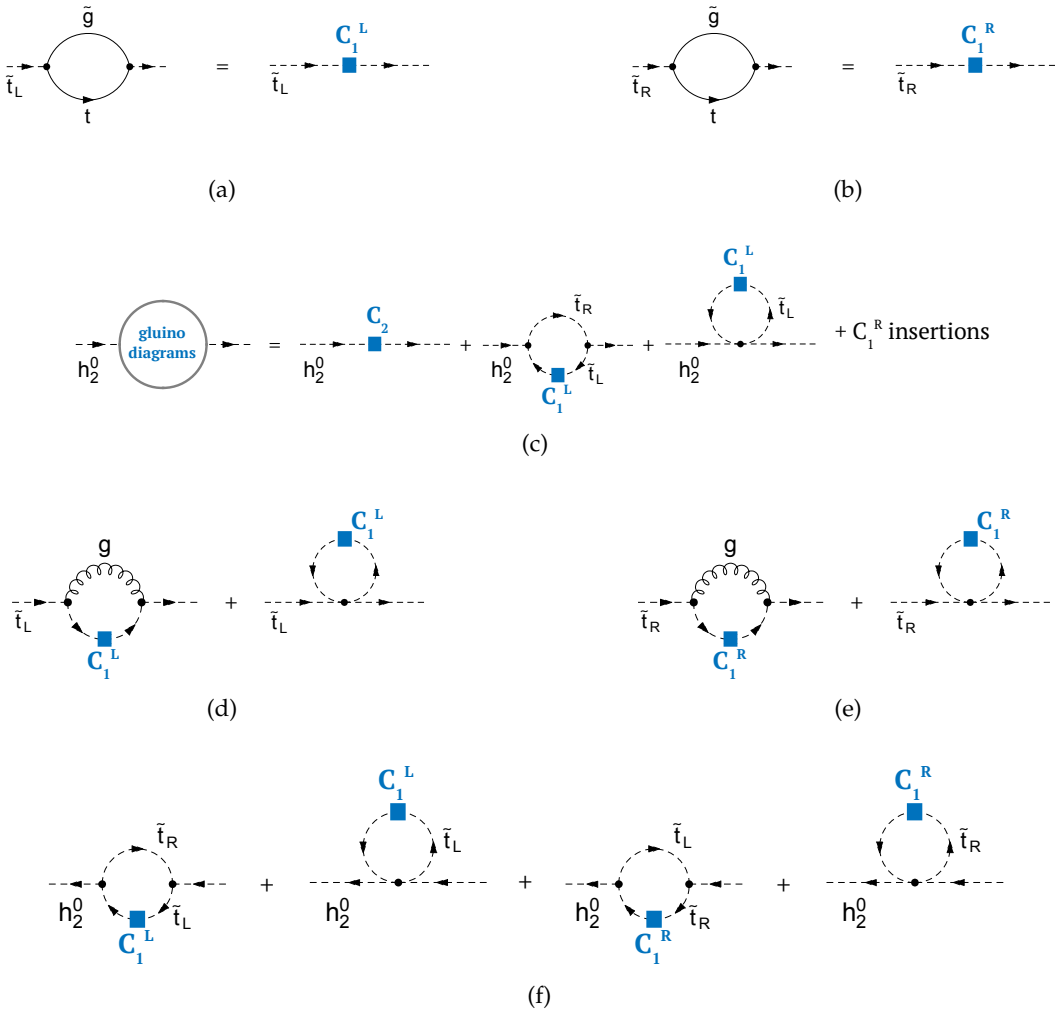

Figure 3.14: **Contributions to the matching of $C_1^{L,R}$ and C_2 and their respective anomalous dimensions.** Figures 3.14a-3.14c show the matching conditions for the Wilson coefficients C_1^L, C_1^R and C_2, respectively. The C_1^R insertions in Figure 3.14c are the same as the ones for C_1^L with $\tilde{t}_L$ replaced by $\tilde{t}_R$. Figures 3.14d-3.14f depict the contributions to the anomalous dimensions of C_1^L, C_1^R and C_2, respectively. For clarity, counterterm diagrams are not shown.

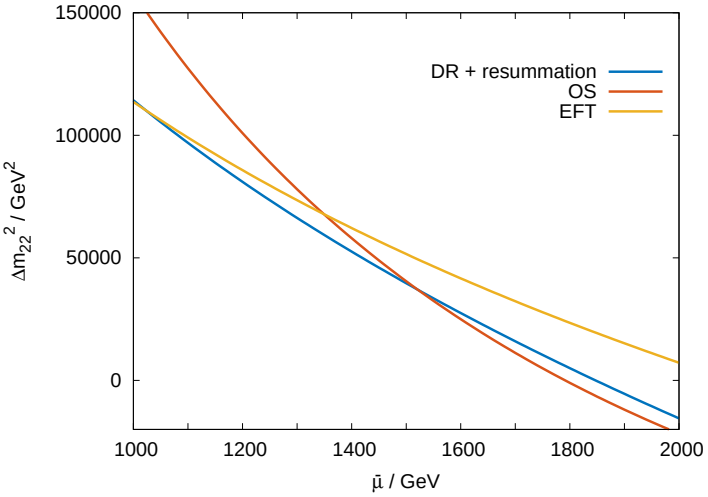

Figure 3.15: **Comparison of the matching procedures.** The two-loop corrections to m_{ij}^2 are compared to each other regarding the matching scale $\bar{\mu}$. The matching in Sections 3.2.2-3.2.4 is performed at once whereas the EFT result of Section 3.2.5 integrates out the gluino and top squarks at separate scales.

scale. Afterwards we study the renormalisation group of the effective couplings generated from integrating out the gluino. We then perform the matching to m_{ij}^2 at the scale $\bar{\mu}$ and compare the results to the matching procedure of the previous sections. Both procedures are illustrated in Figure 3.2.

If the gluino is integrated out at the scale M_3, it generates effective mass terms for the top squarks and the Higgs field. In the following, let us treat them as effective vertices described by the effective Hamiltonian

$$\mathcal{H}_{\text{eff.}} = C_1^L \, \tilde{t}_L^\star \tilde{t}_L + C_1^R \, \tilde{t}_R^\star \tilde{t}_R + C_2 \, h_2^{0,\star} h_2^0 \, . \tag{3.84}$$

The Wilson coefficients $C_1^{L,R}$ and C_2 have mass dimension two and are defined by the matching conditions sketched diagrammatically in Figures 3.14a-3.14c. In addition to the shown diagrams also the corresponding counterm diagrams contribute, i. e. the matching is performed between renormalised theories. For C_1^L and C_1^R we have, at the matching scale $\bar{\mu} = M_3$

$$C_1^L(\bar{\mu} = M_3) = \frac{4\, C_F \, g_3^2}{16\, \pi^2} \, M_3^2 = C_1^R(\bar{\mu} = M_3) \, . \tag{3.85}$$

See [243] for a pedagogical introduction to the application of effective operators in the context flavour physics.

The dominant two-loop contributions to C_2 are the same as in eq. (3.52). Below M_3 the RGEs of the Wilson coefficients are

$$\bar{\mu} \frac{\mathrm{d}}{\mathrm{d}\bar{\mu}} \vec{C}(\bar{\mu}) = \gamma^T \vec{C}(\bar{\mu}) \, . \tag{3.86}$$

The vector of Wilson coefficients is $\vec{C}^T = (C_1^L, C_1^R, C_2)$ and γ is the anomalous dimension matrix of the corresponding operators. It can be calculated from the diagrams in Figures 3.14d-3.14f

$$\gamma = \begin{pmatrix} 0 & † & \gamma_0 \\ † & 0 & \gamma_0 \\ * & * & 0 \end{pmatrix}, \qquad \text{with } \gamma_0 = -\frac{2\,N\,|y_t|^2}{16\,\pi^2}\,. \tag{3.87}$$

Note that the ε poles of the diagrams in Figures 3.14d and 3.14e exactly cancel each other and therefore yield no QCD contribution the anomalous dimension matrix. The entries in eq. (3.87) that are labelled with a star ($*$) are of the order $|y_t|^4\,g_3^2$ and therefore not relevant for the discussion of the matching scale. The same holds for those entries labelled with a dagger (†) that mainly induce operator mixing of the $C_1^{L,R}$ but are not enhanced by M_3^2.

Below M_3, there is no renormalisation group running of C_1^L and C_2^R to leading order in $|y_t|^2$ and hence

$$C_1(\bar{\mu}) = C_1(\bar{\mu} = M_3)\,, \qquad C_2(\bar{\mu}) = C_2(\bar{\mu} = M_3)\,. \tag{3.88}$$

The operator mixing with C_1^L and C_1^R induces the RGE running of C_2

$$C_2(\bar{\mu}) = C_2(M_3) + \Big(C_1^L(M_3) + C_1^R(M_3)\Big) \int_{\log M_3}^{\log \bar{\mu}} \mathrm{d}\log\mu\;\gamma_0\,. \tag{3.89}$$

The integral measure can be rewritten in terms of y_t using the beta function $\beta_{y_t} = \frac{\mathrm{d}\,y_t}{\mathrm{d}\log\bar{\mu}} = y_t\,(6\,y_t^2 - 16\,g_3^2/3)/16\pi^2 = \beta_0\,y_t$

$$C_2(\bar{\mu}) = C_2(M_3) + \Big(C_1^L(M_3) + C_1^R(M_3)\Big) \int_{y_t(M_3)}^{y_t(\bar{\mu})} \mathrm{d}y_t\;\frac{\gamma_0}{y_t\,\beta_0}\,. \tag{3.90}$$

In perturbation theory, C_1^L and C_1^R are of the order of g_3^2. The matching is correct up to order $y_t^2\,g_3^2$. β_0 and γ_0 are consequently expanded to order in y_t^2, resulting in $\gamma_0/\beta_0 = -1$

$$C_2(\bar{\mu}) = C_2(M_3) - \Big(C_1^L(M_3) + C_1^R(M_3)\Big)\log\frac{y_t(\bar{\mu})}{y_t(M_3)}\,. \tag{3.91}$$

$\log\frac{y_t(\bar{\mu}=1\,\mathrm{TeV})}{y_t(\bar{\mu}=3\,\mathrm{TeV})} = 0.047$.

Numerically, the running of y_t is of the order of few percent as can be seen from the data in Table 2.3.

In a second matching step, the corrections to m_{22}^2 are calculated at the renormalisation scale $\bar{\mu}$. The calculation is the same as in the previous sections except for the diagrams with gluinos. These are now replaced by the diagrams with insertions of the effective couplings $C_1^{L,R}$ and C_2. These diagrams also appear in the matching condition for C_2, see Figure 3.14c. Despite that, these diagrams are now evaluated at the renormalisation scale $\bar{\mu}$ rather than at M_3.

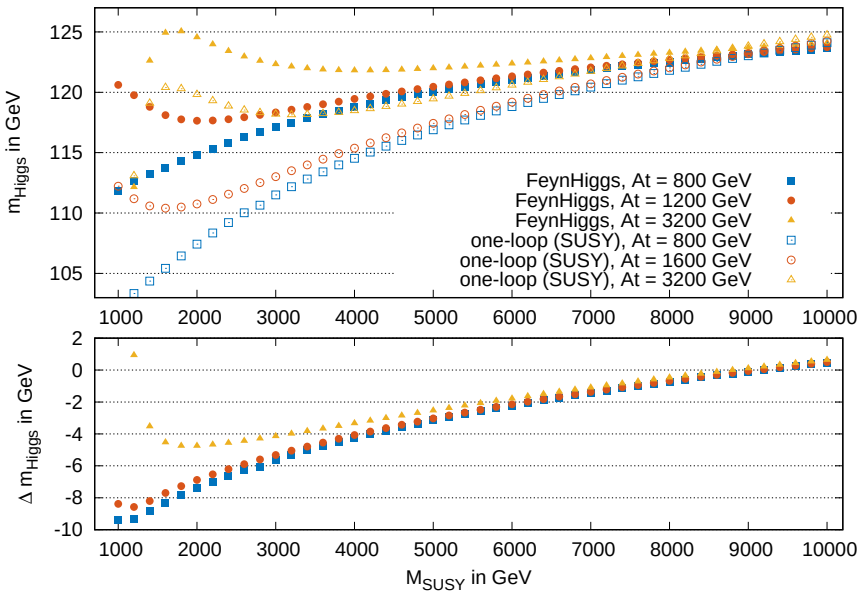

Figure 3.16: **Comparison of the Higgs mass calculation.** In the upper plot, results obtained with FeynHiggs ("FH") are compared to our one-loop SUSY corrections. In the lower plot, the difference to between both result is given. For larger values of M_{SUSY} the logarithmic terms dominate the result and are correctly reproduced by our calculation. The input values are given in eqs.(3.92)-(3.94)

Using the same parameters as in eqs. (3.48)-(3.51) and additionally $M_3 = 3\,\text{TeV}$, the results of this section are compared to the results of the previous sections for different values of $\bar{\mu}$. Figure 3.15 shows that for $\bar{\mu} = \sqrt{m_L m_R} = 1.44\,\text{TeV}$ the results of the previous sections are in accordance with the twofold matching and RGE evolution of this section which is additionally less dependent on the matching scale $\bar{\mu}$. The schemes differ by about a factor of 10% from each other.

From eq. (3.91) we can further conclude that all gluino interactions are to be evaluated at the scale of M_3. For our analysis of the fine-tuning we will therefore use $g_3 = g_3(M_3)$ even if all SUSY particles are integrated out at once.

3.2.6 *The mass of the lightest CP even Higgs boson*

As we have discussed in Section 3.1, the mass of the lightest CP even Higgs boson in the MSSM is at tree-level bounded by the Z mass, $m_h \leq |\cos 2\beta|\, M_Z$. In order to identify this boson with the SM Higgs boson, rather large loop corrections are needed. These corrections are dominated by the stop masses and the stop mixing $X_t = A_t - \mu \cot\beta$ which are also relevant for the discussion of fine-tuning where we include an approximation for the Higgs mass as important constraint.

The precise determination of the mass of the Higgs bosons in the MSSM has been a productive field of study for many years. Full one-loop [244–247] and two-loop results [239, 248–264] and partial three-loop [265–267] results have been calculated in a diagrammatic approach. Furthermore there are EFT calculations [238, 268–274] where the contributions of heavy SUSY particles are treated as corrections to the parameters in the Higgs potential. For comparisons of those methods see e. g. [275, 276].

Due to the relevance of the loop corrections to m_h in the MSSM, they can hardly be neglected in a numerical study of the fine-tuning in the MSSM. In our approach the mass of the CP even Higgs bosons is given by eq. (3.16). The loop corrections to the mass parameters m_{ij}^2 have already been discussed in the previous section. The corrections to the quartic couplings Δ_{ij} are calculated at the one-loop level including now a finite top mass $m_t^{\text{pole}} = 173.1 \pm 0.9\,\text{GeV}$ [202]. We do not consider RGE running of the Δ_{ij} and therefore choose the renormalisation scale to be $\bar{\mu} = m_t$. The dominant contributions then are of the form $\log m_{L,R}^2 / m_t^2$ and are checked analytically with the compact expressions in [235]. This also provides a useful check of our computational setup.

Our approach is still only an estimation since electro-weak corrections and corrections from the finite VEVs, besides m_t, are not taken into account. Hence we compare our numerical results to those of `FeynHiggs-2.14.3` [247, 248, 277–281] in order to quantify these uncertainties.

For the comparison the following strategy is adopted: `FeynHiggs` uses M_Z and the mass of the CP odd Higgs boson m_A as input. For this reason, we fit the $\overline{\text{DR}}$ parameters m_{11}^2 and m_{22}^2 to M_Z and m_A, which in our setup are obtained by eqs. (3.9) and (3.15). For the global scan we export the analytical expressions from `Mathematica` to `C++`. Dilogarithms are evaluated with the GNU Scientific Library [282]. For the fitting routines the `ISRES` algorithms [194, 195] from the `C++` implementation of the `NLopt2.4.2` library [196] is used.

The masses of the CP even Higgs bosons are given by the eigenvalues of the mass matrix given in eq. (3.16). The following input parameters are used

$$m_A = 800\,\text{GeV}\,, \qquad |\mu| = 400\,\text{GeV}\,, \tag{3.92}$$

$$\tan\beta = 5\,, \qquad M_1 = 100\,\text{GeV}\,, \tag{3.93}$$

$$M_2 = 100\,\text{GeV}\,, \qquad M_3 = 1000\,\text{GeV}\,. \tag{3.94}$$

The parameters M_1 and M_2 are mandatory for the usage of FeynHiggs. Their value is chosen small to avoid large contributions from this sector.

We further keep the mass splitting $m_L - m_R = 200\,\text{GeV}$ fixed and vary A_t and $M_{\text{SUSY}} = \sqrt{m_L m_R}$ as shown in Figure 3.16. The stop masses are given in the $\overline{\text{DR}}$ scheme. For comparison, only the contribution from top and stop quarks are included at the one-loop level when calling `FeynHiggs`. Thus contributions from finite momenta in the propagator, resummed logarithms and RGE running of the top quark mass as well as CP violation are neglected. Figure 3.16 finally shows

These options are set calling `FeynHiggs` with the octal code `12110000`.

that we generally underestimate m_h, especially for smaller values of M_{SUSY}. The reason is that for larger values of M_{SUSY}, the logarithms $\log M_{SUSY}/m_t$, which in our approach are reproduced, dominate the result. Figure 3.16 also shows difference to the `FeynHiggs` result. This difference is used to improve our estimate for the Higgs mass in our analysis of the fine-tuning in the MSSM.

3.3 THE FINE-TUNING IN THE MSSM

So far, the gluino corrections to the Higgs potential in the MSSM have been studied from different perspectives, some of them rather technical. Let us summarise our results, before applying them to the study of the fine-tuning in the MSSM.

A heavy gluino leads to large corrections to the mass parameters m_{ij}^2 in the Higgs potential. Regarding the fine-tuning in the MSSM those contributions shift the electro-weak scale towards higher values, see Section 3.2.2.

The gluino contributes to the Higgs potential at two-loop via top squark loops. If the top squarks are renormalised in the $\overline{\text{DR}}$ scheme these corrections appear recurringly at higher orders in perturbation theory and therefore need to be summed to all orders, see Section 3.2.3. This resummation is, however, not necessary, if an on-shell scheme is applied to the top squarks. The gluino contributions increase the on-shell mass of the top squarks compared the $\overline{\text{DR}}$ mass. As we have argued in Section 3.2.4, the splitting can allow $\overline{\text{DR}}$ mass parameters to be several hundreds of GeV below the current collider bounds, that are sensitive to the physical mass.

Concerning the fine-tuning in the MSSM, the question of the renormalisation scheme is actually the question of which parameters define the theory. The fine-tuning is a measure to assess these theory parameters. Assuming the SUSY parameters are set at a high scale in an underlying, more general theory, the fine-tuning of the EW scale should be studied with respect to these parameters. In practical calculations these will mostly be the $\overline{\text{DR}}$ parameter. From that perspective, the on-shell mass is an observable that can be determined from the theory parameters.

It is rather interesting that the gluino mass M_3 may increase the on-shell mass compared to the $\overline{\text{DR}}$ mass. As we have seen in Section 3.2.4 this allows $\overline{\text{DR}}$ masses to be closer to the EW scale than one would expect from LHC mass limits. As our analysis will show, the fine-tuning is hence reduced. We will compare the fine-tuning calculated from the naive one-loop corrections to m_{ij}^2 to the fine-tuning calculated from the two-loop corrections. Formally, the one-loop results have no control over the renormalisation scheme dependence of the top squark. For the two-loop corrections we adopt the OS scheme for the top squarks and expand the result in terms of the $\overline{\text{DR}}$ mass.

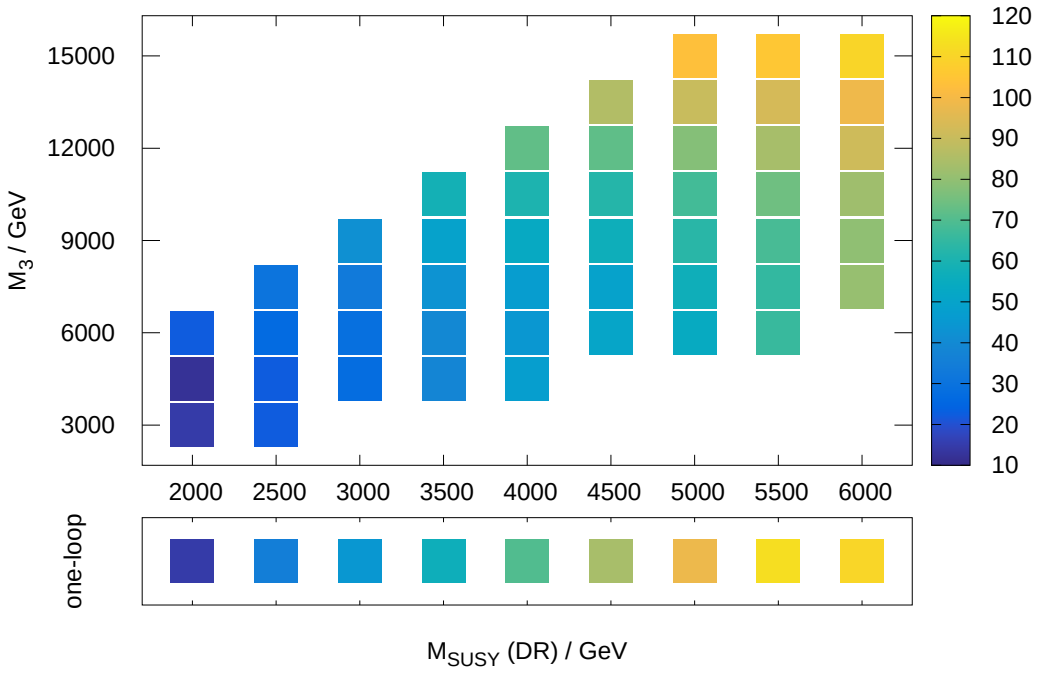

(a)

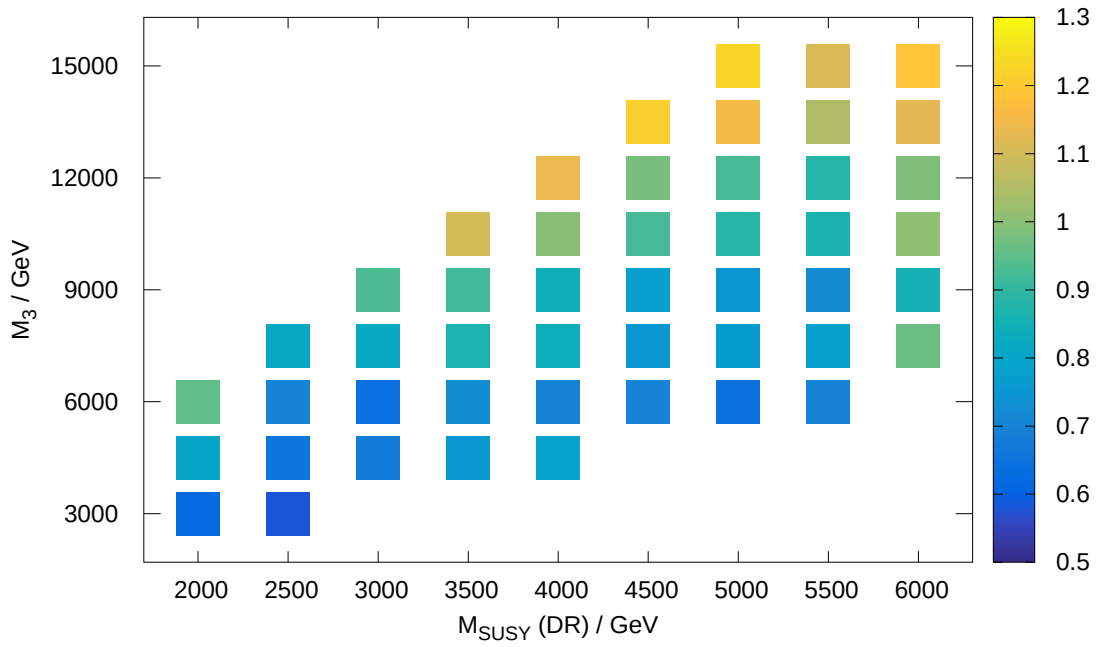

(b)

Figure 3.17: **The fine-tuning of M_Z for sample points in the M_3-M_{SUSY}-plane.** Upper plot: The colour-coded areas show the median fine-tuning of 100 sample point that have been fitted to M_Z and m_h. For reference, the one-loop result is shown for each value of $M_{\mathrm{SUSY}} = \sqrt{m_L\, m_R}$. Lower plot: For comparison the two-loop result from the upper plot has been divided by the one-loop results. A decrease in the fine-tuning at two-loop compared to one-loop is marked with blue colours.

Each point in the MSSM parameter space has a certain fine-tuning. Our considerations are nonetheless of more general kind. Hence we will not focus so much on the fine-tuning of a single set of parameters but try to formulate a more general statement about the MSSM parameter space. This is done by performing a global scan in the $M_{\text{SUSY}} = \sqrt{m_L\, m_R}$ and M_3 plane. For each value in this plane, a χ^2 function defined by

$$\chi^2 = \left(\frac{M_Z^{\text{exp}} - M_Z^{\text{theo}}}{\sigma_{M_Z}}\right)^2 + \left(\frac{m_h^{\text{exp}} - m_h^{\text{theo}} - m_h^{\text{offset}}}{\sigma_{m_h}}\right)^2 , \tag{3.95}$$

is evaluated. For $\sigma_{M_Z} = 2.1\,\text{MeV}$ the experimental uncertainty from [120] is used. To account for the uncertainty in the Higgs mass calculation the difference to the `FeynHiggs` calculation found in Section 3.2.6 is used as an offset to the experimental values to account for the corrections to the Higgs mass that are neglected and $\sigma_{m_h} = 1\,\text{GeV}$. The χ^2 function is minimised by varying the values of m_{11}^2, m_{22}^2, m_R and A_t over the following ranges

Having fixed M_{SUSY}, the choice of m_R also fixes M_L.

$$m_{11}^{\text{tree}} = 10 \ldots 600\,\text{GeV} , \qquad m_{22}^{\text{tree}} = 10 \ldots 600\,\text{GeV} , \tag{3.96}$$

$$m_R^{\overline{\text{DR}}} = 400\,\text{GeV} \ldots M_{\text{SUSY}} , \qquad A_t = 10\,\text{GeV} \ldots 3\,M_{\text{SUSY}} . \tag{3.97}$$

Starting from 100 random points in this parameter space we thus generate 100 sets of parameters with $\chi^2 < 1$. For each point M_Z is calculated from the right-hand side of eq. (3.9) including the complete two-loop corrections for m_{ij}^2 with the top squarks renormalised on-shell and the complete one-loop corrections to Δ_{ij} with the stop masses converted to the OS scheme. The fine-tuning of M_Z is then determined as a function of m_R, according to eq. (3.2). During the parameter scan the following values are kept fix

$$\tan\beta = 5 , \qquad |\mu| = 400\,\text{GeV} . \tag{3.98}$$

The $\overline{\text{DR}}$ couplings y_t and g_3 are evaluated at the scales $y_t = y_t(M_{\text{SUSY}})$ and $g_3 = g_3(M_3)$, as has been discussed in Section 3.2.5. The parameter scan is performed in `C++` as described in Section 3.2.6.

The plots that show the mean and the quartiles are not shown since qualitatively they all look alike.

For illustration, Figure 3.17a shows the median of the fine-tuning measure over all 100 sampling points for each point in the M_{SUSY}-M_3 plane. For comparison, the scan is also performed including only the one-loop corrections. The result is indicated by the colour bar in Figure 3.17a. The one-loop corrections are independent of the gluino mass M_3.

Let us illustrate how to read this plot for $M_{\text{SUSY}} = 3500\,\text{GeV}$: Considering the one-loop results we find a median for fine-tuning of about 1 in 70, i. e. half of the points in the scan are less fine-tuned. In the column for $M_{\text{SUSY}} = 3500\,\text{GeV}$ of the two-loop result, we find a similar fine-tuning for a gluino mass of 12 TeV. For gluino masses below

12 TeV the colour coding indicates lower values of the fine-tuning reaching down to about 1 in 40.

For comparison, the lower plot of Figure 3.17b shows the ratio of the fine-tuning obtained at two-loop divided by the one-loop result. The colour coding is chosen such that ratios around one appear to be greenish, i. e. when both methods yield the same fine-tuning. If the fine-tuning for the two-loop result decreases compared to the one-loop result a blue colour is chosen, while a yellow colour marks the opposite case.

Overall, the fine-tuning including the gluino contributions is typically smaller than the one found at one-loop for the same values of M_{SUSY}. That is an astonishing result because it shows that the electroweak scale might not be as fine-tuned as one would naively expect from a one-loop analysis.

There are still two caveats. As indicated by Figure 3.17b, for high values of M_3 the fine-tuning starts to increase compared to the one-loop result, e. g. for $M_{\text{SUSY}} = 5\,\text{TeV}$ and $M_3 = 15\,\text{TeV}$. The reason is that the dominant two-loop contributions to m_{ij}^2 and therefore to M_Z stem from terms scaling as $M_3^2 \log M_3 / m_{L,R}$ (see eq. (3.52)). The fine-tuning measure is basically the logarithmic derivative with respect to m_R and hence proportional to M_3 for those contributions. At some point the two-loop contributions to the fine-tuning become larger than the one-loop contributions in which case the fine-tuning increases.

Furthermore, the fit only converges well for values of M_{SUSY} starting at 2 TeV. Below these values the Higgs mass of 125 GeV cannot be accounted for with our set of parameters, see Figure 3.16. The parameters in the scan are chosen such that the stop mixing $X_t = A_t - \mu \cot\beta$ is not much larger than the SUSY scale. Allowing for larger values of the stop mixing to account for the Higgs mass would in turn introduce an additional source of fine-tuning.

The fact that both M_Z and m_h receive the largest contributions from the top and stop sector (at least for $\tan\beta > 1$) leads to an implicit connection of the Higgs mass and the fine-tuning. This situation is specific to the MSSM, though. In the next-to-minimal supersymmetric extension of the Standard Model (NMSSM) an additional SM singlet superfield is added whose VEV gives an additional contribution to the masses of the Higgs boson. In such a scenario the $\overline{\text{DR}}$ masses could be of the order of a hundred GeV if the gluino is heavy enough for sufficiently large on-shell masses. Thus, we conclude that a mild hierarchy between stop and gluinos masses could be the answer to the little hierarchy problem.

For a review of the NMSSM see, e. g. [283, 284].

3.4 AN APPLICATION TO MESON MIXING

In March 2019, the LHCb collaboration announced the observation of CP violation in charm decays [285]. CP violation was first discovered

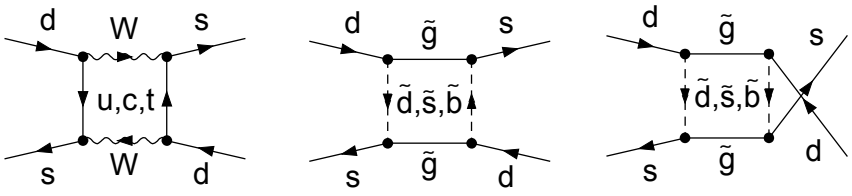

(a) (b) (c)

Figure 3.18: **Sample diagrams for kaon mixing I.** Diagram (a) appears in the SM. The gluino boxes in diagrams (b) and (c) cancel each other for $M_3 \approx 1.5\, m_{\tilde{q}}$. The clashing arrows in diagram (c) that denote fermion flow are due to the Majorana nature of the gluino.

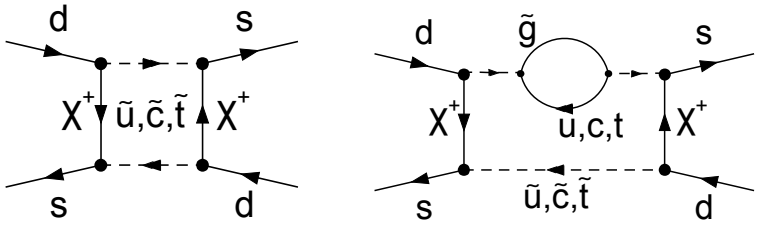

(a) (b)

Figure 3.19: **Sample diagrams for kaon mixing II.** The chargino box does at one-loop not depend on the gluino mass M_3. At two-loop, gluino insertions into the up-type squark propagator scale as M_3^2 and introduce a dependence of the renormalisation scheme of the squarks.

in the system of neutral kaons in 1964 [286]. The weak interaction allows the flavour eigenstate $K^0 = (\bar{s}d)$ to oscillate into $\overline{K^0} = (s\bar{d})$, see Figure 3.18a. But the rate of that process is not the same as for the reversed process. This leads to the fact that the mass eigenstates K_L and K_S, which are superpositions of K^0 and $\overline{K^0}$, are not CP eigenstates. The existence of the CP violating decay $K_L \to \pi\pi$ at a rate of two per mille then lead to the discovery in 1964. At the quark level, the mixing of K^0 into $\overline{K^0}$ and vice versa is described by the effective Hamiltonian

$$\mathcal{H}_{\text{eff}}^{\Delta s=2} = \sum_{i=1}^{8} C_i(\bar{\mu})\, Q_i(\bar{\mu}) + \text{H.c.}\,. \tag{3.99}$$

In the SM only the operator $Q_1 = \bar{s}\gamma_\mu \mathbb{P}_L d\ \bar{s}\gamma^\mu \mathbb{P}_L d$ contributes due to the chiral structure of the weak interaction. The corresponding Wilson coefficient at the mass scale of top quark is at leading order

$$C_1^{\text{SM}}(\bar{\mu} = m_t) = \frac{G_F^2}{16\,\pi^2} \left(V_{\text{CKM}}^{ts} V_{\text{CKM}}^{td,\star}\right)^2 m_W^2\, S\left(\frac{\bar{m}_t{}^2}{m_W^2}\right)\,, \tag{3.100}$$

with the Inami-Lim function $S(\bar{m}_t{}^2/m_W^2) = 2.35$ [287, 288].

In SUSY models also the operators $Q_2 \ldots Q_8$ contribute [289–294]. Since we are interested in the effect of the renormalisation scheme

adopted for the squarks, we will only discuss the SUSY corrections to C_1 and compare them to the SM value. The dominant contributions originate from gluino and chargino boxes [295], see Figures 3.18 and 3.19

$$C_1^{\tilde{g}\tilde{g}} = -\frac{g_3^4}{16\,\pi^2}\sum_{i,j}^{6}\Big(\frac{11}{36}\,D_2(m_{\tilde{d}_i}, m_{\tilde{d}_j}, M_3, M_3) + \frac{1}{9}\,M_3^2\,(m_{\tilde{d}_i}, m_{\tilde{d}_j}, M_3, M_3)\Big)\,V_{i\,12}^{d\,LL}\,V_{j\,12}^{d\,LL}\,, \tag{3.101}$$

$$C_1^{\tilde{\chi}^+\tilde{\chi}^+} = -\frac{g_2^4}{128\,\pi^2}\sum_{i,j}^{6}\,D_2(m_{\tilde{u}_i}, m_{\tilde{u}_j}, M_3, M_3)\,V_{i\,12}^{u\,LL}\,V_{j\,12}^{u\,LL}\,. \tag{3.102}$$

For the definition of the loop functions D_0 and D_2 and the Mixing matrices $V^{u,d}$ see Appendix A.3.4 or references [296, 297].

These Wilson coefficients are defined at $M_{\text{SUSY}} = 1\,\text{TeV}$. At the mass scale of the top quark they are [298]

$$C_1^{\text{SUSY}}\left(\bar{\mu} = m_t\right) = \left(\frac{\alpha_s(M_{\text{SUSY}})}{\alpha_s(m_t)}\right)^{6/21} C_1^{\text{SUSY}}(M_{\text{SUSY}})\,. \tag{3.103}$$

With the input of Table 2.2, $(\dots)^{6/21} = 0.963$

The squark masses are $m_{\tilde{u}} = m_{\tilde{d}} = m_{\tilde{q}} = M_{\text{SUSY}} = 1\,\text{TeV}$. Following the approach by the authors of [299] we include mixing between the weak doublets and parametrise the squark mass matrices in the super-CKM basis as follows

$$\mathbf{M}_{\tilde{d}}^2 = \begin{pmatrix} M_{\tilde{q}}^2 & \mathbf{0} \\ \mathbf{0} & M_{\tilde{d}}^2 \end{pmatrix}\,, \qquad \mathbf{M}_{\tilde{u}}^2 = \begin{pmatrix} V_{\text{CKM}}\,M_{\tilde{q}}^2\,V_{\text{CKM}}^\dagger & \mathbf{0} \\ \mathbf{0} & M_{\tilde{u}}^2 \end{pmatrix}\,, \tag{3.104}$$

where $M_{\tilde{u}}^{2,ij} = m_u^2\,\delta^{ij}$, $M_{\tilde{d}}^{2,ij} = m_d^2\,\delta^{ij}$ and $M_{\tilde{q}}^{2,ij} = m_q^2\,(\delta^{ij} + \Delta^{ij})$. The off-diagonal elements are set to $\Delta_{12} = \Delta_{13} = \Delta_{23} = 0.005$ and all others to zero. In addition, we choose $M_2 = 600\,\text{GeV}$.

It has already been pointed out in [295], that there is an interesting interplay between the chargino and the gluino boxes depending on the value of the gluino mass M_3, see the dashed lines in Figure 3.20a. For M_3 of the order of 1 TeV, i. e. the squark masses, the gluino contributions dominate over the chargino contributions that are proportional to the weak coupling g_2. Interestingly, at $M_3 \approx 1.5\,m_{\tilde{q}}$ the gluino loops become zero due to the interference with the crossed diagrams (Figure 3.18c). For larger values of M_3, the gluino decouples and the chargino loops dominate the result.

At two-loop, however, the gluino contributes via squark loops that scale as M_3^2 as shown in Figure 3.19b. As we have argued in Section 3.2.4, the resummation of these loops is equivalent to renormalising the squarks in an OS scheme. To account for this corrections, the scheme difference for $m_{\tilde{q}}$ induced by the flavour universal gluino corrections is calculated according to eq. (3.82). The results for the

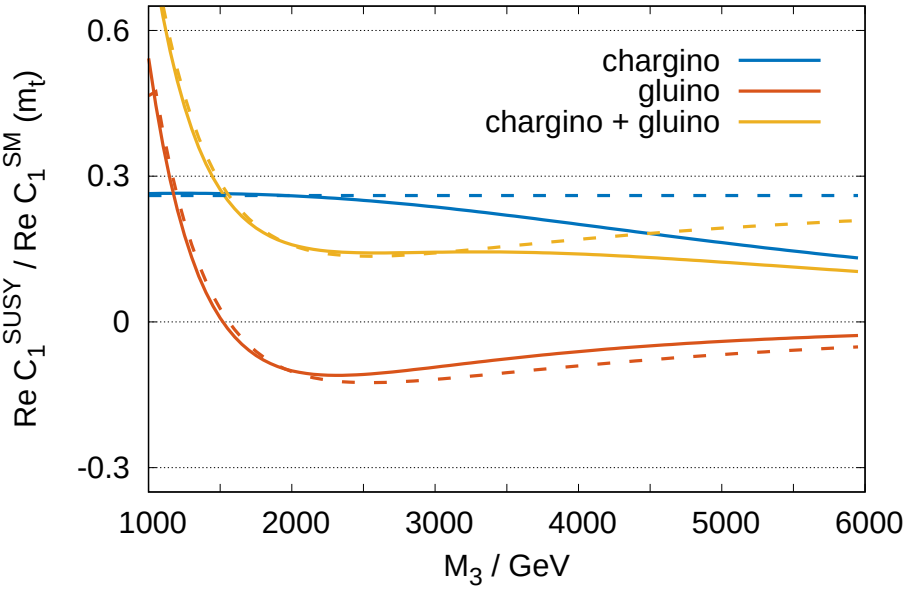

(a)

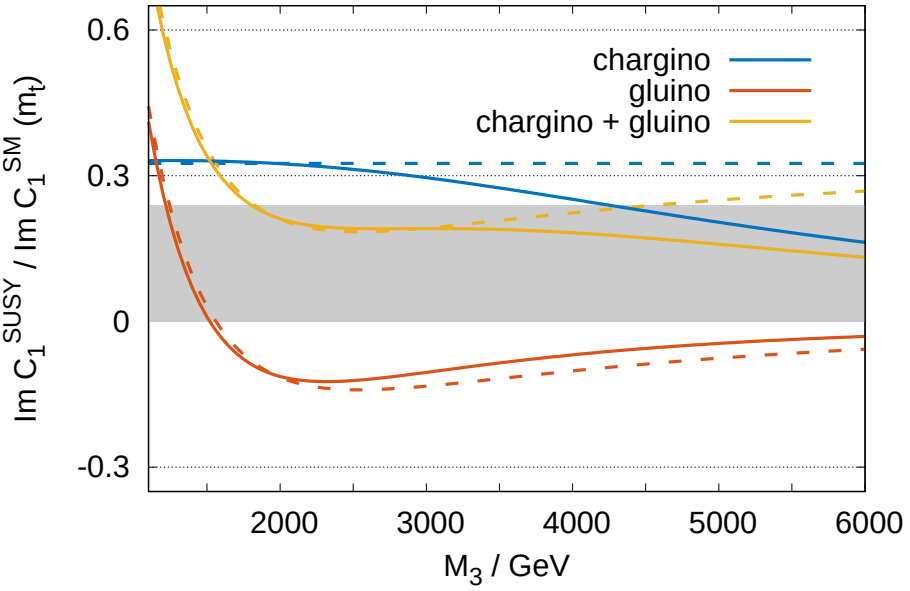

(b)

Figure 3.20: **Renormalisation scheme comparison for Kaon mixing.** The plots show the real (top) and imaginary (bottom) part of the SUSY contributions to C_1 at the scale m_t, normalised to $C_1^{SM}(m_t)$. Above $M_3 \approx m_{\tilde{q}} = 1\,\text{TeV}$, chargino boxes are dominant. The dashed lines depict the case where the squark masses are given in the $\overline{\text{DR}}$ scheme while the solid lines depict the case where the squark masses have been converted to the OS scheme. The area shaded in grey shows the 68% confidence interval for $C_{\epsilon K}$ from the 2018 new physics fit by UTfit. $M_2 = 600\,\text{GeV}$ and all squark masses are set to 1 TeV.

Wilson coefficient C_1 are represented by solid lines in Figure 3.20a. Because the OS mass for the squarks is increased compared to $\overline{\text{DR}}$ mass, the size of the chargino loops that scale as $1/m_{\tilde{q}}^2$ is decreased. Still, they dominate the SUSY contributions for values of M_3 above 3000 GeV. Note that the size of the scheme difference increases up to a factor of two.

The shaded area in Figure 3.20b corresponds to the 68% confidence interval from the 2018 new physics fit by the UTfit collaboration [300, 301] that suggests $C_{\epsilon K} = 1.12 \pm 0.12$. Neglecting the contributions from charm and light quarks that value corresponds to $C_{\epsilon K} - 1 = \operatorname{Im} C_1^{\text{SUSY}} / \operatorname{Im} C_1^{\text{SM}}$ in our scenario. Note that the RGE running below m_t and the hadronic matrix elements cancel in this ratio. For $M_3 > 4000\,\text{GeV}$, the $\overline{\text{DR}}$ results (dashed lines) show a slight tension in $C_{\epsilon K}$ whereas the OS result does not (solid lines).

In Figure 3.20a a similar constraint from the mass difference of the Kaons applies. This constraint, however, depends on long-distance effects that are not yet fully understood, see e. g. [91, 302–305].

As a result, we summarise that also in predictions for flavour processes the OS mass for squarks should be used in presence of a heavy gluino, in order to avoid the resummation of higher orders. This scheme difference does in addition have an effect on the constraints of new physics.

3.5 CONCLUSIONS

In this chapter we have considered the quantum corrections to the MSSM Higgs potential in case the gluino mass M_3 is larger than the masses of the top squarks. The gluino contributes to the Higgs potential at two-loop. Its contributions to the mass parameters in the Higgs potential scale as M_3^2 and therefore can exceed the one-loop corrections. These corrections also affect the renormalisation scheme of the top squarks. If those are renormalised in the $\overline{\text{DR}}$ scheme the gluino contributions repeat themselves also at higher loop order and hence need to be resummed. We have demonstrated that the resummation of the $\overline{\text{DR}}$ contributions can be avoided by adopting the OS scheme for the top squarks. As a consequence, the OS mass of the top squarks becomes considerably larger than the $\overline{\text{DR}}$ mass.

This relation is crucial if the SUSY parameters are set in some high-scale scenario and evolved to the scale of SUSY particles. Then the $\overline{\text{DR}}$ masses should be translated to the OS scheme for comparison with collider experiments that are sensitive to the on-shell mass of particles. As an example we have studied the influence of the squark renormalisation scheme in kaon mixing. The scheme difference can change the SUSY contributions by a factor of two. We emphasize that this observation is universal for any model of new physics with an additional scalar at an intermediate mass scale.

Moreover, this relation is interesting concerning the little hierarchy problem in the MSSM. The fine-tuning in the MSSM may be lower compared to the naive one-loop loop result if the contributions of a heavy gluino are included. As has been shown in a numerical scan this holds for large ranges of the MSSM parameter space. This effect could be even stronger in supersymmetric models with an extended Higgs sector.

The `Mathematica` package `Medusa` has been developed by C. Wiegand to calculate two-loop amplitudes with heavy particles in the framework of EFT. Our work provided a unique opportunity to test this new package and for this reason we laid special emphasis on cross-checking and self-consistency of our results.

4

CONCLUSIONS

Charm *is a way of getting the answer 'Yes' without asking a clear question.*
—Albert Camus

THE OTHER SIDE OF THE DESERT. Gauge coupling unification in the MSSM calls for two important assumptions, namely the absence of generic new physics beyond the MSSM that would modify the RGEs and the magnitude of the SUSY scale being in the TeV range. This hypothetical picture of physics beyond the SM has often been compared to that of a desert with no new particles between the SUSY and the see-saw or GUT scale.

From today's perspective, this picture is a two-sided one. On the one hand, it offered the prospect of finding new particles and interactions with searches at collider experiments. On the other hand, this simplified picture can narrow our view on the dynamics of new physics. In this work we have approached possible SUSY scenarios both from high and low energies and studied the implications thereof.

In Chapter 2 we have followed a top-down approach confronting a minimal SUSY SO(10) GUT model with recent data from lattice and neutrino experiments. An extensive numerical treatment of the RGEs has enabled us to constrain the SUSY threshold corrections in the Yukawa sector. This analysis has impact on GUT inspired SUSY model building while at the same time it remains agnostic regarding the details of the SUSY spectrum. With increasing precision of both neutrino observables and of our knowledge of the light quark masses, we expect that the Yukawa sector of SUSY SO(10) will further be challenged.

Following a bottom-up approach in Chapter 3, we have investigated the fine-tuning in the MSSM in the presence of a hierarchy between the top squarks and the gluino. We have found that a heavy gluino induces a sizeable shift between the on-shell mass and the $\overline{\text{DR}}$ mass of the stops. As a consequence, the little hierarchy problem and the fine-tuning can be milder compared to a one-loop analysis if one includes two-loop corrections to the Higgs sector. Furthermore we have demonstrated that in case of a hierarchical SUSY spectrum the on-shell mass definition should be applied for calculating low-energy observables in order to avoid large loop corrections at every order in perturbation theory by explicitly performing the resummation of these terms.

Both approaches have in common that the theory predictions from higher energy scales are massively altered through quantum corrections that make the treatment in an EFT framework necessary. In the future, the challenge for particle theory may be to deal with the reality that new physics could be more hierarchical than the desert picture

But, Mousie, thou art no thy-lane,
In proving foresight may be vain;
The best-laid schemes *o' mice an' men*
Gang aft agley,
An' lea'e us nought but grief an' pain,
For promis'd joy!
—Robert Burns

suggests. Eventually, nature, as we observe it, is hierarchical in terms of energy scales. New physics might be not different from that.

A

APPENDIX

A.1 CONVENTIONS

This conventions coincide with those in reference [306].

Throughout this thesis, a system of units is used, where the Planck constant $\hbar$ and the speed of light c equal one.

SPACE AND TIME. A Lorentz vector and its derivative are defined by their timely and spatial components as

$$x^\mu = (t, \vec{x}) \,, \qquad \partial^\mu = \left(\frac{\partial}{\partial t}, -\vec{\nabla} \right) \,. \tag{A.1}$$

Lorentz indices can be raised and lowered using the metric tensor

$$g^{\mu\nu} = g_{\mu\nu} = \mathrm{diag}(1, -1, -1, -1) \,. \tag{A.2}$$

If not explicitely stated otherwise, all Greek indices are Lorentz indices and double occuring indices are automatically summed over.

The Dirac algebra obeys the anti-commutation relation

$$\{\gamma^\mu, \gamma^\nu\} = \gamma^\mu\gamma^\nu + \gamma^\nu\gamma^\mu = 2\, g^{\mu\nu} \,. \tag{A.3}$$

For contractions of Lorentz vectors with Dirac matrices Feynman's slash notation is used $\not{k} = k_\mu \gamma^\mu$. Traces over even numbers of Dirac matrices can iteratively be rewritten as

$$\mathrm{tr}\left(\gamma^{\mu_1} \cdots \gamma^{\mu_n}\right) = \sum_{i=2}^{n} (-1)^i g^{\mu_1\mu_i} \,\mathrm{tr}\left(\gamma^{\mu_2} \cdots \gamma^{\mu_{i-1}} \gamma^{\mu_{i+1}} \cdots \gamma^{\mu_n}\right) \,, \tag{A.4}$$

whereas traces of odd numbers of Dirac matrices vanish and $\mathrm{tr}\left(\gamma^\mu\gamma^\nu\right) = 2\, g^{\mu\nu}$. For a discussion of the Dirac algebra outside of four dimensions see Section 3.2.1.

With $\gamma_5 = \mathrm{i}\gamma^0\gamma^1\gamma^2\gamma^3$ the projectors onto left-handed and right-handed states are

$$\mathbb{P}_L = \frac{1}{2}\left(1 - \gamma_5\right) \,, \qquad \mathbb{P}_R = \frac{1}{2}\left(1 + \gamma_5\right) \,. \tag{A.5}$$

COLOUR ALGEBRA. The group generators of $\mathrm{SU}(3)_C$ are $T^a = \lambda^a/2$ with λ^a being the Gell-Mann matrices, see e. g. [306]. The structure constants f^{abc} are defined by the commutation relation of the group generators

$$[T^a, T^b] = T^a T^b - T^b T^a = \mathrm{i}\, f^{abc}\, T^c \,. \tag{A.6}$$

For the Casimir operators we write $C_F = (N^2-1)/2N$ and $C_A = N$ for SU(N). They obey

$$(T^a T^a)_{ij} = C_F\,\delta_{ij}\,, \qquad (T^a T^b)_{ii} = \frac{1}{2}\,\delta^{ab} \tag{A.7}$$

$$f^{acd} f^{bcd} = C_A\,\delta^{ab}\,, \qquad f^{abc}(T^b T^c)_{ij} = \frac{i}{2}\,C_A\,T^a_{ij}\,. \tag{A.8}$$

For the calculation of the renormalisation constant of the strong coupling the Fierz identity of SU(N) is used

$$(T^a)_{ij}(T^b)_{kl} = \frac{1}{2}\,\delta_{il}\delta_{kj} - \frac{1}{2N}\,\delta_{ij}\delta_{kl}\,. \tag{A.9}$$

In all final results, N is set to three.

SPECIAL FUNCTIONS The real and imaginary part of a complex number z are denoted by $\mathrm{Re}\,z$ and $\mathrm{Im}\,z$, respectively. In polar coordinates we have $z = r\,e^{i\varphi}$, with $r = |z|$ and $\varphi = \arg z$. We write $z^\star$ for the complex conjugate.

The logarithm of real arguments $x \in \mathbb{R}$ is defined by

$$\log x = \int_1^x \mathrm{d}t\,\frac{1}{t}\,. \tag{A.10}$$

For complex arguments $z \in \mathbf{C}$ the principal value of the logarithm is defined by

$$\log z = \log|z| + i\arg z\,, \tag{A.11}$$

with $-\pi < \arg z \leq \pi$, i. e. the branch cut is on the negative real axis.

The dilogarithm is defined by

$$\mathrm{Li}_2(z) = -\int_0^z \mathrm{d}t\,\frac{\log(1-t)}{t} \tag{A.12}$$

and fulfils the identity

$$\mathrm{Li}_2(1-z) + \mathrm{Li}_2\left(1-\frac{1}{z}\right) = -\frac{1}{2}(\log z)^2\,. \tag{A.13}$$

The Γ function is defined by

$$\Gamma(z) = \int_0^\infty \mathrm{d}t\; t^{z-1}e^{-t}\,, \quad \mathrm{Re}\,z > 0\,, \tag{A.14}$$

and obeys the functional equation $\Gamma(z+1) = z\,\Gamma(z)$, i. e. for positive integers $n \in \mathbf{N}$, $\Gamma(n) = (n+1)!$ It can be analytically continued to the complex plane with single poles for negativ integers.

The hypergeometric function is defined by

$${}_2\mathrm{F}_1(a,b;c;z) = \frac{\Gamma(c)}{\Gamma(b)\,\Gamma(c-b)}\int_0^1 \mathrm{d}t\;\frac{t^{b-1}\,(1-t)^{c-b-1}}{(1-z\,t)^a}\,, \tag{A.15}$$

for $0 < \mathrm{Re}\,b < \mathrm{Re}\,c$ and $a, z \in \mathbf{C}$.

The trace of a matrix A is defined by the sum of its diagonal entries

$$\mathrm{tr}\,\{A\} = \sum_i A_{ii}\,. \tag{A.16}$$

PARAMETRISATION OF FLAVOUR ROTATIONS. Any unitary 3×3 matrix can be parametrised as

$$U = \text{diag}\left(e^{i\delta_1}, e^{i\delta_2}, e^{i\delta_3}\right) \cdot V \cdot \text{diag}\left(e^{-i\phi_1/2}, e^{-i\phi_2/2}, 1\right) . \quad \text{(A.17)}$$

For the CKM matrix, the additional phases δ_1, δ_2, δ_3, ϕ_1 and ϕ_2 can be absorbed into redefinitions of the fields. The matrix V is given in the standard parametrisation of the PDG

$$V = \begin{pmatrix} c_{12}c_{13} & s_{12}c_{13} & s_{13}e^{-i\delta} \\ -s_{12}c_{23} - c_{12}s_{23}s_{13}e^{i\delta} & c_{12}c_{23} - s_{12}s_{23}s_{13}e^{i\delta} & s_{23}c_{13} \\ s_{12}s_{23} - c_{12}c_{23}s_{13}e^{i\delta} & -c_{12}s_{23} - s_{12}c_{23}s_{13}e^{i\delta} & c_{23}c_{13} \end{pmatrix} , \quad \text{(A.18)}$$

where the sines and cosines of the mixing angles are $s_{ij} = \sin\theta_{ij}$ and $c_{ij} = \cos\theta_{ij}$ and the δ is the CP phase.

The PMNS matrix can be parametrised in the same way. However, only the phases δ_i can be absorbed and the Majorana phases ϕ_1 and ϕ_2 could be physical although they have not been measured yet. In the analyses of Chapter 2 they are therefore treated as being zero.

A.2 GUT SCALE PARAMETERS FOR THE GLOBAL MINIMA

This section gives the coordinates of the global minima found in Section 2.2. The parametrisation of the GUT Yukawa matrices Y_{10} and Y_{126} is as follows

$$Y_{10} = \text{diag}\left(H_1, H_2, H_3\right) , \qquad Y_{126} = \begin{pmatrix} F_1 & F_2 & F_3 \\ F_2 & F_4 & F_5 \\ F_3 & F_5 & F_6 \end{pmatrix} .$$

All results are given with a high numerical precision so that they can be reproduced. For the correspondence to the MSSM Yukawa matrices see Section 2.1.5.

A.2.1 *Global Minima without SUSY Threshold Corrections*

$\tan\beta = 10$, $\chi^2 = 127.016$

$$\begin{aligned} r &= 8.93109 , & s &= 0.40219 + 0.0537018\,i , \\ r_R &= 5.7222 \times 10^{14}\,\text{GeV} , & H_1 &= -8.13678 \times 10^{-6} , \\ H_2 &= 0.000546749 , & H_3 &= 0.0587967 , \\ F_1 &= (3.62943 + 1.11577\,i) \times 10^{-5} , & F_2 &= (-4.86448 - 6.8181\,i) \times 10^{-5} , \\ F_3 &= -8.669 \times 10^{-5} + 0.00101114\,i , & F_4 &= -0.00122229 + 0.000483037\,i , \\ F_5 &= 0.00229999 - 0.00243838\,i , & F_6 &= -0.00436435 + 0.000144527\,i . \end{aligned}$$

$\tan\beta = 38$, $\chi^2 = 94.6859$

$$
\begin{aligned}
r &= 2.09333\,, & s &= 0.361579 + 0.00221939\,\mathrm{i}\,,\\
r_R &= -1.01454 \times 10^{14}\,\mathrm{GeV}\,, & H_1 &= -3.76306 \times 10^{-5}\,,\\
H_2 &= 0.0017972\,, & H_3 &= 0.254405\,,\\
F_1 &= 0.000100472 + 0.000137311\,\mathrm{i}\,, & F_2 &= 3.1103 \times 10^{-5} + 0.000457557\,\mathrm{i}\,,\\
F_3 &= -0.00260288 + 0.0039351\,\mathrm{i}\,, & F_4 &= -0.00474944 + 0.00161864\,\mathrm{i}\,,\\
F_5 &= -0.0107501 + 0.00940057\,\mathrm{i}\,, & F_6 &= -0.0119578 - 0.047225\,\mathrm{i}\,.
\end{aligned}
$$

$\tan\beta = 50$, $\chi^2 = 75.438$

$$
\begin{aligned}
r &= -1.351\,, & s &= 0.380723 + 0.0112833\,\mathrm{i}\,,\\
r_R &= 7.08356 \times 10^{13}\,\mathrm{GeV}\,, & H_1 &= -5.44756 \times 10^{-5}\,,\\
H_2 &= 0.00295336\,, & H_3 &= 0.418203\,,\\
F_1 &= 0.000198815 + 0.000167965\,\mathrm{i}\,, & F_2 &= 0.000197095 + 0.00060758\,\mathrm{i}\,,\\
F_3 &= 0.00302059 - 0.00664685\,\mathrm{i}\,, & F_4 &= -0.00713153 + 0.00251093\,\mathrm{i}\,,\\
F_5 &= 0.0167445 - 0.0153386\,\mathrm{i}\,, & F_6 &= -0.0253209 - 0.0530162\,\mathrm{i}\,.
\end{aligned}
$$

A.2.2 *Global Minima with SUSY Threshold Corrections*

$\tan\beta = 10$, $\chi^2 = 40.3671$

$$
\begin{aligned}
r &= 2.68759\,, & s &= 0.146006 - 0.258778\,\mathrm{i}\,,\\
r_R &= 4.05262 \times 10^{13}\,\mathrm{GeV}\,, & H_1 &= 5.28137 \times 10^{-6}\,,\\
H_2 &= 0.000694187\,, & H_3 &= 0.186542\,,\\
F_1 &= (-7.52986 - 11.2321\,\mathrm{i}) \times 10^{-6}\,, & F_2 &= (-5.92321 - 9.76299\,\mathrm{i}) \times 10^{-5}\,,\\
F_3 &= 0.000578945 + 0.000363829\,\mathrm{i}\,, & F_4 &= 6.89316 \times 10^{-5} - 0.000631902\,\mathrm{i}\,,\\
F_5 &= 0.0100828 + 0.000256401\,\mathrm{i}\,, & F_6 &= 0.0424372 + 0.028391\,\mathrm{i}\,,\\
\epsilon_q &= 0.05000\,, & \epsilon_b &= -0.07348963\,,\\
\epsilon_l &= -0.02999953\,.
\end{aligned}
$$

$\tan\beta = 38$, $\chi^2 = 1.74389$

$$
\begin{aligned}
r &= 0.739487\,, & s &= 0.171775 - 0.0527206\,\mathrm{i}\,,\\
r_R &= 3.00163 \times 10^{12}\,\mathrm{GeV}\,, & H_1 &= 1.74192 \times 10^{-5}\,,\\
H_2 &= 0.00263311\,, & H_3 &= 0.873783\,,\\
F_1 &= (-4.52508 - 1.40042) \times 10^{-5}\,\mathrm{i}\,, & F_2 &= -0.000670712 - 0.000352788\,\mathrm{i}\,,\\
F_3 &= 0.00257905 + 0.000499293\,\mathrm{i}\,, & F_4 &= -0.00325008 - 0.0013532\,\mathrm{i}\,,\\
F_5 &= 0.0128581 + 0.0601288\,\mathrm{i}\,, & F_6 &= 0.474974 + 0.216717\,\mathrm{i}\,,\\
\epsilon_q &= 0.02796541\,, & \epsilon_b &= -0.04061278\,,\\
\epsilon_l &= -0.006000\,.
\end{aligned}
$$

$\tan\beta = 50,\ \chi^2 = 3.73552$

$$
\begin{aligned}
r &= 0.699764\,, & s &= 0.137602 - 0.0279775\,\mathrm{i}\,,\\
r_R &= 2.33 \times 10^{12}\,\mathrm{GeV}\,, & H_1 &= 1.21069 \times 10^{-5}\,,\\
H_2 &= 0.00246264\,, & H_3 &= 0.988718\,,\\
F_1 &= (-4.09545 - 1.24086\,\mathrm{i}) \times 10^{-5}\,, & F_2 &= 0.000472532 + 0.00031884\,\mathrm{i}\,,\\
F_3 &= 0.00483506 + 0.00119957\,\mathrm{i}\,, & F_4 &= -0.00190458 + 0.00028723\,\mathrm{i}\,,\\
F_5 &= -0.0316564 - 0.0584933\,\mathrm{i}\,, & F_6 &= 0.607543 + 0.0633526\,\mathrm{i}\,,\\
\epsilon_q &= 0.04720754\,, & \epsilon_b &= -0.006000\,,\\
\epsilon_l &= 0.001271233\,.
\end{aligned}
$$

A.2.3 *Local Minima with SUSY Threshold Corrections*

$\tan\beta = 38,\ \chi^2 = 3.71108$

$$
\begin{aligned}
r &= 0.670043\,, & s &= 0.11989 - 0.0413042\,\mathrm{i}\,,\\
r_R &= 2.03128 \times 10^{12}\,\mathrm{GeV}\,, & H_1 &= 1.09545 \times 10^{-5}\,,\\
H_2 &= 0.00255376\,, & H_3 &= 1.05489\,,\\
F_1 &= -3.38058 \times 10^{-5} - 5.63 \times 10^{-10}\,\mathrm{i}\,, & F_2 &= -0.00040558 - 0.00026938\,\mathrm{i}\,,\\
F_3 &= 0.00523839 + 0.000883983\,\mathrm{i}\,, & F_4 &= -0.00226047 + 0.00066294\,\mathrm{i}\,,\\
F_5 &= 0.0259931 + 0.063712\,\mathrm{i}\,, & F_6 &= 0.622678 + 0.0958844\,\mathrm{i}\,,\\
\epsilon_q &= 0.04999992\,, & \epsilon_b &= -0.01243252\,,\\
\epsilon_l &= -0.0048000\,.
\end{aligned}
$$

$\tan\beta = 50,\ \chi^2 = 4.6864$

$$
\begin{aligned}
r &= 0.719454\,, & s &= 0.17033 - 0.0410235\,\mathrm{i}\,,\\
r_R &= 2.89057 \times 10^{12}\,\mathrm{GeV}\,, & H_1 &= 1.14972 \times 10^{-5}\,,\\
H_2 &= 0.00276048\,, & H_3 &= 0.898288\,,\\
F_1 &= (-3.87624 - 1.31146\,\mathrm{i}) \times 10^{-5}\,, & F_2 &= -0.000600001 - 0.000317934\,\mathrm{i}\\
F_3 &= -0.00275464 - 0.00102727\,\mathrm{i}\,, & F_4 &= -0.00375989 - 0.00115394\,\mathrm{i}\\
F_5 &= -0.0164547 - 0.0618966\,\mathrm{i}\,, & F_6 &= 0.552 + 0.0273906\,\mathrm{i}\\
\epsilon_q &= 0.4246740\,, & \epsilon_b &= -0.03408847\,,\\
\epsilon_l &= 0.0020000\,.
\end{aligned}
$$

A.3 TECHNICAL DETAILS OF THE CALCULATIONS IN CHAPTER 3

A.3.1 *Two and four-component spinors.*

Supersymmetry is typically defined in terms of Weyl spinors since they are the components of supermultiplets. For practical calculations, e. g. in `FeynArts`, it is often useful to translate them into the language of four component spinors. All relations are taken from reference [27] and also work without introducing spinor indices as we will see.

Let ξ and η be two two-component spinors of degenerate mass m that transform under $M \in \mathrm{SL}(2, \mathbf{C})$. The spinors ξ^T and $\bar{\xi}$ then transform under M^{-1} and $(M^{-1})^*$, respectively, such that $\xi^T\eta = \eta^T\xi$

and $\bar{\xi}^T\bar{\eta} = \bar{\eta}^T\bar{\xi}$ are invariants. For simplicity, the scalar products are written as $\xi\eta$, etc. outside this Appendix. From the trasformation properties follows that $(\xi^T\eta)^\dagger = \bar{\eta}^T\bar{\xi}$. The Weyl equations for those spinors read

$$p_\mu\bar{\sigma}^\mu\xi = m\bar{\eta}\,, \qquad p_\mu\sigma^\mu\bar{\eta} = m\xi\,, \tag{A.19}$$

where the Pauli matrices

$$\sigma_1 = \begin{pmatrix} 0 & 1 \\ 1 & 0 \end{pmatrix}\,, \qquad \sigma_2 = \begin{pmatrix} 0 & -\mathrm{i} \\ \mathrm{i} & 0 \end{pmatrix}\,, \qquad \sigma_3 = \begin{pmatrix} 1 & 0 \\ 0 & -1 \end{pmatrix}\,, \tag{A.20}$$

are used to define $\sigma^\mu = (1, \vec{\sigma})$ and $\bar{\sigma}^\mu = (1, -\vec{\sigma})$. Introducing four component notation

$$\psi = \begin{pmatrix} \xi \\ \bar{\eta} \end{pmatrix}\,, \qquad \gamma^\mu = \begin{pmatrix} 0 & \sigma^\mu \\ \bar{\sigma}^\mu & 0 \end{pmatrix}\,, \tag{A.21}$$

the Weyl equations can be rewritten as the Dirac equation

$$p_\mu\gamma^\mu\psi = m\psi\,. \tag{A.22}$$

Let us define two Dirac spinors

$$\psi_t = \begin{pmatrix} t_L \\ \bar{t}_R^T \end{pmatrix}, \qquad \psi_b = \begin{pmatrix} b_L \\ \bar{b}_R^T \end{pmatrix}. \tag{A.23}$$

The conjugated Dirac spinors $\overline{\psi} = \psi^\dagger\gamma^0$ are

$$\overline{\psi}_t = \begin{pmatrix} t_R^T, & \bar{t}_L \end{pmatrix}, \qquad \overline{\psi}_b = \begin{pmatrix} b_R^T, & \bar{b}_L \end{pmatrix}. \tag{A.24}$$

For Yukawa interactions we need the bilinear forms

$$\overline{\psi}_b\psi_t = b_R^T t_L + \bar{b}_L\bar{t}_R^T\,, \tag{A.25}$$

$$\overline{\psi}_t\psi_b = t_R^T b_L + \bar{t}_L\bar{b}_R^T\,. \tag{A.26}$$

We can project onto the chiral components by

$$\overline{\psi}_b\mathbb{P}_L\psi_t = b_R^T t_L\,, \qquad \overline{\psi}_b\mathbb{P}_R\psi_t = \bar{b}_L\bar{t}_R^T\,, \tag{A.27}$$

$$\overline{\psi}_t\mathbb{P}_L\psi_b = t_R^T b_L\,, \qquad \overline{\psi}_t\mathbb{P}_R\psi_b = \bar{t}_L\bar{b}_R^T\,. \tag{A.28}$$

For the fermion coupling to gluons the vector bilinear forms are needed, e. g.

$$\overline{\psi}_t\gamma^\mu\mathbb{P}_L\psi_t = \bar{t}_L\bar{\sigma}^\mu t_L\,, \qquad \overline{\psi}_t\gamma^\mu\mathbb{P}_R\psi_t = t_R^T\sigma^\mu\bar{t}_R^T\,. \tag{A.29}$$

Majorana particles, however, have to be treated differently. The gluino can e. g. be put in four component notation as

$$\psi_{\tilde{g}} = \begin{pmatrix} \tilde{g} \\ \bar{\tilde{g}}^T \end{pmatrix}\,. \tag{A.30}$$

For the top-stop-gluino couplings the following bilinear forms are needed

$$\overline{\psi}_t \mathbb{P}_L \psi_{\tilde{g}} = t_R^T \bar{\tilde{g}} \,, \qquad \overline{\psi}_t \mathbb{P}_R \psi_{\tilde{g}} = \bar{t}_L \bar{\tilde{g}}^T \,, \tag{A.31}$$

$$\overline{\psi}_{\tilde{g}} \mathbb{P}_L \psi_t = \tilde{g}^T t_L \,, \qquad \overline{\psi}_{\tilde{g}} \mathbb{P}_R \psi_t = \bar{\tilde{g}} \bar{t}_R^T \,. \tag{A.32}$$

Finally, also a vector bilinear appears in the gluino-gluino-gluon coupling

$$\overline{\psi}_{\tilde{g}} \gamma^\mu \mathbb{P}_L \psi_{\tilde{g}} = \bar{\tilde{g}} \bar{\sigma}^\mu \tilde{g} \,, \qquad \overline{\psi}_{\tilde{g}} \gamma^\mu \mathbb{P}_R \psi_{\tilde{g}} = \tilde{g}^T \sigma^\mu \bar{\tilde{g}}^T \,. \tag{A.33}$$

A.3.2 *Lagrangian*

The Feynman rules are derived from the superpotential in 3.20 according to [26]. For the translation into four component spinors the expressions from the previous section are used. The interactions of gluons and gluinos in Feynman gauge are

The Feynman rules get an additional factor of i *because, instead of* $\mathcal{L}$, $\mathrm{i}\mathcal{L}$ *appears in the definition of Green's functions in perturbation theory.*

$$\begin{aligned}
\mathcal{L}_{\mathrm{SQCD}} = {} & \mathrm{i}\, g_3\, f^{abc}\, \overline{\psi}^a_{\tilde{g}} \gamma^\mu (\mathbb{P}_L + \mathbb{P}_R) \psi^b_{\tilde{g}}\, G^c_\mu \\
& - g_3\, G^a_\mu \left(\overline{\psi}_t \gamma^\mu T^a (\mathbb{P}_L + \mathbb{P}_R) \psi_t + \overline{\psi}_b \gamma^\mu T^a \mathbb{P}_L \psi_b \right) \\
& - \mathrm{i}\, g_3\, G^a_\mu \left(\tilde{t}^\star_L\, T^a\, \partial^\mu\, \tilde{t}_L + \tilde{t}_R\, T^a\, \partial^\mu\, \tilde{t}^\star_R + \tilde{b}^\star_L\, T^a\, \partial^\mu\, \tilde{b}_L \right) \\
& + \sqrt{2}\, g_3 \left(\tilde{t}^\star_L\, T^a\, \overline{\psi}_{\tilde{g}} \mathbb{P}_L \psi_t - \overline{\psi}_t \mathbb{P}_R \psi_{\tilde{g}}\, T^a\, \tilde{t}_L \right) \\
& + \sqrt{2}\, g_3 \left(\tilde{b}^\star_L\, T^a\, \overline{\psi}_{\tilde{g}} \mathbb{P}_L \psi_b - \overline{\psi}_b \mathbb{P}_R \psi_{\tilde{g}}\, T^a\, \tilde{b}_L \right) \\
& + \sqrt{2}\, g_3 \left(\overline{\psi}_t \mathbb{P}_L \psi_{\tilde{g}}\, T^a\, \tilde{t}^\star_R - t_R\, T^a\, \overline{\psi}_{\tilde{g}} \mathbb{P}_R \psi_t \right) \\
& + g_3^2\, G^a_\mu G^{b,\mu} \left(\tilde{t}^\star_L\, T^a T^b\, \tilde{t}_L + \tilde{t}_R\, T^a T^b\, \tilde{t}^\star_R + \tilde{b}^\star_L\, T^a T^b\, \tilde{b}_L \right) \\
& + \frac{1}{2}\, g_3^2 \left(\tilde{t}^\star_L\, T^a\, \tilde{t}_L + \tilde{t}_R\, T^a\, \tilde{t}^\star_R + \tilde{b}^\star_L\, T^a\, \tilde{b}_L \right) \\
& \qquad \times \left(\tilde{t}^\star_L\, T^a\, \tilde{t}_L + \tilde{t}_R\, T^a\, \tilde{t}^\star_R + \tilde{b}^\star_L\, T^a\, \tilde{b}_L \right) \\
& - \frac{1}{4}\, F^a_{\mu\nu} F^{a,\mu\nu} - \bar{c}^a\, \partial_\mu \left(\delta^{ab}\, \partial^\mu + g_3\, f^{abc}\, G^{c,\mu} \right) c^c \,,
\end{aligned} \tag{A.34}$$

where colour indices have been suppressed. In colour space ψ_t, ψ_b, $\tilde{t}_L$, $\tilde{b}_L$, $\tilde{t}^\star_R$ are column vectors while their respective conjugates are row vectors. The field strength tensor is

$$F^a_{\mu\nu} = \partial_\mu G^a_\nu - \partial_\nu G^a_\mu + g_3\, f^{abc}\, G^b_\mu G^c_\nu \,, \tag{A.35}$$

and c^a is the Faddeev-Popov ghost [307].

The Yukawa interactions derived from 3.20 are

$$\begin{aligned}-\mathcal{L}_{\text{Yukawa}} = {} & y_t\,\overline{\psi}_t \mathbb{P}_L \psi_t\, h_2^0 + y_t^\star\,\overline{\psi}_t \mathbb{P}_R \psi_t\, h_2^{0,\star} \\ & + y_t\,\tilde{t}_R\,\overline{\psi}_{h,2} \mathbb{P}_L \psi_t + y_t^\star\,\overline{\psi}_t \mathbb{P}_R \psi_{h,2}\,\tilde{t}_R^\star \\ & + y_t\,\overline{\psi}_t \mathbb{P}_L \psi_{h,2}\,\tilde{t}_L + y_t^\star\,\tilde{t}_L^\star\,\overline{\psi}_{h,2} \mathbb{P}_R \psi_t \\ & - y_t\,\overline{\psi}_t \mathbb{P}_L \psi_b\, h_2^+ - y_t^\star \overline{\psi}_b \mathbb{P}_R \psi_t\, h_2^{+,\star} \\ & - y_t\,\overline{\psi}_t \mathbb{P}_L \psi_+\,\tilde{b}_L - y_t^\star\,\tilde{b}_L^\star\,\overline{\psi}_+ \mathbb{P}_R \psi_t \\ & - y_t\,\tilde{t}_R\,\overline{\psi_+^C} \mathbb{P}_L \psi_b - y_t^\star\,\overline{\psi}_b \mathbb{P}_R \psi_+^C\,\tilde{t}_R^\star\,, \end{aligned} \tag{A.36}$$

where four-component spinors of the higgsinos are given by

$$\psi_{h,2} = \begin{pmatrix} \tilde{h}_2^0 \\ \overline{\tilde{h}}_2^{0,T} \end{pmatrix}, \qquad \psi_+ = \begin{pmatrix} \tilde{h}_2^+ \\ \overline{\tilde{h}}_1^{-,T} \end{pmatrix}, \qquad \psi_+^C = \begin{pmatrix} \tilde{h}_1^- \\ \overline{\tilde{h}}_2^{+,T} \end{pmatrix}. \tag{A.37}$$

Finally, the F-terms are

$$\begin{aligned}-\mathcal{L}_F = {} & |y_t|^2\,\tilde{t}_R \tilde{t}_R^\star\, h_2^0\, h_2^{0,\star} + |y_t|^2\,\tilde{t}_L^\star \tilde{t}_L\, h_2^0\, h_2^{0,\star} + |y_t|^2\,\tilde{b}_L^\star \tilde{b}_L\, h_2^+\, h_2^{+,\star} \\ & + |y_t|^2\,\tilde{t}_R \tilde{t}_R^\star\, h_2^+\, h_2^{+,\star} - |y_t|^2\,\tilde{b}_L^\star \tilde{t}_L\, h_2^0\, h_2^{+,\star} - |y_t|^2\,\tilde{t}_L^\star \tilde{b}_L\, h_2^\star\, h_2^+ \\ & + |y_t|^2\,\tilde{t}_R \tilde{t}_L\,\tilde{t}_L^\star \tilde{t}_R^\star + y_t\,\mu^\star\, h_1^{0,\star}\,\tilde{t}_R \tilde{t}_L + y_t^\star\,\mu\, h_1^0\,\tilde{t}_L^\star \tilde{t}_R^\star \\ & + |y_t|^2\,\tilde{t}_R \tilde{b}_L\,\tilde{b}_L^\star \tilde{t}_R^\star + y_t\,\mu^\star\, h_1^{-,\star}\,\tilde{t}_R \tilde{b}_L + y_t^\star\,\mu\, h_1^-\,\tilde{b}_L^\star \tilde{t}_R^\star \\ & + |\mu|^2\, h_1^0\, h_1^{0,\star} + |\mu|^2\, h_2^0\, h_2^{0,\star}\,. \end{aligned} \tag{A.38}$$

A.3.3 *Beta functions*

The beta functions that result from this subset of the MSSM can be derived from the one-loop and two-loop expression in [104]. Defining

$$\frac{\mathrm{d}}{\mathrm{d}\log\bar{\mu}} X = \frac{1}{16\,\pi^2}\,\beta_x^{(1)} + \frac{1}{(16\,\pi^2)^2}\,\beta_x^{(2)}\,, \tag{A.39}$$

one finds

$$\beta_{g_3}^{(1)} = -\frac{15}{2} g_3^3\,, \tag{A.40}$$

$$\beta_{y_t}^{(1)} = y_t \left(6|y_t|^2 - \frac{16}{3} g_3^2\right)\,, \tag{A.41}$$

$$\beta_{A_t}^{(1)} = A_t \left(18\,|y_t|^2 - \frac{16}{3} g_3^2\right) + \frac{32}{3}\, y_t\, g_3^2\, M_3\,, \tag{A.42}$$

$$\beta_{m_L^2}^{(1)} = 2\,|y_t|^2 (m^2_{m_{h_2}^2} + m_L^2 + m_R^2) + 2\,|A_t|^2 - \frac{32}{3} g_3^2 M_3^2\,, \tag{A.43}$$

$$\beta_{m_R^2}^{(1)} = 4\,|y_t|^2 (m^2_{m_{h_2}^2} + m_L^2 + m_R^2) + 4\,|A_t|^2 - \frac{32}{3} g_3^2 M_3^2\,, \tag{A.44}$$

$$\beta_{M_3}^{(1)} = -15\, g_3^2\, M_3\,, \tag{A.45}$$

$$\beta_{m_{h_2}^2}^{(1)} = 6\,|y_t|^2 (m^2_{m_{h_2}^2} + m_L^2 + m_R^2)\,, \tag{A.46}$$

$$\begin{aligned}\beta^{(2)}_{m^2_{h_2}} &= -36\,|y_t|^2\left(|y_t|^2\,(m^2_{m^2_{h_2}}+m^2_L+m^2_R)+2\,|A_t|^2\right)\\ &\quad+32\,g_3^2\Big(|y_t|^2\,(m^2_{m^2_{h_2}}+m^2_L+m^2_R)+|A_t|^2+2\,|y_t|^2\,M_3^2\\ &\quad-y_t^\star\,A_t\,M_3-y_t\,A_t^\star\,M_3\Big)\,. \end{aligned}\tag{A.47}$$

We have checked all counterterms from our calculations with these expressions and found perfect agreement.

A.3.4 *Loop functions and squark mixing*

The loop functions that appear in eqs. (3.101) and (3.102) from references [296, 297] are

$$\begin{aligned}C_0(m_1,m_2,m_3) &= \frac{m_1^2\,m_2^2\log\left(\frac{m_1^2}{m_2^2}\right)+m_2^2\,m_3^2\log\left(\frac{m_2^2}{m_3^2}\right)}{(m_1^2-m_2^2)(m_2^2-m_3^2)(m_3^2-m_1^2)}\\ &\quad+\frac{m_3^2\,m_1^2\log\left(\frac{m_3^2}{m_1^2}\right)}{(m_1^2-m_2^2)(m_2^2-m_3^2)(m_3^2-m_1^2)}\,,\end{aligned}\tag{A.48}$$

$$D_0(m_1,m_2,m_3,m_4)=\frac{C_0(m_1,m_2,m_3)-C_0(m_1,m_2,m_4)}{m_3^2-m_4^2}\,,\tag{A.49}$$

$$D_2(m_1,m_2,m_3,m_4)=C_0(m_1,m_2,m_3)+m_4^2\,D_0(m_1,m_2,m_3,m_4)\,.\tag{A.50}$$

The squark mixing is described by

$$V^{q\,LL}_{i\,12}=W^q_{1i}\,W^{q,\star}_{2i}\,,\qquad q=u,d\,,\tag{A.51}$$

with no sum over $i=1,\ldots,6$ and W^q_{ij} diagonalise the up-type squark and down-type squark mass matrices of eq. 3.104

$$W^{q,\dagger}\,M^2_{\tilde q}\,W^q=\mathrm{diag}\,(\tilde q_1,\ldots\tilde q_6)\,,\qquad q=u,d\,.\tag{A.52}$$

BIBLIOGRAPHY

[1] Vladimir A. Smirnov. "Analytic tools for Feynman integrals." In: *Springer Tracts Mod. Phys.* 250 (2012), pp. 1–296.

[2] Gerard 't Hooft and M. J. G. Veltman. "Regularization and Renormalization of Gauge Fields." In: *Nucl. Phys.* B44 (1972), pp. 189–213.

[3] William A. Bardeen et al. "Deep Inelastic Scattering Beyond the Leading Order in Asymptotically Free Gauge Theories." In: *Phys. Rev.* D18 (1978), p. 3998.

[4] S. L. Glashow. "Partial Symmetries of Weak Interactions." In: *Nucl. Phys.* 22 (1961), pp. 579–588.

[5] Abdus Salam and John Clive Ward. "Electromagnetic and weak interactions." In: *Phys. Lett.* 13 (1964), pp. 168–171.

[6] Steven Weinberg. "A Model of Leptons." In: *Phys. Rev. Lett.* 19 (1967), pp. 1264–1266.

[7] H. Fritzsch, Murray Gell-Mann, and H. Leutwyler. "Advantages of the Color Octet Gluon Picture." In: *Phys. Lett.* 47B (1973), pp. 365–368.

[8] Harald Fritzsch and Murray Gell-Mann. "Current algebra: Quarks and what else?" In: *eConf* C720906V2 (1972), pp. 135–165. arXiv: hep-ph/0208010 [hep-ph].

[9] C. S. Wu et al. "Experimental Test of Parity Conservation in Beta Decay." In: *Phys. Rev.* 105 (1957), pp. 1413–1414.

[10] Peter W. Higgs. "Broken symmetries, massless particles and gauge fields." In: *Phys. Lett.* 12 (1964), pp. 132–133.

[11] Peter W. Higgs. "Broken Symmetries and the Masses of Gauge Bosons." In: *Phys. Rev. Lett.* 13 (1964), pp. 508–509.

[12] G. Arnison et al. "Experimental Observation of Lepton Pairs of Invariant Mass Around 95-GeV/c**2 at the CERN SPS Collider." In: *Phys. Lett.* B126 (1983), pp. 398–410.

[13] G. Arnison et al. "Experimental Observation of Isolated Large Transverse Energy Electrons with Associated Missing Energy at s**(1/2) = 540-GeV." In: *Phys. Lett.* B122 (1983), pp. 103–116.

[14] M. Banner et al. "Observation of Single Isolated Electrons of High Transverse Momentum in Events with Missing Transverse Energy at the CERN anti-p p Collider." In: *Phys. Lett.* B122 (1983), pp. 476–485.

[15] P. Bagnaia et al. "Evidence for Zo —> e+ e- at the CERN anti-p p Collider." In: *Phys. Lett.* B129 (1983), pp. 130–140.

[16] Georges Aad et al. "Observation of a new particle in the search for the Standard Model Higgs boson with the ATLAS detector at the LHC." In: *Phys. Lett.* B716 (2012), pp. 1–29. arXiv: 1207.7214 [hep-ex].

[17] Serguei Chatrchyan et al. "Observation of a new boson at a mass of 125 GeV with the CMS experiment at the LHC." In: *Phys. Lett.* B716 (2012), pp. 30–61. arXiv: 1207.7235 [hep-ex].

[18] Y. Fukuda et al. "Evidence for oscillation of atmospheric neutrinos." In: *Phys. Rev. Lett.* 81 (1998), pp. 1562–1567. arXiv: hep-ex/9807003 [hep-ex].

[19] Y. Abe et al. "Indication of Reactor $\bar{\nu}_e$ Disappearance in the Double Chooz Experiment." In: *Phys. Rev. Lett.* 108 (2012), p. 131801. arXiv: 1112.6353 [hep-ex].

[20] F. P. An et al. "Observation of electron-antineutrino disappearance at Daya Bay." In: *Phys. Rev. Lett.* 108 (2012), p. 171803. arXiv: 1203.1669 [hep-ex].

[21] A. Aguilar-Arevalo et al. "Evidence for neutrino oscillations from the observation of anti-neutrino(electron) appearance in a anti-neutrino(muon) beam." In: *Phys. Rev.* D64 (2001), p. 112007. arXiv: hep-ex/0104049 [hep-ex].

[22] Steven Weinberg. "Baryon and Lepton Nonconserving Processes." In: *Phys. Rev. Lett.* 43 (1979), pp. 1566–1570.

[23] V. N. Aseev et al. "An upper limit on electron antineutrino mass from Troitsk experiment." In: *Phys. Rev.* D84 (2011), p. 112003. arXiv: 1108.5034 [hep-ex].

[24] D. M. Capper, D. R. T. Jones, and P. van Nieuwenhuizen. "Regularization by Dimensional Reduction of Supersymmetric and Nonsupersymmetric Gauge Theories." In: *Nucl. Phys.* B167 (1980), pp. 479–499.

[25] Warren Siegel. "SUPERGRAVITY SUPERGRAPHS." In: *Phys. Lett.* 84B (1979), pp. 197–200.

[26] Janusz Rosiek. "Complete set of Feynman rules for the MSSM: Erratum." In: (1995). arXiv: hep-ph/9511250 [hep-ph].

[27] Howard E. Haber and Gordon L. Kane. "The Search for Supersymmetry: Probing Physics Beyond the Standard Model." In: *Phys. Rept.* 117 (1985), pp. 75–263.

[28] Pierre Ramond. "Dual Theory for Free Fermions." In: *Phys. Rev.* D3 (1971), pp. 2415–2418.

[29] Jean-Loup Gervais and B. Sakita. "Field Theory Interpretation of Supergauges in Dual Models." In: *Nucl. Phys.* B34 (1971). [,154(1971)], pp. 632–639.

[30] A. Neveu and J. H. Schwarz. "Factorizable dual model of pions." In: *Nucl. Phys.* B31 (1971), pp. 86–112.

[31] Yu. A. Golfand and E. P. Likhtman. "Extension of the Algebra of Poincare Group Generators and Violation of p Invariance." In: *JETP Lett.* 13 (1971). [Pisma Zh. Eksp. Teor. Fiz.13,452(1971)], pp. 323–326.

[32] D. V. Volkov and V. P. Akulov. "Is the Neutrino a Goldstone Particle?" In: *Phys. Lett.* 46B (1973), pp. 109–110.

[33] J. Wess and B. Zumino. "Supergauge Transformations in Four-Dimensions." In: *Nucl. Phys.* B70 (1974), pp. 39–50.

[34] Pierre Fayet. "Supersymmetry and Weak, Electromagnetic and Strong Interactions." In: *Phys. Lett.* 64B (1976), p. 159.

[35] Pierre Fayet. "Spontaneously Broken Supersymmetric Theories of Weak, Electromagnetic and Strong Interactions." In: *Phys. Lett.* 69B (1977), p. 489.

[36] Glennys R. Farrar and Pierre Fayet. "Phenomenology of the Production, Decay, and Detection of New Hadronic States Associated with Supersymmetry." In: *Phys. Lett.* 76B (1978), pp. 575–579.

[37] Pierre Fayet. "Relations Between the Masses of the Superpartners of Leptons and Quarks, the Goldstino Couplings and the Neutral Currents." In: *Phys. Lett.* 84B (1979), p. 416.

[38] Hans Peter Nilles. "Supersymmetry, Supergravity and Particle Physics." In: *Phys. Rept.* 110 (1984), pp. 1–162.

[39] Pierre Fayet and J. Iliopoulos. "Spontaneously Broken Supergauge Symmetries and Goldstone Spinors." In: *Phys. Lett.* 51B (1974), pp. 461–464.

[40] L. O'Raifeartaigh. "Spontaneous Symmetry Breaking for Chiral Scalar Superfields." In: *Nucl. Phys.* B96 (1975), pp. 331–352.

[41] L. Girardello and Marcus T. Grisaru. "Soft Breaking of Supersymmetry." In: *Nucl. Phys.* B194 (1982), p. 65.

[42] Chen-Ning Yang and Robert L. Mills. "Conservation of Isotopic Spin and Isotopic Gauge Invariance." In: *Phys. Rev.* 96 (1954), pp. 191–195.

[43] H. Georgi and S. L. Glashow. "Unity of All Elementary Particle Forces." In: *Phys. Rev. Lett.* 32 (1974), pp. 438–441.

[44] Howard Georgi. "The State of the Art-Gauge Theories." In: *AIP Conf. Proc.* 23 (1975), pp. 575–582.

[45] Harald Fritzsch and Peter Minkowski. "Unified Interactions of Leptons and Hadrons." In: *Annals Phys.* 93 (1975), pp. 193–266.

[46] Stephen L. Adler. "Axial vector vertex in spinor electrodynamics." In: *Phys. Rev.* 177 (1969), pp. 2426–2438.

[47] J. S. Bell and R. Jackiw. "A PCAC puzzle: $\pi^0 \to \gamma\gamma$ in the σ model." In: *Nuovo Cim.* A60 (1969), pp. 47–61.

[48] C. S. Aulakh and Rabindra N. Mohapatra. "Implications of Supersymmetric SO(10) Grand Unification." In: *Phys. Rev.* D28 (1983), p. 217.

[49] T. E. Clark, Tzee-Ke Kuo, and N. Nakagawa. "A SO(10) SUPERSYMMETRIC GRAND UNIFIED THEORY." In: *Phys. Lett.* 115B (1982), pp. 26–28.

[50] Charanjit S. Aulakh et al. "SO(10) theory of R-parity and neutrino mass." In: *Nucl. Phys.* B597 (2001), pp. 89–109. arXiv: hep-ph/0004031 [hep-ph].

[51] Takeshi Fukuyama and Nobuchika Okada. "Neutrino oscillation data versus minimal supersymmetric SO(10) model." In: *JHEP* 11 (2002), p. 011. arXiv: hep-ph/0205066 [hep-ph].

[52] Noriyuki Oshimo. "Antisymmetric Higgs representation in SO(10) for neutrinos." In: *Phys. Rev.* D66 (2002), p. 095010. arXiv: hep-ph/0206239 [hep-ph].

[53] Noriyuki Oshimo. "Model for neutrino mixing based on SO(10)." In: *Nucl. Phys.* B668 (2003), pp. 258–272. arXiv: hep-ph/0305166 [hep-ph].

[54] Bhaskar Dutta, Yukihiro Mimura, and R. N. Mohapatra. "Neutrino masses and mixings in a predictive SO(10) model with CKM CP violation." In: *Phys. Lett.* B603 (2004), pp. 35–45. arXiv: hep-ph/0406262 [hep-ph].

[55] Walter Grimus and Helmut Kuhbock. "Fermion masses and mixings in a renormalizable SO(10) x Z(2) GUT." In: *Phys. Lett.* B643 (2006), pp. 182–189. arXiv: hep-ph/0607197 [hep-ph].

[56] Charanjit S. Aulakh. "Pinning down the new minimal supersymmetric GUT." In: *Phys. Lett.* B661 (2008), pp. 196–200. arXiv: 0710.3945 [hep-ph].

[57] Charanjit S. Aulakh and Sumit K. Garg. "The New Minimal Supersymmetric GUT : Spectra, RG analysis and Fermion Fits." In: *Nucl. Phys.* B857 (2012), pp. 101–142. arXiv: 0807.0917 [hep-ph].

[58] Guido Altarelli and Gianluca Blankenburg. "Different $SO(10)$ Paths to Fermion Masses and Mixings." In: *JHEP* 03 (2011), p. 133. arXiv: 1012.2697 [hep-ph].

[59] Anjan S. Joshipura and Ketan M. Patel. "Fermion Masses in SO(10) Models." In: *Phys. Rev.* D83 (2011), p. 095002. arXiv: 1102.5148 [hep-ph].

[60] Guido Altarelli and Davide Meloni. "A non supersymmetric SO(10) grand unified model for all the physics below M_{GUT}." In: *JHEP* 08 (2013), p. 021. arXiv: 1305.1001 [hep-ph].

[61] Alexander Dueck and Werner Rodejohann. "Fits to SO(10) Grand Unified Models." In: *JHEP* 09 (2013), p. 024. arXiv: 1306.4468 [hep-ph].

[62] K. S. Babu and R. N. Mohapatra. "Predictive neutrino spectrum in minimal SO(10) grand unification." In: *Phys. Rev. Lett.* 70 (1993), pp. 2845–2848. arXiv: hep-ph/9209215 [hep-ph].

[63] L. Lavoura. "Predicting the neutrino spectrum in minimal SO(10) grand unification." In: *Phys. Rev.* D48 (1993), pp. 5440–5443. arXiv: hep-ph/9306297 [hep-ph].

[64] B. Brahmachari and R. N. Mohapatra. "Unified explanation of the solar and atmospheric neutrino puzzles in a minimal supersymmetric SO(10) model." In: *Phys. Rev.* D58 (1998), p. 015001. arXiv: hep-ph/9710371 [hep-ph].

[65] Borut Bajc, Goran Senjanovic, and Francesco Vissani. "How neutrino and charged fermion masses are connected within minimal supersymmetric SO(10)." In: *PoS* HEP2001 (2001), p. 198. arXiv: hep-ph/0110310 [hep-ph].

[66] Borut Bajc, Goran Senjanovic, and Francesco Vissani. "b - tau unification and large atmospheric mixing: A Case for non-canonical seesaw." In: *Phys. Rev. Lett.* 90 (2003), p. 051802. arXiv: hep-ph/0210207 [hep-ph].

[67] H. S. Goh, R. N. Mohapatra, and Siew-Phang Ng. "Minimal SUSY SO(10), b tau unification and large neutrino mixings." In: *Phys. Lett.* B570 (2003), pp. 215–221. arXiv: hep-ph/0303055 [hep-ph].

[68] H. S. Goh, R. N. Mohapatra, and Siew-Phang Ng. "Minimal SUSY SO(10) model and predictions for neutrino mixings and leptonic CP violation." In: *Phys. Rev.* D68 (2003), p. 115008. arXiv: hep-ph/0308197 [hep-ph].

[69] Charanjit S. Aulakh et al. "The Minimal supersymmetric grand unified theory." In: *Phys. Lett.* B588 (2004), pp. 196–202. arXiv: hep-ph/0306242 [hep-ph].

[70] Charanjit S. Aulakh and Aarti Girdhar. "SO(10) MSGUT: Spectra, couplings and threshold effects." In: *Nucl. Phys.* B711 (2005), pp. 275–313. arXiv: hep-ph/0405074 [hep-ph].

[71] Stefano Bertolini, Michele Frigerio, and Michal Malinsky. "Fermion masses in SUSY SO(10) with type II seesaw: A Non-minimal predictive scenario." In: *Phys. Rev.* D70 (2004), p. 095002. arXiv: hep-ph/0406117 [hep-ph].

[72] Borut Bajc et al. "The Minimal supersymmetric grand unified theory. 1. Symmetry breaking and the particle spectrum." In: *Phys. Rev.* D70 (2004), p. 035007. arXiv: hep-ph/0402122 [hep-ph].

[73] Borut Bajc, Goran Senjanovic, and Francesco Vissani. "Probing the nature of the seesaw in renormalizable SO(10)." In: *Phys. Rev.* D70 (2004), p. 093002. arXiv: hep-ph/0402140 [hep-ph].

[74] Charanjit Singh Aulakh and Sumit Kumar Garg. "MSGUT : From bloom to doom." In: *Nucl. Phys.* B757 (2006), pp. 47–78. arXiv: hep-ph/0512224 [hep-ph].

[75] K. S. Babu and Cosmin Macesanu. "Neutrino masses and mixings in a minimal SO(10) model." In: *Phys. Rev.* D72 (2005), p. 115003. arXiv: hep-ph/0505200 [hep-ph].

[76] Stefano Bertolini and Michal Malinsky. "On CP violation in minimal renormalizable SUSY SO(10) and beyond." In: *Phys. Rev.* D72 (2005), p. 055021. arXiv: hep-ph/0504241 [hep-ph].

[77] Borut Bajc et al. "Fermion mass relations in a supersymmetric SO(10) theory." In: *Phys. Lett.* B634 (2006), pp. 272–277. arXiv: hep-ph/0511352 [hep-ph].

[78] Stefano Bertolini, Thomas Schwetz, and Michal Malinsky. "Fermion masses and mixings in SO(10) models and the neutrino challenge to SUSY GUTs." In: *Phys. Rev.* D73 (2006), p. 115012. arXiv: hep-ph/0605006 [hep-ph].

[79] Charanjit S. Aulakh and Sumit K. Garg. "The New Minimal Supersymmetric GUT : Spectra, RG analysis and fitting formulae." In: (2006). arXiv: hep-ph/0612021 [hep-ph].

[80] Charanjit S. Aulakh and Sumit Kumar Garg. "Correcting alpha(3)(M(Z)) in the NMSGUT." In: *Mod. Phys. Lett.* A24 (2009), pp. 1711–1719. arXiv: 0710.4018 [hep-ph].

[81] Borut Bajc, Ilja Dorsner, and Miha Nemevsek. "Minimal SO(10) splits supersymmetry." In: *JHEP* 11 (2008), p. 007. arXiv: 0809.1069 [hep-ph].

[82] K. Matsuda, T. Fukuyama, and H. Nishiura. "SO(10) GUT and quark lepton mass matrices." In: *Phys. Rev.* D61 (2000), p. 053001. arXiv: hep-ph/9906433 [hep-ph].

[83] Takeshi Fukuyama, Koichi Matsuda, and Hiroyuki Nishiura. "Zero texture model and SO(10) GUT." In: *Int. J. Mod. Phys.* A22 (2007), pp. 5325–5343. arXiv: hep-ph/0702284 [HEP-PH].

[84] Graham Ross and Mario Serna. "Unification and fermion mass structure." In: *Phys. Lett.* B664 (2008), pp. 97–102. arXiv: 0704.1248 [hep-ph].

[85] S. Dev et al. "Four Zero Texture Fermion Mass Matrices in SO(10) GUT." In: *Eur. Phys. J.* C72 (2012), p. 1940. arXiv: 1203.1403 [hep-ph].

[86] Franco Buccella et al. "Squeezing out predictions with leptogenesis from SO(10)." In: *Phys. Rev.* D86 (2012), p. 035012. arXiv: 1203.0829 [hep-ph].

[87] K. S. Babu, Borut Bajc, and Shaikh Saad. "Yukawa Sector of Minimal SO(10) Unification." In: *JHEP* 02 (2017), p. 136. arXiv: 1612.04329 [hep-ph].

[88] K. S. Babu, Borut Bajc, and Shaikh Saad. "Resurrecting Minimal Yukawa Sector of SUSY SO(10)." In: *JHEP* 10 (2018), p. 135. arXiv: 1805.10631 [hep-ph].

[89] Stefano Bertolini, Thomas Schwetz, and Michal Malinsky. "Fermion masses and mixings in SO(10) models and the neutrino challenge to SUSY GUTs." In: *Phys. Rev.* D73 (2006), p. 115012. arXiv: hep-ph/0605006 [hep-ph].

[90] Alexander Dueck and Werner Rodejohann. "Fits to SO(10) Grand Unified Models." In: *JHEP* 09 (2013), p. 024. arXiv: 1306.4468 [hep-ph].

[91] S. Aoki et al. "Review of lattice results concerning low-energy particle physics." In: *Eur. Phys. J.* C77.2 (2017), p. 112. arXiv: 1607.00299 [hep-lat].

[92] J. Charles et al. "CP violation and the CKM matrix: Assessing the impact of the asymmetric *B* factories." In: *Eur. Phys. J.* C41.1 (2005), pp. 1–131. arXiv: hep-ph/0406184 [hep-ph].

[93] Ivan Esteban et al. "Updated fit to three neutrino mixing: exploring the accelerator-reactor complementarity." In: *JHEP* 01 (2017), p. 087. arXiv: 1611.01514 [hep-ph].

[94] R. Slansky. "Group Theory for Unified Model Building." In: *Phys. Rept.* 79 (1981), pp. 1–128.

[95] Mark Srednicki. "Supersymmetric Grand Unified Theories and the Early Universe." In: *Nucl. Phys.* B202 (1982), pp. 327–335.

[96] S. F. King. "Neutrino mass models." In: *Rept. Prog. Phys.* 67 (2004), pp. 107–158. arXiv: hep-ph/0310204 [hep-ph].

[97] H. S. Goh et al. "Proton decay in a minimal SUSY SO(10) model for neutrino mixings." In: *Phys. Lett.* B587 (2004), pp. 105–116. arXiv: hep-ph/0311330 [hep-ph].

[98] Takeshi Fukuyama et al. "Detailed analysis of proton decay rate in the minimal supersymmetric SO(10) model." In: *JHEP* 09 (2004), p. 052. arXiv: hep-ph/0406068 [hep-ph].

[99] K. S. Babu and S. Khan. "Minimal nonsupersymmetric $SO(10)$ model: Gauge coupling unification, proton decay, and fermion masses." In: *Phys. Rev.* D92.7 (2015), p. 075018. arXiv: 1507.06712 [hep-ph].

[100] K. Abe et al. "Search for proton decay via $p \to e^+\pi^0$ and $p \to \mu^+\pi^0$ in 0.3 megaton years exposure of the Super-Kamiokande water Cherenkov detector." In: *Phys. Rev.* D95.1 (2017), p. 012004. arXiv: 1610.03597 [hep-ex].

[101] Marie E. Machacek and Michael T. Vaughn. "Two Loop Renormalization Group Equations in a General Quantum Field Theory. 1. Wave Function Renormalization." In: *Nucl. Phys.* B222 (1983), pp. 83–103.

[102] Marie E. Machacek and Michael T. Vaughn. "Two Loop Renormalization Group Equations in a General Quantum Field Theory. 2. Yukawa Couplings." In: *Nucl. Phys.* B236 (1984), pp. 221–232.

[103] Marie E. Machacek and Michael T. Vaughn. "Two Loop Renormalization Group Equations in a General Quantum Field Theory. 3. Scalar Quartic Couplings." In: *Nucl. Phys.* B249 (1985), pp. 70–92.

[104] Stephen P. Martin and Michael T. Vaughn. "Two loop renormalization group equations for soft supersymmetry breaking couplings." In: *Phys. Rev.* D50 (1994), p. 2282. arXiv: hep-ph/9311340 [hep-ph].

[105] Stefan Antusch and Michael Ratz. "Supergraph techniques and two loop beta functions for renormalizable and nonrenormalizable operators." In: *JHEP* 07 (2002), p. 059. arXiv: hep-ph/0203027 [hep-ph].

[106] Stefan Antusch et al. "Neutrino mass operator renormalization in two Higgs doublet models and the MSSM." In: *Phys. Lett.* B525 (2002), pp. 130–134. arXiv: hep-ph/0110366 [hep-ph].

[107] Stefan Antusch et al. "Neutrino mass operator renormalization revisited." In: *Phys. Lett.* B519 (2001), pp. 238–242. arXiv: hep-ph/0108005 [hep-ph].

[108] Stefan Antusch et al. "Running neutrino mass parameters in see-saw scenarios." In: *JHEP* 03 (2005), p. 024. arXiv: hep-ph/0501272 [hep-ph].

[109] K. Ahnert and M. Mulansky. "Odeint - Solving Ordinary Differential Equations in C++." In: *AIP Conference Proceedings* 1389 (2011), p. 001.

[110] Gaël Guennebaud, Benoît Jacob, et al. *Eigen v3*. 2010. URL: http://eigen.tuxfamily.org.

[111] Thomas Deppisch and Florian Herren. "RGE++, A C++ tool for running and decoupling of singlets in the SM and beyond." In: *to be published* (2019).

[112] Nicola Cabibbo. "Unitary Symmetry and Leptonic Decays." In: *Phys. Rev. Lett.* 10 (1963), pp. 531–533.

[113] Makoto Kobayashi and Toshihide Maskawa. "CP Violation in the Renormalizable Theory of Weak Interaction." In: *Prog. Theor. Phys.* 49 (1973), pp. 652–657.

[114] N. Carrasco et al. "Up, down, strange and charm quark masses with N_f = 2+1+1 twisted mass lattice QCD." In: *Nucl. Phys.* B887 (2014), pp. 19–68. arXiv: 1403.4504 [hep-lat].

[115] Bipasha Chakraborty et al. "High-precision quark masses and QCD coupling from $n_f = 4$ lattice QCD." In: *Phys. Rev.* D91.5 (2015), p. 054508. arXiv: 1408.4169 [hep-lat].

[116] B. Colquhoun et al. "Y and Y′ Leptonic Widths, a_μ^b and m_b from full lattice QCD." In: *Phys. Rev.* D91.7 (2015), p. 074514. arXiv: 1408.5768 [hep-lat].

[117] Alexei Bazavov et al. "Determination of α_s from the QCD static energy: An update." In: *Phys. Rev.* D90.7 (2014), p. 074038. arXiv: 1407.8437 [hep-ph].

[118] S. Aoki et al. "Precise determination of the strong coupling constant in N(f) = 2+1 lattice QCD with the Schrodinger functional scheme." In: *JHEP* 10 (2009), p. 053. arXiv: 0906.3906 [hep-lat].

[119] K. Maltman et al. "The Realistic Lattice Determination of alpha(s)(M(Z)) Revisited." In: *Phys. Rev.* D78 (2008), p. 114504. arXiv: 0807.2020 [hep-lat].

[120] C. Patrignani et al. "Review of Particle Physics." In: *Chin. Phys.* C40.10 (2016), p. 100001.

[121] K. G. Chetyrkin, Johann H. Kuhn, and M. Steinhauser. "RunDec: A Mathematica package for running and decoupling of the strong coupling and quark masses." In: *Comput. Phys. Commun.* 133 (2000), pp. 43–65. arXiv: hep-ph/0004189 [hep-ph].

[122] J. C. Hardy and I. S. Towner. "Superallowed 0+ —> 0+ nuclear beta decays: A New survey with precision tests of the conserved vector current hypothesis and the standard model." In: *Phys. Rev.* C79 (2009), p. 055502. arXiv: 0812.1202 [nucl-ex].

[123] K. A. Olive et al. "Review of Particle Physics." In: *Chin. Phys.* C38 (2014), p. 090001.

[124] Y. Amhis et al. "Averages of b-hadron, c-hadron, and τ-lepton properties as of summer 2014." In: (2014). arXiv: 1412.7515 [hep-ex].

[125] Roel Aaij et al. "Determination of the quark coupling strength $|V_{ub}|$ using baryonic decays." In: *Nature Phys.* 11 (2015), pp. 743–747. arXiv: 1504.01568 [hep-ex].

[126] J. P. Lees et al. "Evidence of $B^+ \to \tau^+\nu$ decays with hadronic B tags." In: *Phys. Rev.* D88.3 (2013), p. 031102. arXiv: 1207.0698 [hep-ex].

[127] Bernard Aubert et al. "A Search for $B^+ \to \ell^+\nu_\ell$ Recoiling Against $B^- \to D^0\ell^-\bar{\nu}X$." In: *Phys. Rev.* D81 (2010), p. 051101. arXiv: 0912.2453 [hep-ex].

[128] I. Adachi et al. "Evidence for $B^- \to \tau^- \bar{\nu}_\tau$ with a Hadronic Tagging Method Using the Full Data Sample of Belle." In: *Phys. Rev. Lett.* 110.13 (2013), p. 131801. arXiv: 1208.4678 [hep-ex].

[129] B. Kronenbitter et al. "Measurement of the branching fraction of $B^+ - > \tau^+ \nu_\tau$ decays with the semileptonic tagging method." In: *Phys. Rev.* D92.5 (2015), p. 051102. arXiv: 1503.05613 [hep-ex].

[130] Vardan Khachatryan et al. "Observation of the rare $B_s^0 \to \mu^+ \mu^-$ decay from the combined analysis of CMS and LHCb data." In: *Nature* 522 (2015), pp. 68–72. arXiv: 1411.4413 [hep-ex].

[131] Bernard Aubert et al. "Improved Measurements of the Branching Fractions for $B^0 \to \pi^+ \pi^-$ and $B^0 \to K^+ \pi^-$, and a Search for $B^0 \to K^+ K^-$." In: *Phys. Rev.* D75 (2007), p. 012008. arXiv: hep-ex/0608003 [hep-ex].

[132] J. P. Lees et al. "Measurement of CP Asymmetries and Branching Fractions in Charmless Two-Body B-Meson Decays to Pions and Kaons." In: *Phys. Rev.* D87.5 (2013), p. 052009. arXiv: 1206.3525 [hep-ex].

[133] Bernard Aubert et al. "Study of $B^0 \to \pi^0 \pi^0$, $B^\pm \to \pi^\pm \pi^0$, and $B^\pm \to K^\pm \pi^0$ Decays, and Isospin Analysis of $B \to \pi\pi$ Decays." In: *Phys. Rev.* D76 (2007), p. 091102. arXiv: 0707.2798 [hep-ex].

[134] Y. T. Duh et al. "Measurements of branching fractions and direct CP asymmetries for $B \to K\pi$, $B \to \pi\pi$ and $B \to KK$ decays." In: *Phys. Rev.* D87.3 (2013), p. 031103. arXiv: 1210.1348 [hep-ex].

[135] I. Adachi et al. "Measurement of the CP violation parameters in $B^0 \to \pi^+ \pi^-$ decays." In: *Phys. Rev.* D88.9 (2013), p. 092003. arXiv: 1302.0551 [hep-ex].

[136] In: (CKM workshop 2014, Vienna). URL: https://belle.kek.jp/belle/b_talk.html.

[137] T. Aaltonen et al. "Measurements of Direct CP Violating Asymmetries in Charmless Decays of Strange Bottom Mesons and Bottom Baryons." In: *Phys. Rev. Lett.* 106 (2011), p. 181802. arXiv: 1103.5762 [hep-ex].

[138] A. Bornheim et al. "Measurements of charmless hadronic two body B meson decays and the ratio B(B → D K) / B(B → D pi)." In: *Phys. Rev.* D68 (2003), p. 052002. arXiv: hep-ex/0302026 [hep-ex].

[139] R Aaij et al. "Measurement of b-hadron branching fractions for two-body decays into charmless charged hadrons." In: *JHEP* 10 (2012), p. 037. arXiv: 1206.2794 [hep-ex].

[140] Bernard Aubert et al. "A Study of Bo —> rho+ rho- Decays and Constraints on the CKM Angle alpha." In: *Phys. Rev.* D76 (2007), p. 052007. arXiv: 0705.2157 [hep-ex].

[141] B. Aubert et al. "Improved Measurement of B+ –> rho+rhoo and Determination of the Quark-Mixing Phase Angle alpha." In: *Phys. Rev. Lett.* 102 (2009), p. 141802. arXiv: 0901.3522 [hep-ex].

[142] Bernard Aubert et al. "Measurement of the Branching Fraction, Polarization, and CP Asymmetries in $B^0 \to \rho^0\rho^0$ Decay, and Implications for the CKM Angle α." In: *Phys. Rev.* D78 (2008), p. 071104. arXiv: 0807.4977 [hep-ex].

[143] P. Vanhoefer et al. "Study of $B^0 \to \rho^+\rho^-$ decays and implications for the CKM angle ϕ_2." In: *Phys. Rev.* D93.3 (2016), p. 032010. arXiv: 1510.01245 [hep-ex].

[144] J. Zhang et al. "Observation of B+ —> rho+ rhoo." In: *Phys. Rev. Lett.* 91 (2003), p. 221801. arXiv: hep-ex/0306007 [hep-ex].

[145] I. Adachi et al. "Study of $B^0 \to \rho^0\rho^0$ decays, implications for the CKM angle ϕ_2 and search for other Bo decay modes with a four-pion final state." In: (2012). arXiv: 1212.4015 [hep-ex].

[146] Roel Aaij et al. "Observation of the $B^0 \to \rho^0\rho^0$ decay from an amplitude analysis of $B^0 \to (\pi^+\pi^-)(\pi^+\pi^-)$ decays." In: *Phys. Lett.* B747 (2015), pp. 468–478. arXiv: 1503.07770 [hep-ex].

[147] J. P. Lees et al. "Measurement of CP-violating asymmetries in $B^0 \to (\rho\pi)^0$ decays using a time-dependent Dalitz plot analysis." In: *Phys. Rev.* D88.1 (2013), p. 012003. arXiv: 1304.3503 [hep-ex].

[148] A. Kusaka et al. "Measurement of CP Asymmetry in a Time-Dependent Dalitz Analysis of Bo —> (rho pi)o and a Constraint on the CKM Angle phi(2)." In: *Phys. Rev. Lett.* 98 (2007), p. 221602. arXiv: hep-ex/0701015 [hep-ex].

[149] P. del Amo Sanchez et al. "Measurement of CP observables in $B^{+-} - > D_{CP}K^{+-}$ decays and constraints on the CKM angle γ." In: *Phys. Rev.* D82 (2010), p. 072004. arXiv: 1007.0504 [hep-ex].

[150] Bernard Aubert et al. "Measurement of Ratios of Branching Fractions and CP-Violating Asymmetries of $B^\pm \to D^*K^\pm$ Decays." In: *Phys. Rev.* D78 (2008), p. 092002. arXiv: 0807.2408 [hep-ex].

[151] Bernard Aubert et al. "Measurement of CP violation observables and parameters for the decays B+- —> D K*+-." In: *Phys. Rev.* D80 (2009), p. 092001. arXiv: 0909.3981 [hep-ex].

[152] K. Trabelsi. "Study of direct CP in charmed B decays and measurement of the CKM angle gamma at Belle." In: *7th International Workshop on the CKM Unitarity Triangle (CKM 2012) Cincinnati, Ohio, USA, September 28-October 2, 2012*. 2013. arXiv: 1301.2033 [hep-ex].

[153] Roel Aaij et al. "Measurement of *CP* observables in $B^{\pm} \to DK^{\pm}$ and $B^{\pm} \to D\pi^{\pm}$ with two- and four-body D decays." In: *Phys. Lett.* B760 (2016), pp. 117–131. arXiv: 1603.08993 [hep-ex].

[154] Roel Aaij et al. "A study of *CP* violation in $B^{\mp} \to Dh^{\mp}$ ($h = K, \pi$) with the modes $D \to K^{\mp}\pi^{\pm}\pi^0$, $D \to \pi^+\pi^-\pi^0$ and $D \to K^+K^-\pi^0$." In: *Phys. Rev.* D91.11 (2015), p. 112014. arXiv: 1504.05442 [hep-ex].

[155] P. del Amo Sanchez et al. "Search for b —> u transitions in $B^- \to DK^-andD^*K^-$ Decays." In: *Phys. Rev.* D82 (2010), p. 072006. arXiv: 1006.4241 [hep-ex].

[156] Y. Horii et al. "Evidence for the Suppressed Decay $B^- \to DK^-$, $D \to K^+\pi^-$." In: *Phys. Rev. Lett.* 106 (2011), p. 231803. arXiv: 1103.5951 [hep-ex].

[157] M. Nayak et al. "Evidence for the suppressed decay $B^- \to DK^-$, $D \to K^+\pi^-\pi^0$." In: *Phys. Rev.* D88.9 (2013), p. 091104. arXiv: 1310.1741 [hep-ex].

[158] Roel Aaij et al. "Measurement of CP violation parameters in $B^0 \to DK^{*0}$ decays." In: *Phys. Rev.* D90.11 (2014), p. 112002. arXiv: 1407.8136 [hep-ex].

[159] P. del Amo Sanchez et al. "Evidence for direct CP violation in the measurement of the Cabibbo-Kobayashi-Maskawa angle gamma with B-+ —> D(*) K(*)-+ decays." In: *Phys. Rev. Lett.* 105 (2010), p. 121801. arXiv: 1005.1096 [hep-ex].

[160] A. Poluektov et al. "Evidence for direct CP violation in the decay B->D(*)K, D->KsPi+Pi- and measurement of the CKM phase phi3." In: *Phys. Rev.* D81 (2010), p. 112002. arXiv: 1003.3360 [hep-ex].

[161] Roel Aaij et al. "Study of $B^- \to D\,K^-\pi^+\pi^-$ and $B^- \to D\pi^-\pi^+\pi^-$ decays and determination of the CKM angle γ." In: *Phys. Rev.* D92.11 (2015), p. 112005. arXiv: 1505.07044 [hep-ex].

[162] Lincoln Wolfenstein. "Parametrization of the Kobayashi-Maskawa Matrix." In: *Phys. Rev. Lett.* 51 (1983), p. 1945.

[163] Stefan Antusch and Vinzenz Maurer. "Running quark and lepton parameters at various scales." In: *JHEP* 11 (2013), p. 115. arXiv: 1306.6879 [hep-ph].

[164] Stephen P. Martin and Michael T. Vaughn. "Regularization dependence of running couplings in softly broken supersymmetry." In: *Phys. Lett.* B318 (1993), pp. 331–337. arXiv: hep-ph/9308222 [hep-ph].

[165] Ralf Hempfling. "Yukawa coupling unification with supersymmetric threshold corrections." In: *Phys. Rev.* D49 (1994), pp. 6168–6172.

[166] Lawrence J. Hall, Riccardo Rattazzi, and Uri Sarid. "The Top quark mass in supersymmetric SO(10) unification." In: *Phys. Rev.* D50 (1994), pp. 7048–7065. arXiv: hep-ph/9306309 [hep-ph].

[167] Marcela Carena et al. "Electroweak symmetry breaking and bottom - top Yukawa unification." In: *Nucl. Phys.* B426 (1994), pp. 269–300. arXiv: hep-ph/9402253 [hep-ph].

[168] Tomas Blazek, Stuart Raby, and Stefan Pokorski. "Finite supersymmetric threshold corrections to CKM matrix elements in the large tan Beta regime." In: *Phys. Rev.* D52 (1995), pp. 4151–4158. arXiv: hep-ph/9504364 [hep-ph].

[169] Ayres Freitas, Esther Gasser, and Ulrich Haisch. "Supersymmetric large tan(beta) corrections to DeltaM(d, s) and B(d, s) $\to \mu^+\mu^-$ revisited." In: *Phys. Rev.* D76 (2007), p. 014016. arXiv: hep-ph/0702267 [HEP-PH].

[170] Stefan Antusch and Martin Spinrath. "Quark and lepton masses at the GUT scale including SUSY threshold corrections." In: *Phys. Rev.* D78 (2008), p. 075020. arXiv: 0804.0717 [hep-ph].

[171] Stefan Antusch and Martin Spinrath. "Quark and lepton masses at the GUT scale including SUSY threshold corrections." In: *Phys. Rev.* D78 (2008), p. 075020. arXiv: 0804.0717 [hep-ph].

[172] Martin Spinrath. "New Aspects of Flavour Model Building in Supersymmetric Grand Unification." PhD thesis. Munich U., 2010. arXiv: 1009.2511 [hep-ph].

[173] Stefan Antusch et al. "From Flavour to SUSY Flavour Models." In: *Nucl. Phys.* B852 (2011), pp. 108–148. arXiv: 1104.3040 [hep-ph].

[174] Bhaskar Dutta, Yukihiro Mimura, and R. N. Mohapatra. "Suppressing proton decay in the minimal SO(10) model." In: *Phys. Rev. Lett.* 94 (2005), p. 091804. arXiv: hep-ph/0412105 [hep-ph].

[175] Bhaskar Dutta, Yukihiro Mimura, and R. N. Mohapatra. "Neutrino mixing predictions of a minimal SO(10) model with suppressed proton decay." In: *Phys. Rev.* D72 (2005), p. 075009. arXiv: hep-ph/0507319 [hep-ph].

[176] Stefan Antusch et al. "Neutrino mass matrix running for non-degenerate seesaw scales." In: *Phys. Lett.* B538 (2002), pp. 87–95. arXiv: hep-ph/0203233 [hep-ph].

[177] B. T. Cleveland et al. "Measurement of the solar electron neutrino flux with the Homestake chlorine detector." In: *Astrophys. J.* 496 (1998), pp. 505–526.

[178] F. Kaether et al. "Reanalysis of the GALLEX solar neutrino flux and source experiments." In: *Phys. Lett.* B685 (2010), pp. 47–54. arXiv: 1001.2731 [hep-ex].

[179] J. N. Abdurashitov et al. "Measurement of the solar neutrino capture rate with gallium metal. III: Results for the 2002–2007 data-taking period." In: *Phys. Rev.* C80 (2009), p. 015807. arXiv: 0901.2200 [nucl-ex].

[180] J. Hosaka et al. "Solar neutrino measurements in super-Kamiokande-I." In: *Phys. Rev.* D73 (2006), p. 112001. arXiv: hep-ex/0508053 [hep-ex].

[181] J. P. Cravens et al. "Solar neutrino measurements in Super-Kamiokande-II." In: *Phys. Rev.* D78 (2008), p. 032002. arXiv: 0803.4312 [hep-ex].

[182] K. Abe et al. "Solar neutrino results in Super-Kamiokande-III." In: *Phys. Rev.* D83 (2011), p. 052010. arXiv: 1010.0118 [hep-ex].

[183] B. Aharmim et al. "Combined Analysis of all Three Phases of Solar Neutrino Data from the Sudbury Neutrino Observatory." In: *Phys. Rev.* C88 (2013), p. 025501. arXiv: 1109.0763 [nucl-ex].

[184] G. Bellini et al. "Measurement of the solar 8B neutrino rate with a liquid scintillator target and 3 MeV energy threshold in the Borexino detector." In: *Phys. Rev.* D82 (2010), p. 033006. arXiv: 0808.2868 [astro-ph].

[185] G. Bellini et al. "Neutrinos from the primary proton-proton fusion process in the Sun." In: *Nature* 512.7515 (2014), pp. 383–386.

[186] P. Adamson et al. "Measurement of Neutrino and Antineutrino Oscillations Using Beam and Atmospheric Data in MINOS." In: *Phys. Rev. Lett.* 110.25 (2013), p. 251801. arXiv: 1304.6335 [hep-ex].

[187] P. Adamson et al. "Electron neutrino and antineutrino appearance in the full MINOS data sample." In: *Phys. Rev. Lett.* 110.17 (2013), p. 171801. arXiv: 1301.4581 [hep-ex].

[188] A. Gando et al. "Constraints on θ_{13} from A Three-Flavor Oscillation Analysis of Reactor Antineutrinos at KamLAND." In: *Phys. Rev.* D83 (2011), p. 052002. arXiv: 1009.4771 [hep-ex].

[189] M. Apollonio et al. "Limits on neutrino oscillations from the CHOOZ experiment." In: *Phys. Lett.* B466 (1999), pp. 415–430. arXiv: hep-ex/9907037 [hep-ex].

[190] A. Piepke. "Final results from the Palo Verde neutrino oscillation experiment." In: *Prog. Part. Nucl. Phys.* 48 (2002), pp. 113–121.

[191] Joachim Kopp et al. "Sterile Neutrino Oscillations: The Global Picture." In: *JHEP* 05 (2013), p. 050. arXiv: 1303.3011 [hep-ph].

[192] M. G. Aartsen et al. "Determining neutrino oscillation parameters from atmospheric muon neutrino disappearance with three years of IceCube DeepCore data." In: *Phys. Rev.* D91.7 (2015), p. 072004. arXiv: 1410.7227 [hep-ex].

[193] T. Rowan. "Functional Stability Analysis of Numerical Algorithms." PhD thesis. Department of Computer Sciences, University of Texas at Austin, 1990.

[194] Thomas P. Runarsson and Xin Yao. "Stochastic ranking for constrained evolutionary optimization." In: *IEEE Trans. Evolutionary Computation* 4 (no. 3) (2000), pp. 284–294.

[195] Thomas Philip Runarsson and Xin Yao. "Search biases in constrained evolutionary optimization." In: *IEEE Trans. on Systems, Man, and Cybernetics Part C: Applications and Reviews* 35 (no. 2) (2005), pp. 233–243.

[196] Steven G. Johnson. *The NLopt nonlinear-optimization package.* URL: http://ab-initio.mit.edu/nlopt.

[197] Francesco Vissani and Alexei Yu. Smirnov. "Neutrino masses and b - tau unification in the supersymmetric standard model." In: *Phys. Lett.* B341 (1994), pp. 173–180. arXiv: hep-ph/9405399 [hep-ph].

[198] P. A. R. Ade et al. "Planck 2015 results. XIII. Cosmological parameters." In: *Astron. Astrophys.* 594 (2016), A13. arXiv: 1502.01589 [astro-ph.CO].

[199] A. Osipowicz et al. "KATRIN: A Next generation tritium beta decay experiment with sub-eV sensitivity for the electron neutrino mass. Letter of intent." In: (2001). arXiv: hep-ex/0109033 [hep-ex].

[200] Marcela Carena et al. "Effective Lagrangian for the $\bar{t}bH^+$ interaction in the MSSM and charged Higgs phenomenology." In: *Nucl. Phys.* B577 (2000), pp. 88–120. arXiv: hep-ph/9912516 [hep-ph].

[201] R. Barate et al. "Search for the standard model Higgs boson at LEP." In: *Phys. Lett.* B565 (2003), pp. 61–75. arXiv: hep-ex/0306033 [hep-ex].

[202] M. Tanabashi et al. "Review of Particle Physics." In: *Phys. Rev.* D98.3 (2018), p. 030001.

[203] S. Heinemeyer, O. Stal, and G. Weiglein. "Interpreting the LHC Higgs Search Results in the MSSM." In: *Phys. Lett.* B710 (2012), pp. 201–206. arXiv: 1112.3026 [hep-ph].

[204] Albert M Sirunyan et al. "Search for supersymmetry in events with a photon, jets, b-jets, and missing transverse momentum in proton-proton collisions at 13 TeV." In: (2019). arXiv: 1901.06726 [hep-ex].

[205] John R. Ellis et al. "Observables in Low-Energy Superstring Models." In: *Mod. Phys. Lett.* A1 (1986), p. 57.

[206] Riccardo Barbieri and G. F. Giudice. "Upper Bounds on Supersymmetric Particle Masses." In: *Nucl. Phys.* B306 (1988), pp. 63–76.

[207] Piotr H. Chankowski, John R. Ellis, and Stefan Pokorski. "The Fine tuning price of LEP." In: *Phys. Lett.* B423 (1998), pp. 327–336. arXiv: hep-ph/9712234 [hep-ph].

[208] Piotr H. Chankowski et al. "Haggling over the fine tuning price of LEP." In: *Nucl. Phys.* B544 (1999), pp. 39–63. arXiv: hep-ph/9808275 [hep-ph].

[209] Riccardo Barbieri and Alessandro Strumia. "About the fine tuning price of LEP." In: *Phys. Lett.* B433 (1998), pp. 63–66. arXiv: hep-ph/9801353 [hep-ph].

[210] John R. Ellis, S. F. King, and J. P. Roberts. "The Fine-Tuning Price of Neutralino Dark Matter in Models with Non-Universal Higgs Masses." In: *JHEP* 04 (2008), p. 099. arXiv: 0711.2741 [hep-ph].

[211] Alessandro Strumia. "The Fine-tuning price of the early LHC." In: *JHEP* 04 (2011), p. 073. arXiv: 1101.2195 [hep-ph].

[212] Manuel Drees, Rohini Godbole, and Probir Roy. *Theory and phenomenology of sparticles : an account of four-dimensional N = 1 supersymmetry in high energy physics / Manuel Drees ; Rohini Godbole ; Probir Roy*. eng. 2005. ISBN: 978-981-256-531-0.

[213] Stephen P. Martin. "A Supersymmetry primer." In: (1997). arXiv: hep-ph/9709356 [hep-ph].

[214] G. C. Branco et al. "Theory and phenomenology of two-Higgs-doublet models." In: *Phys. Rept.* 516 (2012), pp. 1–102. arXiv: 1106.0034 [hep-ph].

[215] Debtosh Chowdhury and Otto Eberhardt. "Global fits of the two-loop renormalized Two-Higgs-Doublet model with soft Z_2 breaking." In: *JHEP* 11 (2015), p. 052. arXiv: 1503.08216 [hep-ph].

[216] Thomas Hahn. "Generating Feynman diagrams and amplitudes with FeynArts 3." In: *Comput.Phys.Commun.* 140 (2001), pp. 418–431. arXiv: hep-ph/0012260 [hep-ph].

[217] Ansgar Denner et al. "Feynman rules for fermion number violating interactions." In: *Nucl. Phys.* B387 (1992), pp. 467–481.

[218] C. Wiegand. "Automatisierte Berechnung von Feynman-Diagrammen auf Zweischleifenordnung." MA thesis. Karlsruhe Institute of Technology, 2013.

[219] C. Wiegand. "Parametrically enhanced two-loop contributions to $b \to s\gamma$ in a Two-Higgs-Doublet Model." PhD thesis. Karlsruhe Institute of Technology, 2017.

[220] Vladimir A. Smirnov. "Applied asymptotic expansions in momenta and masses." In: *Springer Tracts Mod. Phys.* 177 (2002), pp. 1–262.

[221] Andrei I. Davydychev and J.B. Tausk. "Two loop selfenergy diagrams with different masses and the momentum expansion." In: *Nucl.Phys.* B397 (1993), pp. 123–142.

[222] Andrei I. Davydychev and J. B. Tausk. "Tensor reduction of two loop vacuum diagrams and projectors for expanding three point functions." In: *Nucl. Phys.* B465 (1996), pp. 507–520. arXiv: hep-ph/9511261 [hep-ph].

[223] Ulrich Nierste. "Indirect CP violation in the neutral kaon system beyond leading logarithms and related topics." In: (1995). arXiv: hep-ph/9510323 [hep-ph].

[224] U. Nierste, D. Muller, and M. Bohm. "Two loop relevant parts of D-dimensional massive scalar one loop integrals." In: *Z. Phys.* C57 (1993), pp. 605–614.

[225] Charalampos Anastasiou et al. "Two-loop amplitudes and master integrals for the production of a Higgs boson via a massive quark and a scalar-quark loop." In: *JHEP* 01 (2007), p. 082. arXiv: hep-ph/0611236 [hep-ph].

[226] T. Huber and Daniel Maitre. "HypExp: A Mathematica package for expanding hypergeometric functions around integer-valued parameters." In: *Comput. Phys. Commun.* 175 (2006), pp. 122–144. arXiv: hep-ph/0507094 [hep-ph].

[227] Matthias Jamin and Markus E. Lautenbacher. "TRACER version 1.1: A mathematica package for γ-algebra in arbitrary dimensions." In: *Computer Physics Communications* 74.2 (1993), pp. 265 –288. ISSN: 0010-4655.

[228] Hiren H. Patel. "Package-X: A Mathematica package for the analytic calculation of one-loop integrals." In: *Comput. Phys. Commun.* 197 (2015), pp. 276–290. arXiv: 1503.01469 [hep-ph].

[229] Hiren H. Patel. "Package-X 2.0: A Mathematica package for the analytic calculation of one-loop integrals." In: *Comput. Phys. Commun.* 218 (2017), pp. 66–70. arXiv: 1612.00009 [hep-ph].

[230] Florian Herren, Luminita Mihaila, and Matthias Steinhauser. "Gauge and Yukawa coupling beta functions of two-Higgs-doublet models to three-loop order." In: *Phys. Rev.* D97.1 (2018), p. 015016. arXiv: 1712.06614 [hep-ph].

[231] Dominik Stockinger. "Regularization by dimensional reduction: consistency, quantum action principle, and supersymmetry." In: *JHEP* 03 (2005), p. 076. arXiv: hep-ph/0503129 [hep-ph].

[232] John C. Collins. *Renormalization*. Vol. 26. Cambridge Monographs on Mathematical Physics. Cambridge: Cambridge University Press, 1986. ISBN: 9780521311779, 9780511867392.

[233] Robert V. Harlander, Luminita Mihaila, and Matthias Steinhauser. "The SUSY-QCD beta function to three loops." In: *Eur. Phys. J.* C63 (2009), pp. 383–390. arXiv: 0905.4807 [hep-ph].

[234] T. Hahn and M. Perez-Victoria. "Automatized one loop calculations in four-dimensions and D-dimensions." In: *Comput. Phys. Commun.* 118 (1999), pp. 153–165. arXiv: hep-ph/9807565 [hep-ph].

[235] S. Heinemeyer, W. Hollik, and G. Weiglein. "The Mass of the lightest MSSM Higgs boson: A Compact analytical expression at the two loop level." In: *Phys. Lett.* B455 (1999), pp. 179–191. arXiv: hep-ph/9903404 [hep-ph].

[236] A. M. Sirunyan et al. "Combined search for electroweak production of charginos and neutralinos in proton-proton collisions at $\sqrt{s} = 13$ TeV." In: *JHEP* 03 (2018), p. 160. arXiv: 1801.03957 [hep-ex].

[237] J. Fleischer and O. V. Tarasov. "Calculation of Feynman diagrams from their small momentum expansion." In: *Z. Phys.* C64 (1994), pp. 413–426. arXiv: hep-ph/9403230 [hep-ph].

[238] Ralf Hempfling and Andre H. Hoang. "Two loop radiative corrections to the upper limit of the lightest Higgs boson mass in the minimal supersymmetric model." In: *Phys. Lett.* B331 (1994), pp. 99–106. arXiv: hep-ph/9401219 [hep-ph].

[239] Giuseppe Degrassi, Pietro Slavich, and Fabio Zwirner. "On the neutral Higgs boson masses in the MSSM for arbitrary stop mixing." In: *Nucl. Phys.* B611 (2001), pp. 403–422. arXiv: hep-ph/0105096 [hep-ph].

[240] Robert V. Harlander and Matthias Steinhauser. "Hadronic Higgs production and decay in supersymmetry at next-to-leading order." In: *Phys. Lett.* B574 (2003), pp. 258–268. arXiv: hep-ph/0307346 [hep-ph].

[241] Margarete Muhlleitner, Heidi Rzehak, and Michael Spira. "MSSM Higgs Boson Production via Gluon Fusion: The Large Gluino Mass Limit." In: *JHEP* 04 (2009), p. 023. arXiv: 0812.3815 [hep-ph].

[242] Asimina Arvanitaki et al. "Mini-Split." In: *JHEP* 02 (2013), p. 126. arXiv: 1210.0555 [hep-ph].

[243] Andrzej J. Buras. "Weak Hamiltonian, CP violation and rare decays." In: *Probing the standard model of particle interactions. Proceedings, Summer School in Theoretical Physics, NATO Advanced Study Institute, 68th session, Les Houches, France, July 28-September 5, 1997. Pt. 1, 2.* 1998, pp. 281–539. arXiv: hep-ph/9806471 [hep-ph].

[244] Piotr H. Chankowski, Stefan Pokorski, and Janusz Rosiek. "Complete on-shell renormalization scheme for the minimal supersymmetric Higgs sector." In: *Nucl. Phys.* B423 (1994), pp. 437–496. arXiv: hep-ph/9303309 [hep-ph].

[245] A. Dabelstein. "The One loop renormalization of the MSSM Higgs sector and its application to the neutral scalar Higgs masses." In: *Z. Phys.* C67 (1995), pp. 495–512. arXiv: hep-ph/9409375 [hep-ph].

[246] Damien M. Pierce et al. "Precision corrections in the minimal supersymmetric standard model." In: *Nucl. Phys.* B491 (1997), pp. 3–67. arXiv: hep-ph/9606211 [hep-ph].

[247] M. Frank et al. "The Higgs Boson Masses and Mixings of the Complex MSSM in the Feynman-Diagrammatic Approach." In: *JHEP* 02 (2007), p. 047. arXiv: hep-ph/0611326 [hep-ph].

[248] S. Heinemeyer, W. Hollik, and G. Weiglein. "The Masses of the neutral CP - even Higgs bosons in the MSSM: Accurate analysis at the two loop level." In: *Eur. Phys. J.* C9 (1999), pp. 343–366. arXiv: hep-ph/9812472 [hep-ph].

[249] S. Heinemeyer, W. Hollik, and G. Weiglein. "QCD corrections to the masses of the neutral CP - even Higgs bosons in the MSSM." In: *Phys. Rev.* D58 (1998), p. 091701. arXiv: hep-ph/9803277 [hep-ph].

[250] S. Heinemeyer, W. Hollik, and G. Weiglein. "Precise prediction for the mass of the lightest Higgs boson in the MSSM." In: *Phys. Lett.* B440 (1998), pp. 296–304. arXiv: hep-ph/9807423 [hep-ph].

[251] Ren-Jie Zhang. "Two loop effective potential calculation of the lightest CP even Higgs boson mass in the MSSM." In: *Phys. Lett.* B447 (1999), pp. 89–97. arXiv: hep-ph/9808299 [hep-ph].

[252] Jose Ramon Espinosa and Ren-Jie Zhang. "Complete two loop dominant corrections to the mass of the lightest CP even Higgs boson in the minimal supersymmetric standard model." In: *Nucl. Phys.* B586 (2000), pp. 3–38. arXiv: hep-ph/0003246 [hep-ph].

[253] Andrea Brignole et al. "On the O(alpha(t)**2) two loop corrections to the neutral Higgs boson masses in the MSSM." In: *Nucl. Phys.* B631 (2002), pp. 195–218. arXiv: hep-ph/0112177 [hep-ph].

[254] A. Brignole et al. "On the two loop sbottom corrections to the neutral Higgs boson masses in the MSSM." In: *Nucl. Phys.* B643 (2002), pp. 79–92. arXiv: hep-ph/0206101 [hep-ph].

[255] Stephen P. Martin. "Complete Two Loop Effective Potential Approximation to the Lightest Higgs Scalar Boson Mass in Supersymmetry." In: *Phys. Rev.* D67 (2003), p. 095012. arXiv: hep-ph/0211366 [hep-ph].

[256] Athanasios Dedes, Giuseppe Degrassi, and Pietro Slavich. "On the two loop Yukawa corrections to the MSSM Higgs boson masses at large tan beta." In: *Nucl. Phys.* B672 (2003), pp. 144–162. arXiv: hep-ph/0305127 [hep-ph].

[257] Stephen P. Martin. "Strong and Yukawa two-loop contributions to Higgs scalar boson self-energies and pole masses in supersymmetry." In: *Phys. Rev.* D71 (2005), p. 016012. arXiv: hep-ph/0405022 [hep-ph].

[258] B. C. Allanach et al. "Precise determination of the neutral Higgs boson masses in the MSSM." In: *JHEP* 09 (2004), p. 044. arXiv: hep-ph/0406166 [hep-ph].

[259] S. Heinemeyer et al. "High-precision predictions for the MSSM Higgs sector at O(alpha(b) alpha(s))." In: *Eur. Phys. J.* C39 (2005), pp. 465–481. arXiv: hep-ph/0411114 [hep-ph].

[260] S. Heinemeyer et al. "The Higgs sector of the complex MSSM at two-loop order: QCD contributions." In: *Phys. Lett.* B652 (2007), pp. 300–309. arXiv: 0705.0746 [hep-ph].

[261] G. Degrassi, S. Di Vita, and P. Slavich. "Two-loop QCD corrections to the MSSM Higgs masses beyond the effective-potential approximation." In: *Eur. Phys. J.* C75.2 (2015), p. 61. arXiv: 1410.3432 [hep-ph].

[262] S. Borowka et al. "Momentum-dependent two-loop QCD corrections to the neutral Higgs-boson masses in the MSSM." In: *Eur. Phys. J.* C74.8 (2014), p. 2994. arXiv: 1404.7074 [hep-ph].

[263] Wolfgang Hollik and Sebastian Paßehr. "Two-loop top-Yukawa-coupling corrections to the Higgs boson masses in the complex MSSM." In: *Phys. Lett.* B733 (2014), pp. 144–150. arXiv: 1401.8275 [hep-ph].

[264] Wolfgang Hollik and Sebastian Paßehr. "Higgs boson masses and mixings in the complex MSSM with two-loop top-Yukawa-coupling corrections." In: *JHEP* 10 (2014), p. 171. arXiv: 1409.1687 [hep-ph].

[265] R. V. Harlander et al. "Higgs boson mass in supersymmetry to three loops." In: *Phys. Rev. Lett.* 100 (2008). [Phys. Rev. Lett.101,039901(2008)], p. 191602. arXiv: 0803.0672 [hep-ph].

[266] P. Kant et al. "Light MSSM Higgs boson mass to three-loop accuracy." In: *JHEP* 08 (2010), p. 104. arXiv: 1005.5709 [hep-ph].

[267] Stephen P. Martin. "Three-loop Standard Model effective potential at leading order in strong and top Yukawa couplings." In: *Phys. Rev.* D89.1 (2014), p. 013003. arXiv: 1310.7553 [hep-ph].

[268] Howard E. Haber and Ralf Hempfling. "The Renormalization group improved Higgs sector of the minimal supersymmetric model." In: *Phys. Rev.* D48 (1993), pp. 4280–4309. arXiv: hep-ph/9307201 [hep-ph].

[269] J. A. Casas et al. "The Lightest Higgs boson mass in the minimal supersymmetric standard model." In: *Nucl. Phys.* B436 (1995). [Erratum: Nucl. Phys.B439,466(1995)], pp. 3–29. arXiv: hep-ph/9407389 [hep-ph].

[270] Marcela Carena et al. "Analytical expressions for radiatively corrected Higgs masses and couplings in the MSSM." In: *Phys. Lett.* B355 (1995), pp. 209–221. arXiv: hep-ph/9504316 [hep-ph].

[271] Howard E. Haber, Ralf Hempfling, and Andre H. Hoang. "Approximating the radiatively corrected Higgs mass in the minimal supersymmetric model." In: *Z. Phys.* C75 (1997), pp. 539–554. arXiv: hep-ph/9609331 [hep-ph].

[272] Patrick Draper, Gabriel Lee, and Carlos E. M. Wagner. "Precise estimates of the Higgs mass in heavy supersymmetry." In: *Phys. Rev.* D89.5 (2014), p. 055023. arXiv: 1312.5743 [hep-ph].

[273] Emanuele Bagnaschi et al. "Higgs Mass and Unnatural Supersymmetry." In: *JHEP* 09 (2014), p. 092. arXiv: 1407.4081 [hep-ph].

[274] Javier Pardo Vega and Giovanni Villadoro. "SusyHD: Higgs mass Determination in Supersymmetry." In: *JHEP* 07 (2015), p. 159. arXiv: 1504.05200 [hep-ph].

[275] Marcela Carena et al. "Reconciling the two loop diagrammatic and effective field theory computations of the mass of the lightest CP - even Higgs boson in the MSSM." In: *Nucl. Phys.* B580 (2000), pp. 29–57. arXiv: hep-ph/0001002 [hep-ph].

[276] Patrick Draper and Heidi Rzehak. "A Review of Higgs Mass Calculations in Supersymmetric Models." In: *Phys. Rept.* 619 (2016), pp. 1–24. arXiv: 1601.01890 [hep-ph].

[277] Henning Bahl et al. "Reconciling EFT and hybrid calculations of the light MSSM Higgs-boson mass." In: *Eur. Phys. J.* C78.1 (2018), p. 57. arXiv: 1706.00346 [hep-ph].

[278] Henning Bahl and Wolfgang Hollik. "Precise prediction for the light MSSM Higgs boson mass combining effective field theory and fixed-order calculations." In: *Eur. Phys. J.* C76.9 (2016), p. 499. arXiv: 1608.01880 [hep-ph].

[279] T. Hahn et al. "High-Precision Predictions for the Light CP -Even Higgs Boson Mass of the Minimal Supersymmetric Standard Model." In: *Phys. Rev. Lett.* 112.14 (2014), p. 141801. arXiv: 1312.4937 [hep-ph].

[280] G. Degrassi et al. "Towards high precision predictions for the MSSM Higgs sector." In: *Eur. Phys. J.* C28 (2003), pp. 133–143. arXiv: hep-ph/0212020 [hep-ph].

[281] S. Heinemeyer, W. Hollik, and G. Weiglein. "FeynHiggs: A Program for the calculation of the masses of the neutral CP even Higgs bosons in the MSSM." In: *Comput. Phys. Commun.* 124 (2000), pp. 76–89. arXiv: hep-ph/9812320 [hep-ph].

[282] M. Galassi et a. *GNU Scientific Library Reference Manual (2nd Ed.)* ISBN: 0954161734.

[283] Ulrich Ellwanger, Cyril Hugonie, and Ana M. Teixeira. "The Next-to-Minimal Supersymmetric Standard Model." In: *Phys. Rept.* 496 (2010), pp. 1–77. arXiv: 0910.1785 [hep-ph].

[284] M. Maniatis. "The Next-to-Minimal Supersymmetric extension of the Standard Model reviewed." In: *Int. J. Mod. Phys.* A25 (2010), pp. 3505–3602. arXiv: 0906.0777 [hep-ph].

[285] Roel Aaij et al. "Observation of *CP* violation in charm decays." In: (2019). arXiv: 1903.08726 [hep-ex].

[286] J. H. Christenson et al. "Evidence for the 2π Decay of the K_2^0 Meson." In: *Phys. Rev. Lett.* 13 (1964), pp. 138–140.

[287] T. Inami and C. S. Lim. "Effects of Superheavy Quarks and Leptons in Low-Energy Weak Processes k(L) —> mu anti-mu, K+ —> pi+ Neutrino anti-neutrino and Ko <—> anti-Ko." In: *Prog. Theor. Phys.* 65 (1981). [Erratum: Prog. Theor. Phys.65,1772(1981)], p. 297.

[288] A. Lenz et al. "Anatomy of New Physics in $B - \bar{B}$ mixing." In: *Phys. Rev.* D83 (2011), p. 036004. arXiv: 1008.1593 [hep-ph].

[289] Yosef Nir and Nathan Seiberg. "Should squarks be degenerate?" In: *Phys. Lett.* B309 (1993), pp. 337–343. arXiv: hep-ph/9304307 [hep-ph].

[290] Kfir Blum et al. "Combining Ko - anti-Ko mixing and Do - anti-Do mixing to constrain the flavor structure of new physics." In: *Phys. Rev. Lett.* 102 (2009), p. 211802. arXiv: 0903.2118 [hep-ph].

[291] John S. Hagelin, S. Kelley, and Toshiaki Tanaka. "Exact supersymmetric amplitude for Ko - anti-Ko and Bo - anti-Bo mixing." In: *Mod. Phys. Lett.* A8 (1993), pp. 2737–2746. arXiv: hep-ph/9304218 [hep-ph].

[292] F. Gabbiani et al. "A Complete analysis of FCNC and CP constraints in general SUSY extensions of the standard model." In: *Nucl. Phys.* B477 (1996), pp. 321–352. arXiv: hep-ph/9604387 [hep-ph].

[293] Marco Ciuchini et al. "Delta M(K) and epsilon(K) in SUSY at the next-to-leading order." In: *JHEP* 10 (1998), p. 008. arXiv: hep-ph/9808328 [hep-ph].

[294] Oram Gedalia et al. "Lessons from Recent Measurements of Do - anti-Do Mixing." In: *Phys. Rev.* D80 (2009), p. 055024. arXiv: 0906.1879 [hep-ph].

[295] Andreas Crivellin and Momchil Davidkov. "Do squarks have to be degenerate? Constraining the mass splitting with Kaon and D mixing." In: *Phys. Rev.* D81 (2010), p. 095004. arXiv: 1002.2653 [hep-ph].

[296] Andreas Crivellin and Ulrich Nierste. "Supersymmetric renormalisation of the CKM matrix and new constraints on the squark mass matrices." In: *Phys. Rev.* D79 (2009), p. 035018. arXiv: 0810.1613 [hep-ph].

[297] Andreas Crivellin, Ahmet Kokulu, and Christoph Greub. "Flavor-phenomenology of two-Higgs-doublet models with generic Yukawa structure." In: *Phys. Rev.* D87.9 (2013), p. 094031. arXiv: 1303.5877 [hep-ph].

[298] Jonathan A. Bagger, Konstantin T. Matchev, and Ren-Jie Zhang. "QCD corrections to flavor changing neutral currents in the supersymmetric standard model." In: *Phys. Lett.* B412 (1997), pp. 77–85. arXiv: hep-ph/9707225 [hep-ph].

[299] Teppei Kitahara, Ulrich Nierste, and Paul Tremper. "Supersymmetric Explanation of CP Violation in $K \to \pi\pi$ Decays." In: *Phys. Rev. Lett.* 117.9 (2016), p. 091802. arXiv: 1604.07400 [hep-ph].

[300] M. Bona et al. "Constraints on new physics from the quark mixing unitarity triangle." In: *Phys. Rev. Lett.* 97 (2006), p. 151803. arXiv: hep-ph/0605213 [hep-ph].

[301] M. Bona et al. "Model-independent constraints on $\Delta F = 2$ operators and the scale of new physics." In: *JHEP* 03 (2008), p. 049. arXiv: 0707.0636 [hep-ph].

[302] N. H. Christ et al. "Long distance contribution to the KL-KS mass difference." In: *Phys. Rev.* D88 (2013), p. 014508. arXiv: 1212.5931 [hep-lat].

[303] Z. Bai et al. "$K_L - K_S$ Mass Difference from Lattice QCD." In: *Phys. Rev. Lett.* 113 (2014), p. 112003. arXiv: 1406.0916 [hep-lat].

[304] Norman H. Christ et al. "Effects of finite volume on the K_L-K_S mass difference." In: *Phys. Rev.* D91.11 (2015), p. 114510. arXiv: 1504.01170 [hep-lat].

[305] D. Becirevic et al. "Ko - anti-Ko mixing with Wilson fermions without subtractions." In: *Phys. Lett.* B487 (2000), pp. 74–80. arXiv: hep-lat/0005013 [hep-lat].

[306] Michael E. Peskin and Daniel V. Schroeder. *An Introduction to quantum field theory*. Reading, USA: Addison-Wesley, 1995. ISBN: 9780201503975, 0201503972. URL: http://www.slac.stanford.edu/~mpeskin/QFT.html.

[307] L. D. Faddeev and V. N. Popov. "Feynman Diagrams for the Yang-Mills Field." In: *Phys. Lett.* B25 (1967), pp. 29–30.

ACKNOWLEDGEMENTS

- First of all, I would like to thank Ulrich Nierste for offering me the opportunity to do a bit more than three years of research that finally lead to this work. He also came up with the idea of revisiting the fine-tuning in case of heavy gluinos and provided me with advice during that time. I also like to thank Margarete Mühlleitner who agreed to be the second reviewer of this thesis. Her comments on the manuscript lead to many improvements in the final phase of this thesis.

- I am very grateful to all people who read this work or at least parts of it and contributed with their comments, expertise and experience: Stefan de Boer who also had the ungrateful job of cross-checking the formulae, Florian Herren and Marta Moscati who both read through the *whole work*, Martin Spinrath (no GUTs, no glory!) and José Zurita for the phenomenological perspective and legitimate criticisms on German writing habbits.

- I also like to thank Stefan Schacht and Martin Spinrath for two years of collaboration on the GUT project. During our weekly skype meetings across twelve time zones I learned a lot about the practical aspects of scientific publications.

- I further want to apologise to Christoph Wiegand for my—using his words—'chaotic' beta testing of Medusa.

- Furthermore, I thank the following TTPeople for 'fruitful' discussions about the SM and beyond as well as more or less related topics. These are, in no particular order:
  - my room mates Aliaksei Kachanovich, my 'personal' admin and Mathematica expert David Wellmann as well as Marco Bonetti who is next to finish his thesis. Osu!
  - all the admins, especially for helping me out when I broke my account two weeks ago, namely Konstantin Asteriadis, Martin Gabelmann, David Wellmann, my last SUSY brother at arms Mustafa Tabet and all others who preceded them.
  - Daniel Baranowski, Martin Lang and Marvin Gerlach who take (or took) care of the constant supply of coffee and soft drinks.
  - the rest of the 11:30 lunch group: Monika Blanke, Wolfgang 'G.' Hollik, Go Mishima, Ivan Nišandžić and Jakob Schwichtenberg. I hope you won't starve without me.
  - Martina Schorn who keeps track of... everything.

- TD acknowledges emotional support by BWV 1004.

COLOPHON

This document was typeset using the typographical look-and-feel `classicthesis` developed by André Miede and Ivo Pletikosić. The style was inspired by Robert Bringhurst's seminal book on typography "*The Elements of Typographic Style*". `classicthesis` is available for both LaTeX and LyX:

https://bitbucket.org/amiede/classicthesis/

Happy users of `classicthesis` usually send a real postcard to the author, a collection of postcards received so far is featured here:

http://postcards.miede.de/

All Feynman diagrams in this work were drawn with `FeynArts` albeit some were manipulated with Inkscape that was also used to design the flow charts. The plots were created with `GNUplot` using the parula colour scheme available at

www.gnuplotting.org

Final Version as of May 15, 2019 (genehmigte).